University of Alberta

Fault Detection Characterization, Design, and Reliability Analysis

by

Shuonan Yang

A thesis submitted to the Faculty of Graduate Studies and Research
in partial fulfillment of the requirements for the degree of

Doctor of Philosophy

in

Control Systems

Department of Electrical and Computer Engineering

Spring 2013
Edmonton, Alberta

Abstract

This thesis develops fault detection characterization, design, and reliability analysis within a real-time, multilayered fault detection and diagnosis (FDD) framework proposed according to fault tolerant control systems (FTCS). With the development of sophisticated control and monitoring systems, it has become more challenging to carry out routine maintenance, tuning, troubleshooting, and thus keep the systems operate in their desired or optimal states. Nevertheless, the system is required to present competitive performance and timely response to abnormal conditions. Compared with pure data-driven FD techniques, integrated schemes with model-based FD approaches utilize the available inherent dynamic relationship among various signals hence can render more precise diagnosis results. Fitting in the FTCS scope, the real-time integrated FDD framework is thus highlighted as a strategic solution platform, where various specific FD approaches may be conceived and realized.

Within the framework, research has been carried out in various aspects, including but not limited to fault detection (FD) design/characterization, real-time frequency estimation, and reliability of fault detection. Firstly, as the major part of the thesis, FD design/characterization takes up more than two chapters where analytical forms characterizing the (first) detection/hitting time (FHT) are developed based on the general-likelihood ratio (GLR) detection method. Both probability expressions and single-valued performance indices are proposed for both additive and multiplicative faults. Secondly, as a substantial technical solution promoted by FD techniques, online fre-

quency estimation has been researched using the gradient estimator approach with leakage. In the last research topic, semi-Markov kernel modeling and real-time reliability are discussed with respect to long term fault and detector sequences. The characterization and design plans have been tested on practical data sequences and industrial system models, demonstrating the feasibility of implementation.

Acknowledgements

I would like to express my appreciation towards my supervisor, Dr. Qing Zhao, for her guidance and help during my time in the University of Alberta. It is she who has introduced me to the academic field, which is the basis of my research throughout these years and thus decisive to this thesis. Above this point, she always discusses academic topics with me in patience, shares valuable opinions with me, and provide encouragement when my research was stagnant; all these makes her a memorable professor.

I thank the PhD final examination committee and candidacy examination committee for my thesis. Thanks to Dr. Tongwen Chen, Dr. Mahdi Tavakoli, Dr. Stevan Dubljevic, and Dr. Youmin Zhang, for peerly reviewing my work and sparing time to prepare for the defense. Thanks to Dr. Biao Huang and Dr. Yindi Jing, for posing questions in the candidacy exam examination and providing me with valuable comments/suggestions.

I would like to express my gratitude to the advanced control lab of the University of Alberta, where I have been carrying out research work and got to know many colleagues who have given me help. Thanks to Mr. Yue Cheng, Mr. Jiadong Wang, Dr. Hongbin Li, Dr. Jingbo Jiang, Mr. Salman Ahmed, Ms. Ping Duan, Mr. Xiangyu Meng, Mr. Geoff McDonald, Mr. Alireza Mohammadi, Mr. Dawei Shi, Ms. Ying Wang, Mr. Yixin Zhang, Dr. Jian Li, and many others whose name are not listed here, for their help to my research progress and effort on keep the lab a great place for research.

During the past years, I have received financial supports from the Natural Science and Engineering Research Council of Canada (NSERC) and the Faculty of Graduate Studies and Research (FGSR) at the University of Alberta in the form of research assistantship, Queen Elizabeth II Scholarship, and travel award. I hereby give my special gratitude to the organizations and the Queen for their generous supports.

At last, I would like to give my greatest thank to my parents and dedicate the thesis to them. They have been providing me with the utmost selfless support in the world, since they gave me the life.

Contents

List of Tables

List of Figures

Nomenclature

(B)CLR (Biased) Continuous Likelihood Ratio

ARL Average Run Length

CUSUM Cumulative Sum

DD Detection Delay

DMRP Discrete-time Markov Renewal Process

FAR False Alarm Rate

FD(D) Fault detection (and diagnosis)

FDI Fault Detection and Isolation

FHT First Hitting Time

FTC(S) Fault Tolerant Control (System)

GLR General Likelihood Ratio

i.i.d. independently and identically distributed

PE Persistency of Excitation

SPR-Lyapunov Strictly Positive Real-Lyapunov

SPRT Sequential Probability Ratio Test

TBFA Time between False Alarms

w.p. Wiener Process

Chapter 1

Introduction

1.1 Fault Detection and Diagnosis

The automation technologies have been rapidly developing in the past 30 years and are applied widely in dynamical processes and systems. Nowadays, modern control systems become extremely complex by integrating various functions and components for sophisticated performance requirement. With such complexities in hardware and software, it is natural that the system may become vulnerable to faults in practice. It is believed that fault tolerance and reliability are among the most important considerations in the design and operation of control systems and technical processes. The proposed research aims to investigate these important issues and develop efficient diagnosis techniques for component faults from the systems perspective (as opposed to that for circuits and chips). As a family of analysis methods and solutions, fault detection and diagnosis (FDD, or equivalently fault detection/isolation (FDI)) and fault tolerant control (FTC) form the background of the research project.

FD methods can be commonly categorized in two main classes, namely model-based and data-driven fault detection [1], [3], [6], [7]. Approaches in both types generate characteristic signals or information to be evaluated as the judgment of faults. As is widely used, model-based approaches generally utilize the available system model or observer-like structures to generate such

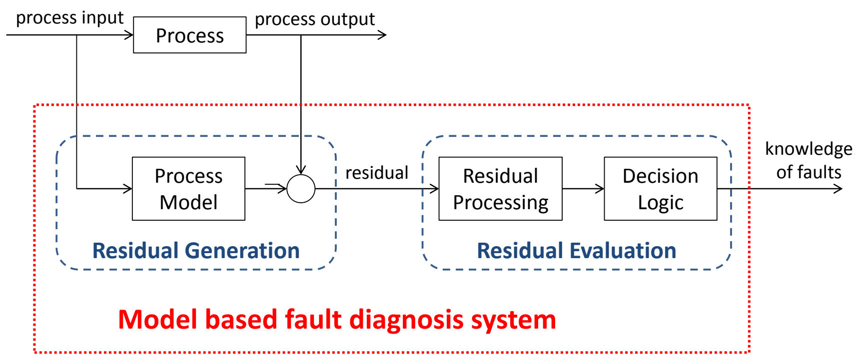

(a) Model-based FD

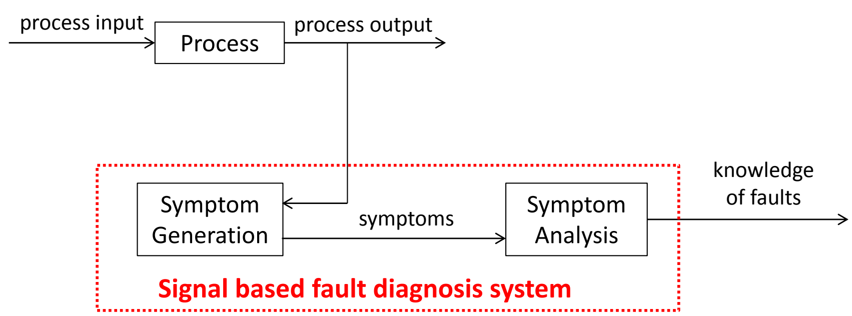

(b) Data-driven FD

Figure 1.1: Schematic description of Model-based and Data-driven FD [1]

a characteristic signal, commonly referred to as a residual signal, which tends to be around 0 if no fault occurs. In contrast, it is unnecessary for data-driven approaches to assume the availability of models; the signal/informations generated for detection are naturally different from model-based residuals and may thus have different characteristics in the sense of detection. In [1] Ding provides the general schemes respectively concerning the model-based and data-driven FD as in Fig. 1.1. Venkatasubramanian and Yang respectively provide in [3] and [6] a more detailed tree hierarchy concerning specific realizations of FD as in Fig. 1.2. Relevant literature review is provided in 1.3.1.

Both types of approaches have their advantages and deficiencies. According to [3], [5], model-based FD are well-defined and can handle unexpected faults, if complete knowledge of all inputs and outputs of the system including their dynamic relationships is available; however, model-based FD may

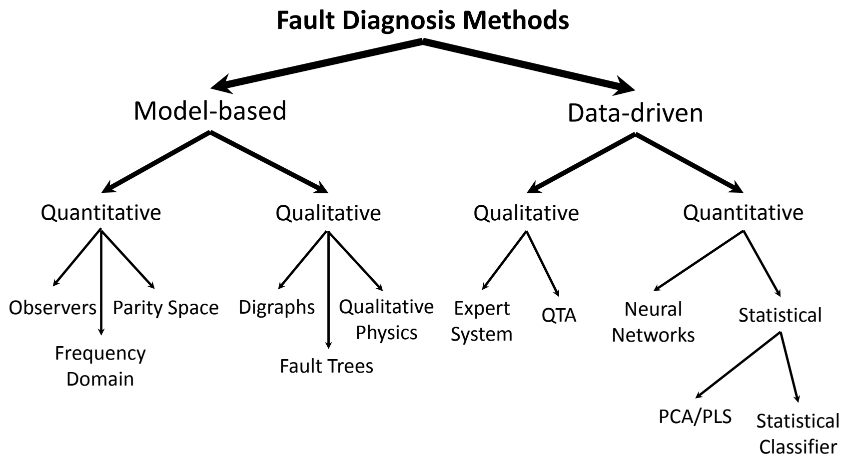

Figure 1.2: A common tree hierarchy of FD [6]

malfunction on lacking such modeling information, and the modeling itself is not always accurate due to system complexities and nonlinearity. In contrast, data-driven FD is easier to implement and thus widely selected for applications due to the lower requirement of *a priori* knowledge, while its performance yield to degradation by sensor failures and the limited coverage in the measurement space of the fault classifiers [3], [5]. In order to maximize the advantages and minimize the disadvantages, researchers integrate both the data-driven and model-based methods together into a new type of compounded approaches, namely the integrated fault diagnosis; our research goals and directions disclosed in Section 1.4 is inspired from this fact.

1.2 Real-time Integrated FDD Framework

Based on the research background and literature review provided in 1.1, we formulate a real-time integrated FDD framework, in which our research is developed. The framework fits in the large scope of intelligent active FTCS, of which a detailed structure is provided, and our concentrations are discussed under this scope. From the practical perspective, our research is expected to develop fault diagnosis analysis to ensure the feasibility of FD and carry out design to improve system safety/performance. In other words, it is desired that FD solutions are stable, implementable using the existing control devices at low costs, and capable of detecting faults/satisfying other requirements. Substantial contributions towards this goal have been made in the following chapters.

1.2.1 Motivations

Our research is developed under the scope of a feasible theoretical framework. From the perspective of FTCS, the framework may contain all or part of F-DI approaches, controller, FDI knowledge/prediction, real-time reconciliation mechanism, and data acquisition, etc. Fig. 1.3 provides one type of explanation between integrated FDD framework and intelligent FTCS scope. Compared with schemes in [77], Fig. 1.3 summarizes a more explicated functional structure in three layers: the top layer functions as reliability maintenance and decision making, the middle layer functions as FDI and controller, and the bottom layer consists of various real subsystems and data collection modules. Our proposed research involves components at the middle and the top layers: FD validation and design are crucial parts of the middle layer; the reliability analysis belongs to the top layer.

The rational behind this contains consideration in more than one aspect. Firstly, the complexity of the large systems (as in the FTCS scope) gradually becomes a potential problem affecting its feasibility and performance, while our research aims to provide satisfactory solutions. As a result, FDI needs to be responsible for dealing with various kinds of raw signal inputs and residuals, and small/narrow-scoped solutions may reflect limitations when applied to such complex environment. For example, multiple types of faults may simultaneously exist in one signal sequence together with noises and disturbances, where detectors/isolators with one simple rule will not function

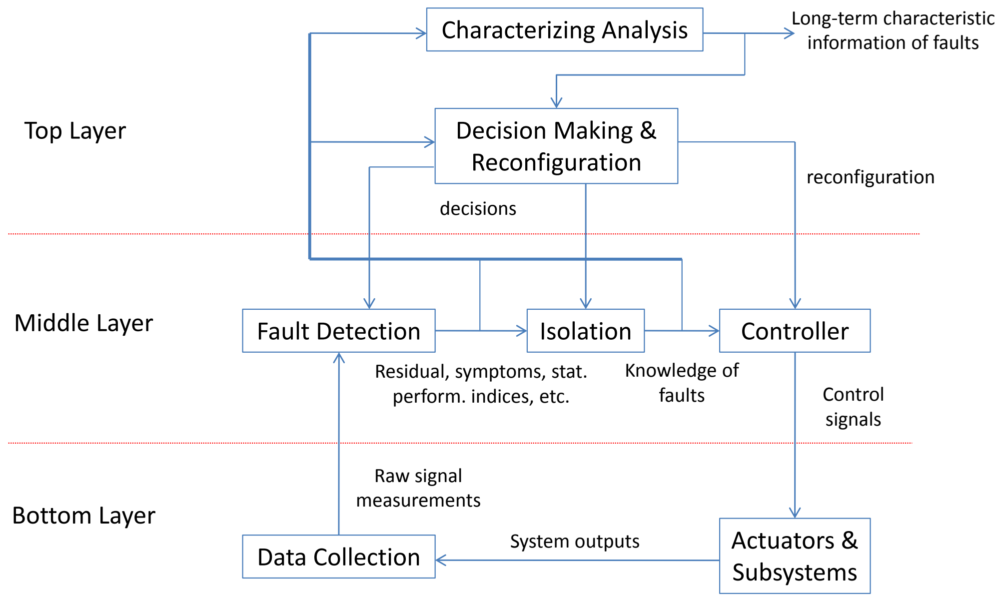

Figure 1.3: A typical structure of FTCS

as desired. Secondly, offline FDI analysis methods are still the major part of FDI approaches in certain applications, e.g. the FD of plant-wide oscillations, which cannot satisfactorily fulfill the requirement on FD methods for abrupt/dynamic changes. Along with high demands on the performance of FDI and its affiliated system, timing response of FD is gradually becoming an urgent and crucial consideration in design, not mentioning its importance on long-term reliability/safety concern and control reconfiguration. Note that detection delays, missing detections, false alarms and their statistical properties in case of random noises are the most prominent performance characteristics of a real-time fault diagnosis scheme [51], [73], which is also part of the motivation that certain methodologies are selected in the research.

The reasons above provide grounds of research under the framework; accordingly, we have developed our research along several FDI-related issues.

1.2.2 Contributions

With the scope determined, the research points are hereby sketched. Note that the previous research efforts mainly concern the fault detection and its evaluation; in contrast, the FTCS scheme shown in Fig. 1.3 contains all the designable parts as FDI, FTC, characterization module, decision/reconfiguration module, etc. New research topics are then conceived and conducted under this intelligent FTC framework, including FD/characterization using new methodologies and/or covering new types of faults, improvement on other modules within the scope, implementation, etc. The following chapters have made substantial contributions towards these topics, which are further discussed according to possible significations in the rest of the subsection.

Detection and Characterization of New Types of Faults

As suggested in Section 1.3.1, the sense of integrated FD based research is not only the integration of methods, but also the capability of dealing with different types of faults or fault induced signals compared with conventional FD approaches by considering more types of residuals. Examples of common fault types are listed as follows, where Chapter 2, 3, 4 have developed FD analysis covering various types of faults, grounding on practical needs.

- Fault simultaneously affecting amplitude, phase, and frequency. Our research about frequency estimation is able to isolate sinusoidal faults corrupted with bounded disturbances, whereas the faults simultaneously affecting amplitude, phase, and frequency may also happen and propose higher requirements.

- Additive fault affecting mean. Researchers have inspected various types of detectors and performance indices, while breakthrough is still expected wirh respect to quantitative performance indices for GLR detection. The

GLR-based test discussed in Chapter 2 has validated the effectiveness in detecting step faults corrupted with Gaussian white noises, and such step faults only change the mean of the noise. Chapter 2 has posed an analytical upper bound of the detection probability upon time with respect to additive bias-type fault, and the comparison between this method and real GLR reflects its feasibility and properties.

- Multiplicative fault affecting variance. Although the step fault (as described in the GLR-based test in the thesis) is considered as additive fault to the noise, in some cases faults may exists as multiplicative gain on noises. This type of faults belongs to those affecting variance. Chapter 3 has provided approximations on both the expectation (mean) of the detection delay and the detection probability upon time with respect to multiplicative fault affecting variance.

- Dynamic faults. This concept denotes a type of faults experiencing dynamic change from their occurrence to the "steady states". For example, the step fault described in our GLR-based test is not a dynamic fault itself; when it happens in a large system consisting of connected subsystems, however, it will perform like a dynamic fault with respect to the data collected from other subsystems. It will be an advanced FD problem when only the data from the propagated subsystems are available, and the diagnosis often has to face this condition. Chapter 4 has exploited dynamic faults in both robust frequency estimation and FD, discussed two types of relevant faults (frequency shift and unexpected additive sinusoids), and examined them in the simulation. Especially, the significance of Chapter 4 is reflected by the improvement of FD evaluation in quantized measures.

Exploit on Other Modules

With the designed integrated FD, it is feasible to define more functions to be realized under the large scope and design the relevant functioning modules. Referring to the FTCS shown in Fig. 1.3, we hereby target to carry out research on other modules, mainly the upper-level analysis of the long-term FD behavior and the FD reliability upon time.

On one hand, the controller receives the fault isolation information and thus can realize FTC on unexpected additive sinusoidal signals, counted as one type of deterministic fault, when the isolation adopts the frequency estimation technique. In practice, this option of the controller design may maintain the system stability by reducing the effect caused by vibrations. On the other hand, the top layer in Fig. 1.3 may characterize and make decisions based on the fault information obtained by both detection and isolation. Take the GLR-based test as an example: it computes the performance indices, which can be helpful in restrict stochastic (random) faults and forwarded to the decisioning module. The decision can be used for operating on the middle-layer controller, e.g. switching between the pre-determined control plans, where the concept of multiple hypothesis will be useful. With research on FD analysis and design provided, Chapter 2, 3, and 4 have carried out simulations respectively on two different DC motor FTCS and one hydraulic rig system. The simulation results give FD response with description of quantitative time distribution and/or mean time expectation, indicating the feasibility of FD-based control within such systems.

Moreover, if the fault time series follows the form of Markov chain, the decision may follow the Markov chain or semi-Markov chain, and the characterization regarding (semi-)Markov chain may generate helpful information for the decision module. The research on Markov chain can characterize the long-term behavior of fault events and may also help to reduce the recovery time from the detection to the confirmation of fault disappearance. Mature research is available on kernel descriptions of Markovian sequences with industrial applications, like image processing and FTCS [63], [112], [48], [49], and the research on kernels of semi-Markov sequences also tend to become popular [114], [50]. Following the direction, Chapter 5 works on kernel modeling of certain types of fault/detection sequences and relevant reliability analysis.

Applications

The application prospects of the research topic can be roughly categorized in two aspects: vibration/oscillation testing and FD performance evaluation. On realizing the desired functions listed in Section 1.2.2, we expect to implement the system on a real industrial process, power system, or mechanical system, with one or both of the functions.

- Vibration & oscillation testing

Oscillations (harmonics) commonly exists in many types of systems, such as chemical processes, rotating machines, power systems [39], etc. It was pointed out that a system running steadily without oscillation is more profitable and safer [36]. On the contrary, the existence of oscillations may keep the components from its optimal performance and even cause the unstableness. Moreover, oscillations generally occur as a plant-wide disturbance by propagating to the neighbor components (then plant-wide) in various paths, e.g. via physical coupling and recycles [43]. For instance, controllers may pass the oscillation to manipulated variables, resulting in poor control performance [44]. Therefore, it is important to diagnose such oscillations and rectify the faulty situations, and FDI expertise may be considered as one type of the potential solutions. Plenty of research achievements have been made concerning the process oscillations and machinery vibrations, and more mechanical and industrial processes are available for implementation compared with confidential systems (e.g. aerospace). Implementation-related methodologies in both frequency and time-domain, such as surrogate data [43], bicoherence [45], ACF [42], IAE [41], are available as alternative FD and decisioning approaches. Based on a complementary research view, we focus on the real-time design on a mechanical system or an industrial process. Chapter 4 poses a set of gear shaft position data upon time, where the crack on the gear perturbs the shaft position by giving a vibration. Accurate frequency estimation is realized on that set of data, with better performance compared with the method in [54].

- FD performance evaluation

From another perspective, our current research can be applied to industrial FD performance evaluation. For example, the detection of mean/variance change of noisy alarm signals (residuals), where the alarm signal is directly used as detector input, is widely applied in process monitoring: it does not belong to the control chart testing standards like CUSUM and GLR, where decision functions are used as detector input. The most common assumption is that the alarm signals are Gaussian i.i.d., and only constant step change exists between hypotheses H_0 and H_1. The method used in Chapter 3 will be applicable to the generation of the analytical discrete (approximated) distribution of FHT with all of the integration removed. Here the distribution of FHT denotes either time between false alarms or detection delay depending on the occurrence of fault, and it also describes the distribution properties of each time duration with the fault decision $\delta(y) = 0$ within one data sequence along the time axis because of the memoryless property. Likewise, industrial indices relevant to run length, especially Average Run Length (ARL) and False Alarm Rate (FAR), can be computed by considering time durations with $\delta(y) = 1$, which has been realized in Chapter 3.

1.3 Literature Review

High volume of literature survey and review work has been done and listed below, in order to contour the research development on FD and acquire materials for possible research directions upon the motivations. Details and complementary information regarding the literature review are available in [69], [70], [71], [72].

1.3.1 Research development on FD

As the first developed FD branch, model-based FD has been mostly researched. Frank explicitly classified quantitative model-based FD into parity space, observer, FD filter, and parameter identification approaches as early as in 1990 [8], while Venkatasubramanian classified qualitative FD into digraph, qualitative physics, and fault trees approaches [4]. Research in all these subcategories has been highly developed. Chang developed research on the possibility of applying sub-optimal extended Kalman filters (EKF) to improve the computation efficiency while maintaining the accuracy of FD [10]. Aiming to achieve the H_2-optimal design of the residual generator, Zhang combined the parity space and H_2 frequency domain approaches, which is able to depict the frequency domain characteristics of the optimal solution generated by the parity space [15]. An example of qualitative model-based FD was given in [9], where the adopted qualitative bond graph (QBG) method was adopted as the modeling scheme to generate a set of qualitative equations used for monitoring faults. Some new developments of model-based FD focuses on dealing with various nonlinearities and uncertainties. Instead of the family of Luenberger-like observers, a type of observers with dynamics in the compensation term was designed to diagnose sensor faults for nonlinear Lipschitz systems and proved to generate optimal residuals, the parameters of which was solved with an LMI numerical method [11]. In [12], a novel FD filter design was provided with extension to a class of nonlinear uncertain systems, using the extended state observer (ESO) theory. In [13], fault detection filter design was explored for linear continuous-time systems with polytopic uncertainties, where the Kalman-Yakubovich-Popov (GKYP) lemma is helpful in dealing with the fault sensitivity performance index. Adaptive observers were also developed for both detection and evaluation regarding a type of singular nonlinear systems with the help of Lyapunov stability, reflecting the combined concerns of nonlinear system, model-based approach, and real-time realization [14].

Research using data-driven (or equivalently, historical knowledge based) FD started in mid-1980s and become prosperous since 1990s. Venkatasubramanian *et al.* classified data-driven FD into qualitative and quantitative approaches, which can be still divided in subclasses such as statistical feature extraction, neural networks, expert systems, and qualitative trend analysis (QTA) [5]. Statistical feature extraction have made the main stream of data-driven FD, under which techniques like principle component analysis (PCA), independent component analysis (ICA), and partial least squares (PLS) have been developed. PCA was applied to the detection and analysis of sensor faults via reconstruction [18], and recursive PCA was developed to adaptively update the fault monitoring [19], [20]. In [21], ICA was used for extracting statistically independent components from the observed data and combine them with process charts, which worked effectively on non-Gaussian faults. As an example of integrating different types of data-driven approaches, a neural network fault detector and an expert system fault isolator were concatenated in [16], forming the integration of not only two different artificial intelligence techniques but also the quantitative and qualitative data-driven FD approaches. New challenges, as claimed in [7], affect data-driven FD performance with the growing complexity of industrial systems and the usage of distributed control systems (DCS), such as nonlinearities, process uncertainties, coupled variables, etc. As a solution, Leung and Romagnoli managed to keep effective FD and FTC performance with the existence of DCS by proposing a three-layer FTCS structure, which applied multivariate statistical process control (MSPC) monitoring to knowledge based FD [17]. Based on such challenges, Wang *et al.* pointed out potential research directions of data-driven FD, including data-driven multi-scale plant-wide modeling and probabilistic density function (PDF) based FD [7].

Recently research has been carried out regarding the integrated FDI, although the development still stays at its primary stage. In many applications, a model can be built on data and signals, based on which modified estimation and identification methods traditionally applied to system models can be useful. For example, subspace based identification methods can be used together with state observers for process fault diagnosis [22]. Another example is that one can achieve comparable goal of spectrum analysis based on Fourier transform by using a signal model [54] and the nonlinear adaptive frequency estimator, an extension from model-based adaptive observer techniques. Sometimes one single technique may contain ideas from both model-based and data driven approaches. One type of structured partial PCA was presented in [26] with ideas borrowed from parity space for isolating sensor and actuator faults. All these approaches will be further investigated for the fault diagnosis problem, where the generated residual or its counterpart will be transformed with signal-based approaches like CUSUM and GLR [51], from which the quantized measures of diagnosis performance may be described as probabilistic distributions. Zhang and Jiang established an FTCS with integrated fault diagnosis and reconfigurable control, in which a two-stage Kalman filter was used for estimating states and fault parameters and then statistical hypothesis tests were developed on the collected information [24]. In [23], a large framework containing FD, hypothesis generation, parameter estimation, and hypothesis validation was proposed, integrating signed direct graph (SDG) based qualitative model and statistical testing (e.g. GLR), in order to deal with extreme cases involving parametric changes in the presence of sensor failures and controller or actuator malfunction. In fact, intrinsic links exist between data and model approaches, as is shown from tests with GLR and stochastic parity space [2], [46].

The sense of integrated FD is reflected not only in the combination of model-based and data-driven methods, but also in the coverage of various type of signals, e.g. deterministic and stochastic disturbances, resulting in a more applicable and robust FD/FTC plan. For example, Ma *et al.* introduced a complex fault isolation design integrating statistic testing and norm-based residual evaluation, following a fault detection filter (FDF) used as the model-based residual generator [25]. More research adaptable to various types of signal inputs is still expected, though; our research has developed under this consideration, which is explicated in Section 1.4.

FDI has plenty of useful applications on aerospace, mechanical systems, electric power systems, production lines, industrial (e.g. chemical) processes, etc. Pirmoradi *et al.* presented a robust scheme for FDI in spacecraft attitude determination (AD) sensors, where dynamics of the spacecraft and the measurement error were used for model-based state estimation and two EKFs were used for fault isolation [27]. Patton *et al.* provided a practical detection and isolation plan regarding faults affecting thrusters of a Mars Express (MEX) satellite system, whose FDI scheme relied on optimal robust disturbance decoupling observers (ORDDOs) [28]. One mostly concerned mechanical fault is rotating machinery vibration, against which model-based, data-driven, and even integrated FD have been researched [29], [30], [31]. Neural networks, as well as other intelligent techniques, has become the most frequently used tool in FDI of electric power systems or their individual components, which has led to a series of novel research results [32], [33], [34]. Wu presented an example of knowledge based FD of car assembly line based on modified support vector machine, where the optimal parameter was computed with the particle swarm optimization (PSO) [35]. As for chemical processes, plant-wide oscillations is the most common fault, without which a steadily running system is more profitable and safer [36]. Oscillations can not only keep the components from its optimal performance but also propagate to the neighbor components (and thus to the entire plant) via physical coupling, recycles, etc., [43], [44]. Thornhill *et al.* introduced the concept of integrated absolute deviation (IAE) between successive zero crossings (caused by the oscillation) of the time series, and a detection method is formed with predefined thresholds on IAE [41]. In [42], the distribution of the time between successive zero crossings of the auto-correlation function (ACF) was inspected, leading to the successful isolation of relevant stochastic performance indices of the oscillation. Jiang *et al.* explained the spectral envelope method, in which the maximum ratio of the power spectrum to the variance among various linear scaled data series was inspected along the frequency axis [37]. These methodologies diagnosing oscillations mentioned above respectively belong to the three main categories in [40], i.e. time-domain, ACF, and spectral methods, which cover both model-based and data-driven FD approaches.

1.3.2 Literature review with respect to specific research points

As introduced in Section 1.2.2, Chapter 2, 3, 4, and 5 have developed in-depth research on different case studies within the integrated FD framework. These case studies cover topics such as likelihood ratio test, covariance matrix, real-time estimation, (Semi-)Markov chain and reliability. Here we list literature reviews relevant to these topics and also the brief discussion on their relationship to the following chapters, in order to help readers comprehend the major points and the usage of our research.

Likelihood ratio test

In certain fault detection algorithms, including the cumulative sum (CUSUM) based, the generalized likelihood ratio (GLR) based, the exponentially weighted moving average (EWMA) based, and other likelihood ratio test based ones, detection of faults is achieved by testing a random residual signal obtained from the process or generated by a filter, which is usually subject to some significant change from the normal system operation to the faulty one. For example, the residual may manifest a stepwise signal changing from one constant level to another superimposed by white noises. In this case, the detection delay can generally be interpreted as the first hitting time (FHT) of a drifted random walk or Brownian motion generated by the recorded residual signal crossing some boundary(-ies), [51], [53]. Research results about the probabilistic properties of FHT are available, e.g. [74], [75], [76], just to name a few. In [53], by means of a continuous approximation of the CUSUM based detection, the probability distributions of (fault) detection delay (DD) and time between false alarms (TBFA) were obtained, which belong to a family of Lévy distributions. However, the results for the most commonly used likelihood-ratio test based detection methods such as the generalized likelihood ratio (GLR) test are not available. One of the motivations of this chapter is to extend the results developed in [53] to the GLR scheme.

In a fault tolerant control system (FTCS), a FD scheme serves as a crucial component. Jiang has surveyed and proposed systematic definition of FTC: in a typical active FTCS, the FD scheme determines the matching faulty situation upon detection; the reconfiguration function then reacts and switches in the best control strategy to keep the desirable closed-loop performance, [77]. In such a system, the FD performance has great impact on the performance of the FTCS. Hence characterization of FD schemes and their performances is important. Markov chains can be used to describe the behavior of fault events as well as the FD process, stated in recent research on stochastic fault tolerant control [60], [63], [61], [78]. Obviously when using Markov chains to describe the FD process, the exponential distribution of the sojourn time is only valid in a single step limit-checking based detection scheme, but will be restrictive for most FD schemes that involved sequential processing and testing of the residual signals. In this case, a semi-Markov chain is more suitable for describing the FD decision process because it allows for different specifications of the sojourn time distributions other than the exponential one, [79]. In the thesis, by analyzing different sequential test based FD schemes, such as GLR and CUSUM based, we can characterize the probability distributions of the fault detection delay and the time between false alarms, which are useful in constructing a semi-Markov FD process in the integrated fault tolerant control system. This chapter only focuses on the statistical characterization of FD, while the semi-Markov process description/constrution will be presented in Chapter 5.

Most online detection schemes operate in discrete-time. A typical detection process in a sequential hypothesis test involves forming a decision signal by taking summation of the residual signal consisting Gaussian i.i.d. noise samples upon time, which can be described by a discrete random walk. In this work, instead of treating the discrete random process directly, we approximate it by the corresponding continuous Brownian motion (i.e. Wiener process), for which more mature analysis tools are available, like [64]. Analytical probabilistic distribution expressions are derived for the CUSUM and GLR based schemes respectively, and are validated via Monte-Carlo simulations. Furthermore, we implement the CUSUM and GLR algorithms in a more realistic DC motor fault tolerant control system, originally seen in [53]. Monte-Carlo simulation results show that the analytical distribution expressions provide satisfactory approximations of the fault detection characteristics. Compared to most existing research work on FD analysis that is mainly focused on developing FD performance indices based on average rates or average run length (ARL), Chapter 2 reveals more detailed and precise statistical profiles of the relevant FD performance criteria. The results from this work are not only useful in design and analysis of intelligent FTCS but also helpful in FD alarms management and assessment, especially for large-scaled processes. For such processes, analysis of detection alarm signals is extremely important in order to reduce the number of nuisance alarm signals, and avoid unnecessary shut-downs, [80], [81].

Variance change detection

From the perspective of stochastic signal monitoring, each of the deterministic properties describing the distribution (mean, variance, skewness) can reflect faults, of which the past research majorally concentrates more on the fault affecting mean change. As a response to rising number of requirements, here we investigate the fault on the detection time and time between false alarms regarding variance change.

So far the cases in which most research work on variance change detection are based on the development of algorithms/mechanisms using covariance matrix. Caliskan posed and compared four algorithms on different performance indices concerning the covariance matrix of the Kalman filter innovation sequence, with the applications as aircraft sensor fault detection and flight control systems [101]. Hung defined a flag matrix determined by the covariance matrix and placed statistical hypothesis testing on certain elements/patterns of the flag matrix [102]. Chiang used sample covariance matrix from unfaulted data to establish a causal map used for fault detection [103]. Yu introduced a data-driven covariance benchmark, where generalized eigenvalue analysis are used for denoting the directions of better or worse control performance [104]. In contrast to these research achievements, we have one step forward to the quantitative description of probabilities/expectations related to FHT, which in this chapter describe detection delay (DD) and time between false alarms (TBFA).

Real-time estimation

The real-time (online) estimation of frequencies and amplitudes of sinusoidal signals is an important and classical problem, which has received much attention from the systems and controls community. In [84], a globally convergent frequency estimator was proposed based on adaptive notch filter design for a sinusoidal signal with single frequency. By using a state space realization of the sinusoidal signal, the frequency estimation problem can be converted to combined state and parameter estimation problem, a well-known yet challenging problem in controls. Adaptive observers based global frequency estimator was then developed, [85], [86]. By considering white noise and time-varying frequencies, a modified Kalman filter was designed for frequency estimation, [87]. A high gain observer has shown great improvement on state estimation for systems with modeling errors or external disturbances, in which the effect from such errors and disturbances can be effectively compressed within a bounded zone that can be narrowed by proper tuning of the design [57], [58]. Recently, the approach was extended to simultaneous reconstruction of multiple frequencies and amplitudes for a signal containing n unknown sinusoids, [54]. Sharma applied the nonlinear contraction to the convergence analysis of the frequency estimator [55]. It was claimed that the selection of the tuning parameters could be obtained analytically. Compared with conventional signal spectrum and time-frequency analysis methods, the adaptive-observer-based frequency estimation provides a promising alternative to deal with online real-time signal analysis, especially for signals with slowly time-varying frequencies. Some research results relevant to the topics of adaptive estimation and disturbance attenuation have appeared recently. Jia provides a disturbance observer incorporating adaptive parameter dynamics based on the least-mean-square (LMS) and recursive least square (RLS) methods [88]. In [89], [90], a modified robust adaptive Newton optimization method was adopted to accomplish frequency estimation on discrete sinusoids with white noise, where instant changes on frequencies are tolerant. In [91], another kind of direct frequency estimator using LMS was formed, dealing with discrete one-frequency sinusoids with white noise. Dash has pointed out one way of time-varying frequency estimation by means of a nonlinear adaptive complex unscented Kalman filter (CUKF) [56].

It is noticed that most current research results generally deal with sinusoids with white noise. In contrast, this chapter focuses on a type of signals with unknown but bounded disturbances, which are difficult to remove by pre-processing the signal. The benchmark research provided in [57] and [58], as well as the extended research in [69], proposed high-gain observer (HGO) based estimation for attenuating the low frequency disturbances so that the dominant frequency components can be isolated, while this scheme may result in a high-dimensional state space model and thus the computation of high-order derivatives of signal, restricting the applicability of this scheme. In Chapter 4, a linear parametric regression model of the signal based on the work of [92] is selected as the signal model instead. A causal filter with proper and stable transfer function is utilized to pre-process the signal such that more information on the frequencies can be gained. Based on the linear parametric model, the adaptive gradient estimator with leakage [92] is analyzed, modified, and adopted to generate frequency estimation in real-time. Due to the existence of the disturbance, the estimation error is inevitable but it is shown to be bounded. The bounds of the frequency estimation are derived, from which one can design the identifier to reduce the bound and enhance the estimation precision.

(Semi-)Markov chain and reliability

As results from Chapter 2, 3, 4, more types of faults become compatible with the FDI framework, and firm connections are established between the research and practical applications, such as frequency tracking, ARL/FAR, troubleshooting of component failure, and movement/speed control system. Long-term signal monitoring, however, is necessary in real industrial production, where multiple transitions between faulty and normal states may be possible. As a result, safe processes and system-level reliability now appear as crucial research topics, in which the Markovian properties and/or assumptions are the basis of theoretical deduction. The research results are mainly used for active fault tolerant control systems, where the real time fault-detection sequences may be important sources of the reconfiguration and even the controller re-design [62].

Abundant research materials like [52] systematically explicated Markov chain and its application on stochastic boundary crossing problems. A widely accepted benchmark of the research is describing the fault with time using a finite-state Markov chain and then modeling the system as a Markovian jump linear system (MJLS) [62]. Fang poses a thorough stability of analysis of continuous-time linear system with stochastic parameter faults, using Lyapunov stability and linear system knowledge [115]. Based on the work of [115], Tao uses Lyapunov and LMI tools to design robust controllers for FTCS under a typical discrete Markovian framework with assumptions for simplification applying [62], [63]. Comparatively, Semi-markov models are more complex and have less mature research, and their better mimic of actual stochastic fault behavior makes them of more research value. Zhao used a semi-Markov chain with sojourn time and renewal process to describe the sequence of fault events and help the FTC switch controllers at the right time [53]. In [114], Barbu pointed out the past research about semi-Markov models like [116], [117], [118] requires strong conditions beyond practical requirements, where a more general theoretic basis is posted with benchmark concepts like Discrete-time Markov Renewal Process (DMRP). Sufficient room for the research on semi-Markov processes still exists, pointing out the direction of Chapter 5.

1.4 Outline

Provided the introduction in Chapter 1, the rest chapters are organized with respect to specific research topics. In Chapter 2, a continuous approximation and characterization is developed for the detection probability of additive faults affecting mean. In Chapter 3, analytical bounds and industrial performance indices are calculated in discrete time domain for the detection probability of multiplicative faults affecting variance. Based on the application background and demands on real-time frequency estimation, a gradient estimator with leakage is proposed in Chapter 4 for sinusoids with perturbation, along with its FD applications to frequency shift and additive sinusoids. In Chapter 5, Semi-Markov models/kernels regarding long-term fault-detection relationship are discussed, and the relevant reliability performance index is also validated. The summary is given in Chapter 6.

Chapter 2

Detection of Additive Fault: Statistical Characterization I

2.1 Introduction

Chapter 2[1] introduces a continuous stochastic filter for characterizing the detection of abrupt mean change on Gaussian signals based on the General Likelihood Ratio (GLR) algorithm. Continuous approximations of GLR test are proposed in the form of Continuous Likelihood Ratio (CLR) test and Biased CLR (BCLR) test. Accordingly, a well-defined probabilistic performance index is given with the accuracy inspected from comparisons, where simulations are applied with both artificial data and motor FTCS to highlight its feasibility. Within the thesis scope, this chapter covers fault detection/isolation procedures, and the feasibility of controllers in the middle layer. The probabilistic performance index provides detailed quantitative information, which can be also used as live complement to the top-layer characterizing-learning mechanism.

The remainder of this chapter is organized as follows: problem definitions and background review are included in Section 2.2; the main results on the

[1] Originally published as:
[70] S. Yang, Q. Zhao, "Statistical characterization of the GLR based fault detection," *Proc. American Control Conference*, 2011, pp. 3778–3783.
[72] S. Yang, Q. Zhao, "Probability distribution characterisation of fault detection delays and false alarms," *IET Control Theory & Applications*, 6(7), 2012, pp. 953–962.

distributions of the delay and time between false alarms are presented for CLR and BCLR test based FD schemes in Section 2.3; in Section 2.4, the simulation study is presented. The results are validated thorough Monte-carlo simulations using idealized synthetic data first and then in a more realistic DC motor fault tolerant control system, where CUSUM and GLR based FD schemes are implemented; finally, conclusions are drawn in section 2.5.

2.2 Problem Formulation

2.2.1 Problem Formulation and Definitions

As a consensus introduced in [53], analysis of a Brownian motion (mathematically Wiener Process (w.p.)) is the key to the sequential hypotheses testing for FD, for which different bounds are proposed and the exit time is specially concerned for characterizing the detection time. The sequential hypotheses testing methods, including CUSUM and GLR, have a common definition form of the detection time as in (2.1), as disclosed in [53]: the detection time T_h is defined as the time instant for the decision signal $g(kT_s)$ (or $g(t)$ as the continuous-time counterpart) to hit the threshold $h(kT_s)$ (or $h(t)$) for the first time, i.e.

$$T_h = \begin{cases} \inf\{k \geq 1 : g(kT_s) \geq h(kT_s)\}, \text{ or} \\ \inf\{t > t_0 : g(t) \geq h(t)\}, \end{cases} \tag{2.1}$$

where T_s is the sample time and t_0 can be 0 for simplicity without loss of generality.

It should be noted that although the standard CUSUM and GLR algorithms are given in discrete-time forms since they treat the discrete-time data sequences, their continuous-time formulations are considered in this work so that the statistical characterization of the detection time can be performed based on the continuous-time random process. This is due to the fact that analytical results for continuous random processes are more mature compared to that for discrete-time random processes, especially for the FHT analysis. The detection time of CUSUM and GLR can generally be treated as the FHT at some boundary(-ies) concerning a drifted random walk (or Brownian motion as the continuous-time approximation) generated by taking full or partial summation (integration) S of the recorded residual signal data $y(kT_s)$ ($y(t)$) or the associated log-likelihood ratio, [51], [82], and abstract results are provided in [83]. A common and descriptive definition of FHT concerning CUSUM and GLR on a constant threshold h is:

$$T_h = \inf\{k \geq 1 : g(S(\Lambda(y)))(k) \geq h\} \tag{2.2}$$

Before any further discussion, it is necessary to clarify the assumptions made on the residual sequence $y(kT_s)$ and the bias fault F when applying the CUSUM or GLR scheme, which will be used throughout this chapter.

At first, the residual random process Y is assumed to be a Gaussian i.i.d. process, and the measured residual signal $y(kT_s)$ is a sample path of Y. The fault reflected in the residual is a constant bias F effective from $k_f T_s$, i.e.

$$Y(kT_s) \sim \left\{ \begin{array}{l} \mathcal{N}(0, \sigma^2 T_s), 1 \leq k < k_f \\ \mathcal{N}(F, \sigma^2 T_s), k \geq k_f \end{array} \right. . \tag{2.3}$$

For Gaussian random variables, the log-likelihood ratio $\Lambda(kT_s) \triangleq \Lambda(y(kT_s))$ becomes, [51]:

$$\Lambda(kT_s) = \ln \frac{f^{(F)}_{Y(kT_s)}(y(kT_s))}{f^{(0)}_{Y(kT_s)}(y(kT_s))} = \frac{F}{\sigma^2 T_s}\left(y(kT_s) - \frac{F}{2}\right). \tag{2.4}$$

where $f^{(\mu)}_{Y(kT_s)}(y(kT_s)) \triangleq \frac{1}{\sqrt{2\pi\sigma^2 T_s}} e^{-\frac{(y(kT_s)-\mu)^2}{2\sigma^2 T_s}}$, $\forall \mu \in \mathbb{R}$.

Since CUSUM and GLR take summation or partial summation of log-likelihood ratios to generate their decision functions, the properties of the (partial) summation should be discussed. The equations have shown that the log-likelihood ratio of Gaussian random variable (r.v.) keeps an affine form of the r.v. sample itself, so the (partial) summation of log-likelihood ratios also keeps an affine relationship with the (partial) summation of the Gaussian independent r.v. samples with the identical variance, which is a random walk (or Brownian motion in the continuous time domain). Hence, the boundary hitting problem of random walk/Brownian motions forms the foundation of CUSUM and GLR. The partial summation S_j^k on $(\Lambda(kT_s))$ has the form, [51]:

$$S_j^k(F) = \sum_{i=j}^{k} \Lambda(kT_s) = \frac{F}{\sigma^2 T_s} \sum_{i=j}^{k} \left(y(iT_s) - \frac{F}{2} \right). \tag{2.5}$$

Define $\nu = F/T_s$ as the scaled bias fault, then it is obtained that the random walk sequence $R(kT_s)$ ($W(kT_s)$ with variance normalized) generated by taking summation on Y, satisfies the following distributions:

$$R(kT_s) \triangleq \sum_{i=1}^{k} Y(iT_s) \sim \begin{cases} \mathcal{N}(0, \sigma^2 kT_s), \text{ when } k < k_f \\ \mathcal{N}(\nu(k - k_f + 1)T_s, \sigma^2 kT_s), \text{ when } k \geq k_f \end{cases} \tag{2.6}$$

$$W(kT_s) \triangleq \frac{1}{\sigma} R(kT_s) \sim \begin{cases} \mathcal{N}(0, kT_s), \text{ when } k < k_f \\ \mathcal{N}(\nu(k - k_f + 1)T_s/\sigma, kT_s), \text{ when } k \geq k_f \end{cases} \tag{2.7}$$

The continuous approximations ($R(t)$ and $W(t)$) should keep the same drift rates as the above discrete-time sequences, hence

$$R(t) \triangleq \int_0^t Y(\tau) d\tau \sim \begin{cases} \mathcal{N}(0, \sigma^2 t), \text{ when } t < t_f \\ \mathcal{N}(\nu(t - t_f), \sigma^2 t), \text{ when } t \geq t_f \end{cases} \tag{2.8}$$

$$W(t) \triangleq \frac{1}{\sigma} R(t) \sim \begin{cases} \mathcal{N}(0, t), \text{ when } t < t_f \\ \mathcal{N}(\nu(t - t_f)/\sigma, t), \text{ when } t \geq t_f \end{cases} \tag{2.9}$$

2.2.2 GLR

The generalized likelihood ratio (GLR) test is based on a double maximization algorithm, which has been commonly utilized as a detection standard. The decision signal is generated following the form defined in [51]:

$$g(kT_s) \triangleq \max_{1 \leq j \leq k} \sup_{F} S_j^k(F), \tag{2.10}$$

where $S_j^k(F)$ is the summation of log-likelihood ratio of the two classes (normal with mean 0 and faulty with mean F), given in (2.4) and (2.5). This algorithm can guarantee the detection of any unknown constant biases (faults).

As $F = \nu T_s$, (2.5) can be transformed into:

$$S_j^k(\nu) = \sum_{i=j}^{k} \frac{\nu}{\sigma^2}\left(y(iT_s) - \frac{\nu T_s}{2}\right). \tag{2.11}$$

Take partial derivative of S_j^k on ν to find a $\hat{\nu}$ maximizing S_j^k:

$$\frac{\partial S_j^k}{\partial \nu}(\hat{\nu}) = 0 \Rightarrow \sum_{i=j}^{k}\left(\frac{y(iT_s)}{\sigma^2}\right) - \frac{\hat{\nu}T_s}{\sigma^2}(k-j+1) = 0$$

$$\Rightarrow \quad \hat{\nu} \triangleq \arg\sup_{\nu} S_j^k(\nu) = \frac{1}{(k-j+1)T_s}\sum_{i=j}^{k} y(iT_s). \tag{2.12}$$

Substitute (2.12) into (2.11):

$$\begin{aligned}
\sup_{\nu} S_j^k(\nu) &= S_j^k(\hat{\nu}) = \frac{1}{2\sigma^2}\sum_{j}^{k}\left(2\hat{\nu}y(iT_s) - \hat{\nu}^2 T_s\right) \\
&= \frac{1}{2\sigma^2}\left[2\hat{\nu}\sum_{j}^{k}(y(iT_s)) - (k-j+1)T_s\hat{\nu}^2\right] \\
&= \frac{1}{2\sigma^2}\left[\frac{2}{(k-j+1)T_s}\left(\sum_{i=j}^{k} y(iT_s)\right)^2 - \frac{(k-j+1)T_s}{(k-j+1)^2 T_s^2}\left(\sum_{i=j}^{k} y(iT_s)\right)^2\right] \\
&= \frac{1}{2\sigma^2}\cdot\frac{1}{(k-j+1)T_s}\left(\sum_{i=j}^{k} y(iT_s)\right)^2.
\end{aligned}$$

Hence, the form of GLR decision function is given as follows:

$$g(kT_s) = \frac{1}{2\sigma^2}\max_{1\le j\le k}\frac{1}{(k-j+1)T_s}\left[\sum_{i=j}^{k} y(iT_s)\right]^2, \tag{2.13}$$

the above decision function has a slightly different form by including the effects of sampling time, which is comparable with the original version in [51]. It is used in the simulation part (Section 2.4) in the GLR algorithm.

2.3 Continuous Likelihood Ratio (CLR)-based detection

Here we firstly present the extension of GLR detection reviewed in Section 2.2.2 to the continuous-time domain, the so-called continuous Likelihood Ratio

(CLR). We assume that the residual $Y(t)$ is a zero-mean Gaussian white noise with the variance σ^2 before the fault happens, and the fault changes its mean to a non-zero unknown value ν in a step manner, i.e.

$$Y(t) \sim \begin{cases} N(0,\sigma^2), & \text{when } t < t_f \\ N(\nu,\sigma^2), & \text{when } t \geq t_f, \end{cases} \tag{2.14}$$

where t_f denotes the time instant when the fault starts to affect the signal. For simplicity, only $\nu > 0$ is considered.

Use $y(t)$ to denote the recorded sample path of $Y(t)$. Due to its Gaussian property, the likelihood ratio at time t is

$$\begin{aligned} \Lambda(t) &= \ln \frac{f_{Y(t)}^{(\nu)}(y(t))}{f_{Y(t)}^{(0)}(y(t))} = \frac{\nu}{\sigma^2}\left(y(t) - \frac{\nu}{2}\right). \\ \text{where} \quad f_{Y(t)}^{(\mu)}(y(t)) &\triangleq \frac{1}{\sqrt{2\pi\sigma^2}} e^{-\frac{(y(t)-\mu)^2}{2\sigma^2}}, \quad \forall \mu \in \mathbb{R}. \end{aligned} \tag{2.15}$$

Define the cumulative integral of likelihood ratio from t_j to t_k:

$$S_{t_j}^{t_k} = \int_{t_j}^{t_k} \Lambda(\tau) d\tau = \frac{\nu}{\sigma^2} \int_{t_j}^{t_k} \left(y(\tau) - \frac{\nu}{2}\right) d\tau. \tag{2.16}$$

Note that ν is unknown, and one solution is to find an estimate $\hat{\nu}$, which generates maximum likelihood for each t_k. Following a similar idea of the double maximization in a discrete GLR regarding both ν and t_j, we may define the decision function $g(t)$ at $\forall t > t_0$:

$$g(t) = \sup_{t_0 < t_j < t} \sup_{\nu > 0} S_{t_j}^t = \sup_{t_0 < t_j < t} \sup_{\nu > 0} \int_{t_j}^{t} \left(\frac{\nu y(\tau)}{\sigma^2} - \frac{\nu^2}{2\sigma^2}\right) d\tau. \tag{2.17}$$

Select a $h > 0$ as the threshold of FD. When $g(t) \geq h$, it generates the alarm.

However the complex form of $g(t)$ limits further analysis of the detection performance. We start by simplifying $g(t)$. Note that the detection standard is equivalent to the proposition: for a fixed t, $\exists t_j \in (t_0, t)$, s.t. $\sup_\nu S_{t_j}^t \geq h$.

It can be transformed as the follows [51]:

$$
\begin{aligned}
\sup_{\nu} S_{t_j}^t \quad \geq \quad h &\Leftrightarrow \sup_{\nu} \left\{ \int_{t_j}^t \left(\frac{y(\tau)}{\sigma} - \frac{\nu}{2\sigma} \right) d\tau - \frac{h\sigma}{\nu} \right\} \geq 0 \\
&\Leftrightarrow \quad \frac{1}{\sigma} \int_{t_j}^t y(\tau) d\tau \geq \inf_{\nu} \left\{ \frac{\nu}{2\sigma}(t - t_j) + \frac{h\sigma}{\nu} \right\} \\
&\Leftrightarrow \quad \frac{1}{\sigma} \int_{t_j}^t y(\tau) d\tau \geq \sqrt{2h(t - t_j)}. \qquad (2.18)
\end{aligned}
$$

Note that the left-hand side of (2.18) defined as

$$
w(t) = \frac{1}{\sigma} \int_{t_j}^t y(\tau) d\tau \qquad (2.19)
$$

is a sample path of a Wiener process $W(t)$ formed by taking the integration of $y(t)$, which starts at t_j and satisfies

$$
W(t) \sim \begin{cases} N(0, t - t_j), \text{ when } t < t_j \\ N(\nu(t - t_j)/\sigma, (t - t_j)), \text{ when } t \geq t_j \end{cases} \qquad (2.20)
$$

The right-hand side of (2.18) is square root function of $(t - t_j)$. Obviously, (2.18) demonstrates a moving window detection method, with the convex of the square root boundary moving along with the wiener process sample path w.

Remark 1 *In (2.18), the superior bound caused by the drift rate ν is removed via optimization. For simplicity we may remove the superior bound caused by t_j, the starting time of Wiener process. As our goal is to analyze the DD and TBFA, the duration between the fault occurrence time t_f and the current time of detection t is of the main interests. For this purpose, we assume that t_j is fixed but not moving along the time axis. Hence, the above CLR based test involves a fixed square root boundary and it is mainly used for analysis purpose instead of implementation. In fact, if implemented, the CLR will not be as sensitive as the original GLR.*

In [59] and [64], the results on the probability of FHT concerning a zero-mean Wiener process and a monotonically non-increasing linear boundary were given. Furthermore the results have been extended to any monotonically non-increasing concave boundary $b(t)$ differentiable on (t_0, ∞) satisfying $b(t_0^+) \geq 0$. Specifically the following equation was given as an upper bound of the probability due to the concavity, [64]:

$$\Pr(t_0 < T_h < t) \leq \int_{t_0}^{t} \frac{b(\tau) - \tau b'(\tau)}{\sqrt{2\pi\tau^3}} e^{-\frac{b^2(\tau)}{2\tau}} d\tau, \text{ if } b'(\tau) \leq 0 \tag{2.21}$$

In fact (2.21) is applicable to all the concave boundaries $b(t)$ satisfying $b(t_0^+) \geq 0$. As a result, it can be applied to analyze the distribution of the FHT of the prosed CLR standard. At first we concentrate on the distribution of the detection delay. Fix $t_f = 0$ for simplicity, and treat it as the start time of CLR detection. Hence the boundary $b(t)$ in (2.18) becomes,

$$b(t) = \sqrt{2ht}. \tag{2.22}$$

By adding a term of $-\nu t/\sigma$ to both $w(t)$ and the boundary, the CLR detection problem can be transformed into an equivalent problem, i.e. the detection of the zero-mean normalized Wiener process $w_0(t) \sim N(0, t)$ hitting the bound

$$b_0(t) = \sqrt{2ht} - \frac{\nu}{\sigma} t. \tag{2.23}$$

Note that both $b(t)$ and $b_0(t)$ are concave, implying that (2.21) can be used for computing the FHT distribution for $w(t)$ to cross $b(t)$ and $b_0(t)$.

Following the discussion above, we can derive an upper bound of the probability of detection delay T_d from $t_0 > 0$ to t based on the results for FTH of Wiener process sample path w_0 hitting the boundary b_0. As $w_0(0) = 0$ and $b_0(0) = 0$ imply the trivial case of "initial hitting" rather than the FHT mentioned above, we assume $t_0 > 0$. Similarly, the false alarm is the case when $w(t)$ hits the bound $b(t)$ at some $t > t_f = 0$ with $\nu = 0$ (no fault). The probability distribution of the time between false alarms is also obtained. The results for FDD and TBFA are shown in the following theorem.

Theorem 2 *For the CLR test described in Remark 1, the probability that the detection delay T_d takes a value in $(t_0,\ t)$ is bounded and the upper bound is given in (2.24); the probability that the time between false alarms T_{fa} takes a value in $(t_0,\ t)$ is bounded and the upper bound is given in (2.25):*

$$\begin{aligned}
\mathrm{Pr}_d^{\mathrm{CLR}}(t_0 < T_d < t) &\leq \int_{t_0}^{t} \frac{b_0(\tau) - \tau b_0'(\tau)}{\sqrt{2\pi\tau^3}} e^{-\frac{b_0^2(\tau)}{2\tau}} d\tau \\
&= \int_{t_0}^{t} \frac{\sqrt{h}}{2\sqrt{\pi\tau}} e^{-h + \frac{\sqrt{2h}\nu}{\sigma}\sqrt{\tau} - \frac{\nu^2\tau}{2\sigma^2}} d\tau \qquad (2.24) \\
\mathrm{Pr}_f^{\mathrm{CLR}}(t_0 < T_{fa} < t) &\leq \int_{t_0}^{t} \frac{\sqrt{h}}{2\sqrt{\pi\tau}} e^{-h} d\tau = \frac{\sqrt{h}}{2\sqrt{\pi}} e^{-h} (\ln t - \ln t_0). \qquad (2.25)
\end{aligned}$$

The proof is obvious from the above discussion and by directly substitution of (2.22) into (2.21). The two expressions give detailed and quantitative description of the possibility of detection up to any time instant; besides CD-F, the mathematical indices of the distribution such as expectation, peak, and skewness are helpful in summarizing quantitative industrial performance indices regarding process (component) fault monitoring.

It is noticed that when t_0 is small, the probability bound tends to increase dramatically. In addition, CLR may provide an over-tightened boundary (low threshold value) especially during the earliest period of time, so that a detection at the beginning is mostly a false alarm. To improve CLR, we introduce a constant bias $\beta > 0$ to the original CLR bound, leading to the so-called biased CLR (BCLR). Under the BCLR test, the boundary becomes

$$b(t) = \sqrt{2ht} + \beta, b_0(t) = \sqrt{2ht} - \frac{\nu}{\sigma}t + \beta, \qquad (2.26)$$

based on which we may describe the distribution following the derivation of (2.24) and (2.25). The results are shown in the following corollary.

Corollary 3 *For the BCLR test with a boundary in (34), the probability that the detection delay T_d takes a value in $(t_0,\ t)$ satisfies an upper bound given* *in (2.27); the probability that the time between false alarms T_{fa} takes a value in $(t_0,\ t)$ satisfies an upper bound given in (2.28):*

$$
\begin{aligned}
\mathrm{Pr}_d^{\mathrm{BCLR}}(t_0 < T_h < t) &\leq \int_{t_0}^{t} \frac{\sqrt{2}\beta + \sqrt{h\tau}}{2\sqrt{\pi\tau^3}} e^{-\frac{(\sqrt{2h\tau}-\frac{\nu}{\sigma}\tau+\beta)^2}{2\tau}} d\tau, \quad (2.27)\\
\mathrm{Pr}_f^{\mathrm{BCLR}}(t_0 < T_h < t) &\leq \int_{t_0}^{t} \frac{\sqrt{2}\beta + \sqrt{h\tau}}{2\sqrt{\pi\tau^3}} e^{-\frac{(\sqrt{2h\tau}+\beta)^2}{2\tau}} d\tau. \quad (2.28)
\end{aligned}
$$

Obviously the problem of infinity bound in (2.24) and (2.25) as $t_0 \to 0$ is solved in (2.27) and (2.28).

Remark 4 *The above results may apply to a more general case that the additive fault is not constant bias but time-varying. The proposed CLR and BCLR can still be used for analyzing the FDD and TBFA, with necessary modification: Define a Gaussian noise $Y(t)$ with time-varying fault $\nu(t)$ after the starting time t_f:*

$$
Y(t) \sim \begin{cases} N(0, \sigma^2), & \textit{when } t < t_f \\ N(\nu(t), \sigma^2), & \textit{when } t \geq t_f, \end{cases} \quad (2.29)
$$

The detection can be treated as a boundary crossing problem between a Wiener process $W(t)$ satisfying

$$
W(t) \sim N\left(\frac{1}{\sigma}\int_{t_j}^{t} \nu(\tau)d\tau,\ t\right), \ \textit{when } t \geq 0 \quad (2.30)
$$

and a bound $b(t)$ as in (2.22), where $t_f = 0$ for simplicity. Equivalently, it is converted to a boundary crossing problem concerning the corresponding detrended Wiener process $W_0(t)$ and a drifted bound $b_0(t)$ satisfying

$$
b_0(t) = \sqrt{2ht} - \frac{1}{\sigma}\int_{0}^{t} \nu(\tau)d\tau. \quad (2.31)
$$

Theorem 2 and Corollary 3 can be readily modified by substituting in (2.31) for the corresponding b_0, as long as $b_0(t)$ is still concave and $b(0^+) \geq 0$.

Another way of treating time-vary faults is by using the known bounds, i.e. $\nu(t) \in [\nu_{\min}, \nu_{\max}]$. *Based on (2.31), we have*

$$b_{\nu_{\max}}(t) \triangleq \sqrt{2ht} - \frac{\nu_{\max}}{\sigma}t \leq b_0(t) \leq \sqrt{2ht} - \frac{\nu_{\min}}{\sigma}t \triangleq b_{\nu_{\min}}(t). \tag{2.32}$$

As a result, the corresponding bounds of the detection delay probabilities in Theorem 2 and Corollary 3 can be formulated as

$$\begin{aligned} Pr_d^{\mathrm{CLR}}(t_0 < T_d < t) &\leq \int_{t_0}^{t} \frac{b_{\nu_{\max}}(\tau) - \tau b'_{\nu_{\max}}(\tau)}{\sqrt{2\pi\tau^3}} e^{-\frac{b^2_{\nu_{\max}}(\tau)}{2\tau}} d\tau \\ &= \int_{t_0}^{t} \frac{\sqrt{h}}{2\sqrt{\pi\tau}} e^{-h+\frac{\sqrt{2h}\nu_{\max}}{\sigma}\sqrt{\tau}-\frac{\nu^2_{\max}\tau}{2\sigma^2}} d\tau, \end{aligned} \tag{2.33}$$

$$Pr_d^{\mathrm{BCLR}}(t_0 < T_d < t) \leq \int_{t_0}^{t} \frac{\sqrt{2}\beta + \sqrt{h\tau}}{2\sqrt{\pi\tau^3}} e^{-\frac{(\sqrt{2h\tau}-\frac{\nu_{\max}}{\sigma}\tau+\beta)^2}{2\tau}} d\tau, \tag{2.34}$$

2.4 Simulation

Simulations are firstly carried out on synthetic data for: 1) validation of the probabilistic properties of CLR and BCLR as in (2.24) and (2.27), and 2) comparison between the proposed CLR and the GLR tests in the analysis. Then simulations are performed on a DC-motor control system to further demonstrate the feasibility of the analytical results developed in this work. Monte-Carlo simulations are performed in all these cases.

2.4.1 Artificial Data

Validation of CLR & BCLR distribution

Here we carry out simulations to validate the theoretical expression regarding the CLR and BCLR tests. Both fault detection (fault $\nu \neq 0$ occurs at $t = 0$) and false alarm cases are discussed, where the PDF of FHT and the normalized experimental histogram (50 divisions) are compared. Random walk samples are used to approximate Wiener processes, where the sampling interval $T_s =$ 0.2s. The residual signal without fault is white Gaussian noise $Y(kT_s) \sim N(0, \sigma)$, and the fault bias is νT_s, yielding the normalized un-drifted random walk $W_0(kT_s) \sim N(0, kT_s)$ and the drifted one $W(kT_s) \sim N(\nu kT_s/\sigma, kT_s)$. FHT is tested with 10,000 randomly generated Gaussian random walk samples with the same distribution, so that the histogram tends to the real distribution.

Select the parameters for the Wiener process $W(t)$ as $\nu = 0.5$, $\sigma = 1$. Select the threshold as $h = 2$, and the drift rate $\nu = 0.5$ for the real detection case with fault, and the bias $\beta = 5$ for BCLR. Simulate both the detection and false alarm test respectively with given 10,000 random walk samples, resulting in Fig. 2.1(a) for CLR and 2.1(b) for BCLR. The time length of observation is set to 150s.

Fig. 2.1(a) shows that the distributions of experimental FHT match the analytical PDF profile well, hence (2.24) and (2.25) are validated. Fig. 2.1(b) shows how the distributions of experimental FHT matches the analytical PDF obtained from (2.27) and (2.28) in both fault detection and false alarm cases. It is also noticed that the CLR has a relative higher false alarm rate compared to BCLR.

Comparison between GLR and CLR

It is desirable to validate the feasibility and accuracy of the CLR algorithm by comparing it with a standard GLR test given in [51]. Select the parameters as $\sigma^2 = 0.09$, $h = 6$, $\nu = 0.5$, and the time of fault occurrence $t_f = 0$. Fig. 2.2 shows the result of the Monte-Carlo simulation. The normalized histogram of 10000 experiments respectively for GLR and CLR and provided, and the PDF expression for CLR as in (2.24) are plotted for comparison. In Fig. 2.2, the CLR experiment matches the PDF expression quite well. The GLR detection presents faster detection than CLR, confirming our speculation as in Remark 1; i.e. CLR is not as sensitive as GLR.

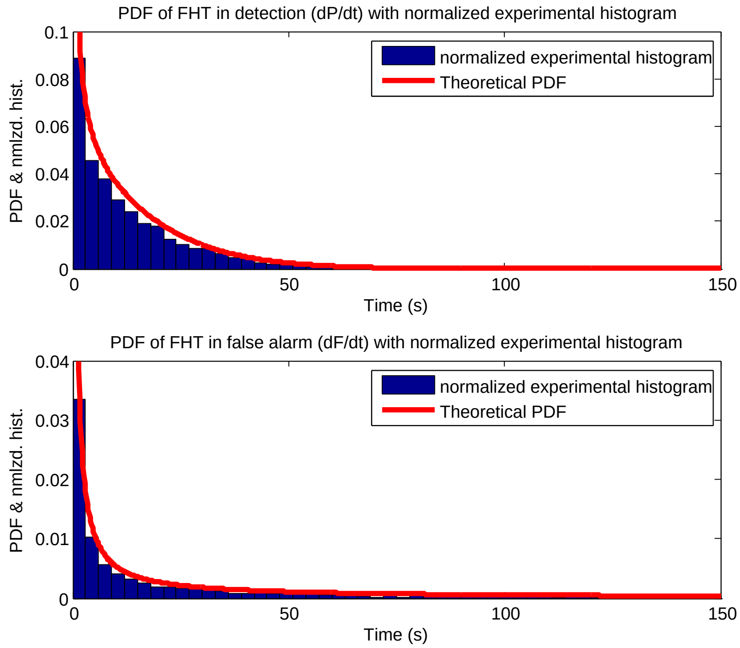

(a) CLR

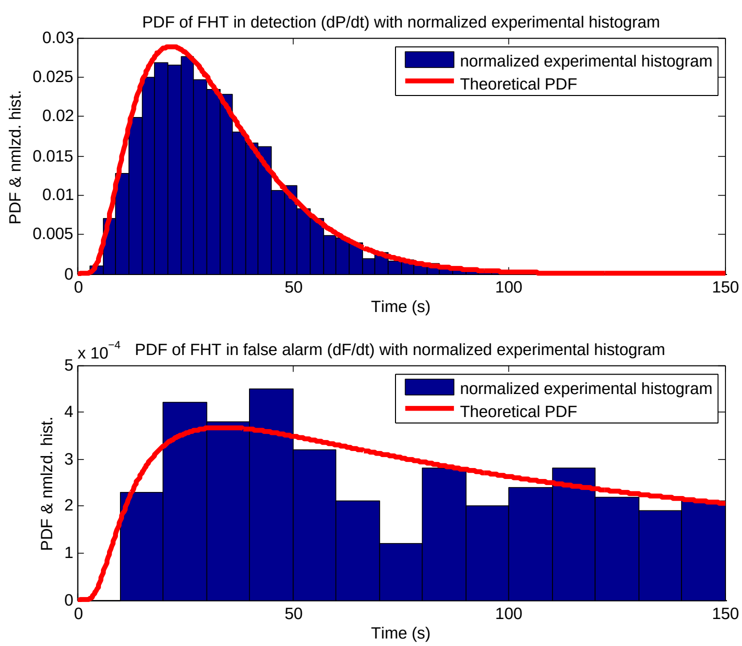

(b) BCLR

Figure 2.1: PDF of FHT in detection (upper) and false alarming (bottom) with normalized experimental histograms.

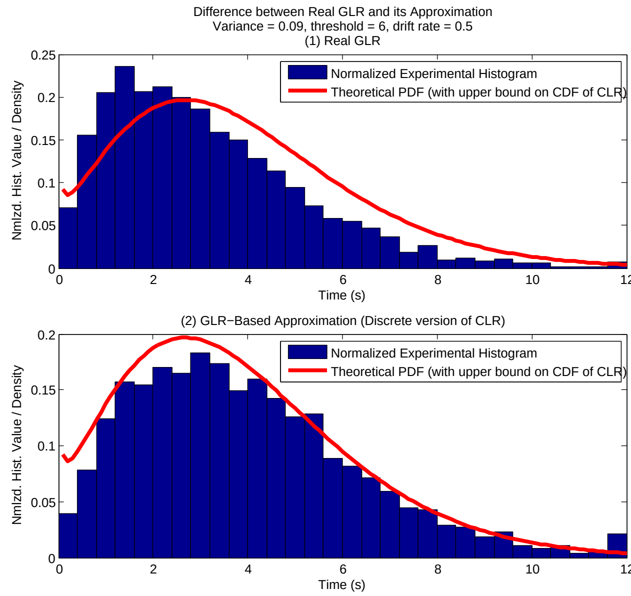

Figure 2.2: Comparison between GLR and CLR

2.4.2 DC Motor Fault Tolerant Control System

Simulations are carried out on a DC-motor system originally seen in [53]. Fig. 2.3 gives the interconnection structure. We hereby succeed relevant concepts and principles from [53] for our experiments:

- Only the speed sensor is subject to fault and noise, regardless that both the speed and position information are acquired from sensors. Faults only occur as step jumps on the speed sensor.

- The auto-switching mechanism based on the FD result and the soft-sensor technique is the kernel of the control: in the normal state the FTCS passes back the real speed measurement, which is subject to be replaced with the speed estimation from the Kalman filter once a fault is detected.

Comparison between GLR and CLR

Here we implement the GLR algorithm in the motor system. The minimum magnitude of detection is selected as zero, indicating that any constant bias

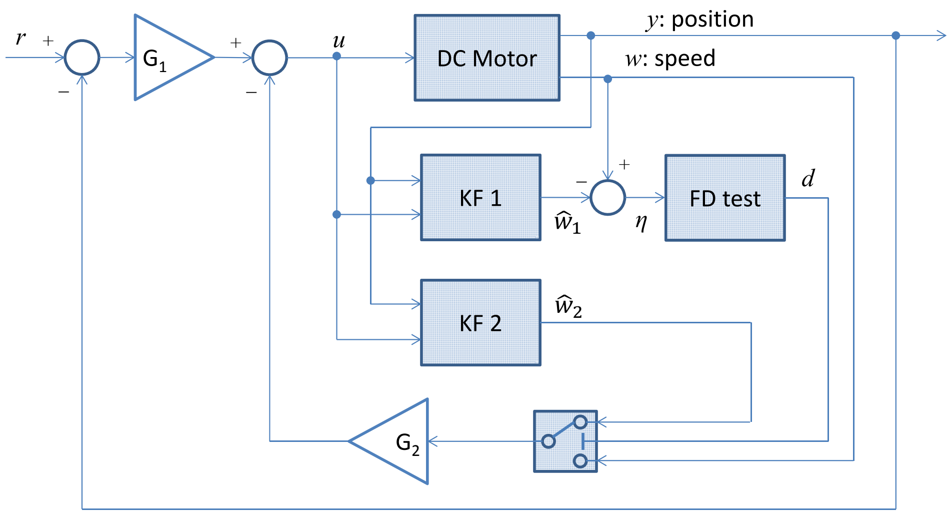

Figure 2.3: Structure of Motor FTCS [53]

in mean will be detected with enough time given. Select the parameters as follows: the variance of Gaussian noise $\sigma^2 = 0.09$, and the threshold $h = 100$. The magnitude speed sensor bias (fault) is selected as $\nu T_s = 10T_s$, so that the average increasing rate (slope) of the cumulative random walk is $\nu = 10$ per second after the fault occurrence time. Fig. 2.4 describes a one-time GLR detection of the motor's speed sensor bias under the parameter set, where the decision function $g(kT_s) = w - \hat{w}_1$ and threshold h are provided.

Likewise, we carry out Monte-Carlo simulations of GLR on the motor system model and compare the results with the theoretical result of CLR as in (2.24). The tests are repeated for 250 times to get a distribution on histogram, and sample time $T_s = 0.002$s. The concepts of real FHT and observed FHT are used. Real FHT means the actual detection time from the fault occurrence to the detection. Observed FHT means the time duration between the time jT_s and the detection time, where the time index j maximizes the decision function, i.e. satisfies $g(kTs) = \max_{1\leq j\leq k} \sup_{\nu>0} S_j^k$ [51]. Fig. 2.5 presents the comparison results. Although Remark 1 and Fig. 2.2 indicate the real GLR detection is more sensitive than CLR, Fig. 2.5 shows a better match, implying

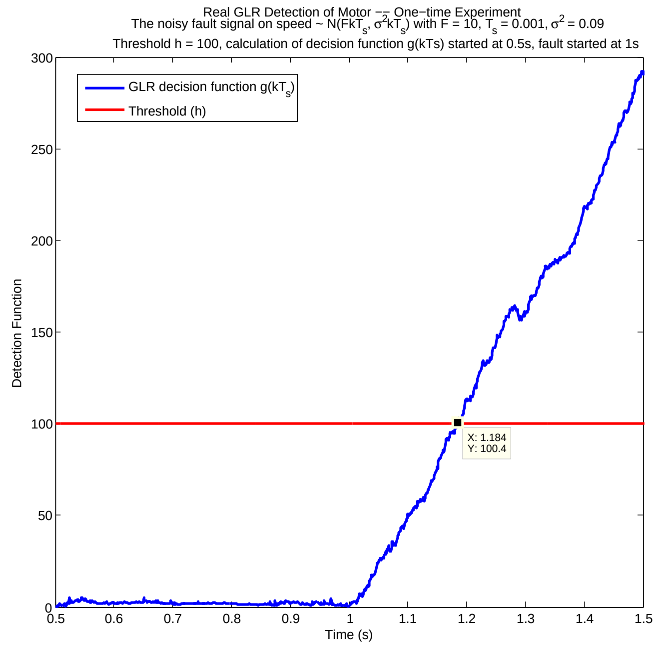

Figure 2.4: One-time GLR detection of the motor's speed sensor bias, sample time $T_s = 0.001$s, FHT (detection delay) $= 0.184$s

the feasibility and accuracy of CLR.

Finally, we can demonstrate that the derived PDF expressions can be used to help select certain user-defined parameters in the detection schemes. For example, for the proposed CLR/BCLR, user-defined parameters include the threshold h and the BCLR tolerance β. Fig. 2.6 shows a plot of FDD expectation with respect to different threshold h and tolerance β values, based on which one can select the values of h and β for desirable mean FDD values. The FHT (expectation) shows an approximately positive linear relationship with respect to h or β, implying that higher threshold (or bias) may result in later detection.

2.5 Conclusion

The chapter has provided methods of approximating discrete FD tests in the continuous time domain and characterized analytical expressions about the probabilistic distribution of FHT based on several FD schemes in continuous

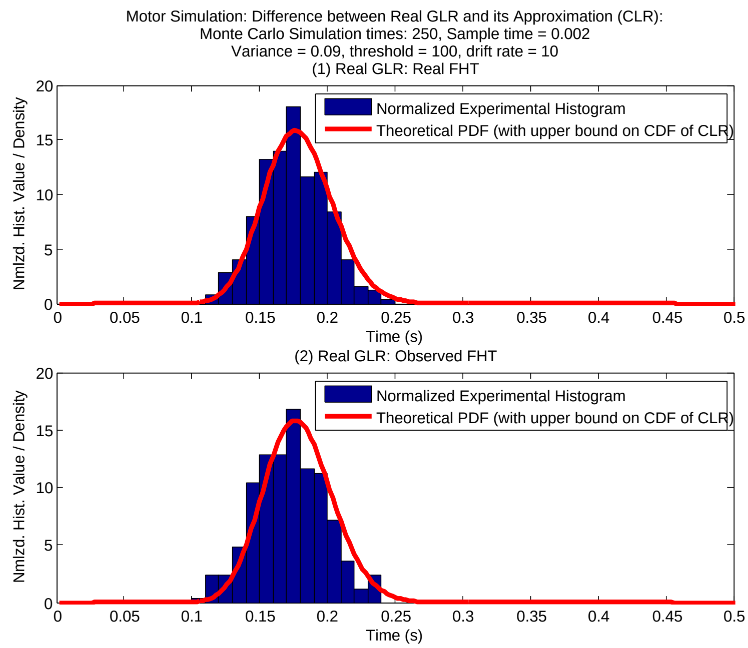

Figure 2.5: Comparison of CLR and motor-based results of GLR, sample time $T_s = 0.002$s

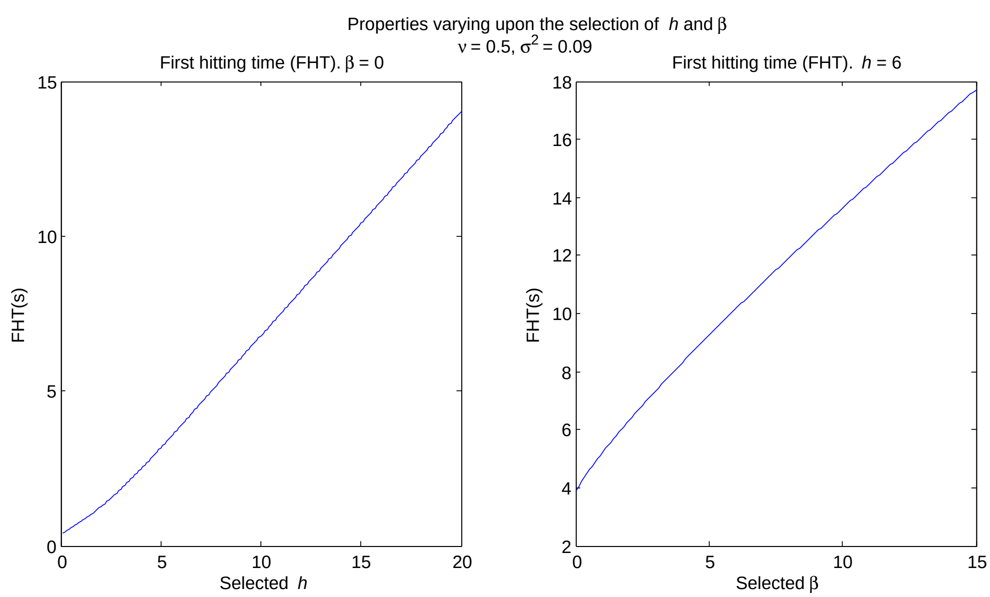

Figure 2.6: Expectation of detection delays (CLR/BCLR) with different parameters h and β

time domain. The proposed CLR and BCLR standards have been established to approximate and simplify the GLR tests. All the analytical expressions has been validated by Monte-Carlo simulations. It is also shown that BCLR has much less false alarm rate despite the longer detection delay on average compared with CLR.

Chapter 3

Detection of Multiplicative Fault: Statistical Characterization II

3.1 Introduction

Chapter 3 is committed to the analysis of multiplicative fault affecting variance on Gaussian signals. The step change on variance is considered here, equivalently the multiplicative fault on white Gaussian signals. Fault detection probability is defined based on a simplified version of GLR; the analytical form of two lower bounds are provided based on two ways of simplification. Like in Chapter 2, both detection time and time between false alarms are considered. The impact of different parameters on probability are investigated and compared. Besides the detailed probabilities, well-accepted industrial performance indices are discussed. Within the thesis scope, the chapter highlights the fault detection on fault affecting variance, multiplicative fault on noise, with the FD performance evaluation for industrial implementation.

The structure of this chapter is as follows. Section 3.2 proposes the background review on the hypothesis testing for the variance change and the log-likelihood ratio (LLR). Section 3.3 gives the sequential probability ratio test (SPRT) for multiplicative fault affecting variance including the decision function. Section 3.4 gives the approximations of usual performance indices used in industries, concerning the detection delay (DD) and the time between false alarms (TBFA). On the other hand, Section 3.5 calculates two lower bounds of the mass probabilities of FHT, also covering DD and TBFA. Section 3.6 provides simulation result concerning a scenario of DC-motor sensor gain. The conclusion section comes at last as Section 3.7.

3.2 Log-likelihood Ratio: Step Change on Variance

Consider an i.i.d. random process $\{Y\}$ with mean μ and variance σ^2. Here we discuss the hypothesis test with

$$\begin{cases} \mathcal{H}_0 : \theta_0 = \sigma_0, \\ \mathcal{H}_1 : \theta_1 = \sigma_1. \end{cases}$$

which is for the detection of step change on variance.

Assume all the elements in $\{Y\}$ are with one identical normal distribution in each, i.e. $\forall i \in N, Y(i) \sim \mathcal{N}(\mu, \sigma^2)$, $\sigma = \sigma_0$ without fault, and $\sigma = \sigma_1$ with fault. Then the probabilistic density functions under the two hypotheses are:

$$\begin{cases} \mathcal{H}_0 : p_{\sigma_0}(y(i)) = \frac{1}{\sqrt{2\pi\sigma_0^2}} e^{-\frac{(y(i)-\mu)^2}{2\sigma_0^2}}, \\ \mathcal{H}_1 : p_{\sigma_1}(y(i)) = \frac{1}{\sqrt{2\pi\sigma_1^2}} e^{-\frac{(y(i)-\mu)^2}{2\sigma_1^2}}. \end{cases}$$

The log-likelihood ratio (LLR) of each sample $y(i)$ and its partial sum can be thus transformed into the following forms, [51]:

$$s(i) \triangleq s(y(i)) \triangleq \ln \frac{p_{\sigma_1}(y(i))}{p_{\sigma_0}(y(i))} = -(\ln \sigma_1 - \ln \sigma_0) + \left(\frac{1}{2\sigma_0^2} - \frac{1}{2\sigma_1^2} \right) (y(i) - \mu)^2, \quad (3.1)$$

$$S(\mathcal{Y}_j^k) \triangleq \sum_{i=j}^{k} s(y(i)) = -(\ln \sigma_1 - \ln \sigma_0)(k - j + 1) + \left(\frac{1}{2\sigma_0^2} - \frac{1}{2\sigma_1^2} \right) \sum_{i=j}^{k} (y(i) - \mu)^2, \quad (3.2)$$

where $\mathcal{Y}_j^k \triangleq \{y_i : j \leq i \leq k\}$ is a partial set of the samples of the faulted Gaussian random process Y. Unlike the case of change on mean, the definition of LLR in (3.2) is no longer normally distributed due to the appearance of the second order term. It is common knowledge, as in [106], that the summation of square of standard normal i.i.d. variables is with χ^2 distribution, i.e. $\sum_{i=j}^{k}\left(\frac{Y(i)-\mu}{\sigma}\right)^2 \sim \chi^2(k-j+1)$. Our main research results are based on the χ^2 and Γ properties of the probabilistic distribution.

Here we briefly show the detectability of the variance step-change problem with the theoretical support from [51], [106], [107]. For simplicity and without loss of generosity, it is assumed $0 < \sigma_0 < \sigma_1$. According to [106] and [107],

$$Y(i) - \mu \sim \begin{cases} \Gamma\left(\frac{1}{2},\ 2\sigma_0^2\right), \text{ without fault,} \\ \Gamma\left(\frac{1}{2},\ 2\sigma_1^2\right), \text{ with fault.} \end{cases} \tag{3.3}$$

with the mean (expectation)

$$\mathrm{E}\left(Y(i) - \mu\right) = \begin{cases} \sigma_0^2, \text{ without fault,} \\ \sigma_1^2, \text{ with fault.} \end{cases} \tag{3.4}$$

Besides, the inequalities of natural logarithms are also provided in [107]:

$$\frac{x-1}{x} \le \ln x \le x - 1,\ \forall x > 0. \tag{3.5}$$

The inequality (3.5) helps to distinguish the faulty and unfaulty cases in the sense of the expectation of LLR. When no fault exists,

$$\mathrm{E}_{\sigma_0}\left(s(i)\right) = \frac{1}{2}\left(-\ln\frac{\sigma_1^2}{\sigma_0^2} + 1 - \frac{\sigma_0^2}{\sigma_1^2}\right) \le \frac{1}{2}\left(-\frac{\sigma_1^2}{\sigma_0^2} + \frac{\sigma_0^2}{\sigma_1^2} + 1 - \frac{\sigma_1^2}{\sigma_0^2}\right) = \frac{1}{2}\left(1 - \frac{\sigma_1^2}{\sigma_0^2}\right) < 0, \tag{3.6}$$

as $\sigma_0 < \sigma_1$. On the other hand, after the fault occurrence,

$$\mathrm{E}_{\sigma_1}\left(s(i)\right) = \frac{1}{2}\left(-\ln\frac{\sigma_1^2}{\sigma_0^2} + \frac{\sigma_1^2}{\sigma_0^2} - 1\right) \ge \frac{1}{2}\left(-\frac{\sigma_1^2}{\sigma_0^2} + \frac{\sigma_1^2}{\sigma_0^2}\right) = 0, \tag{3.7}$$

where the equality only applies when $\sigma_1^2 = \sigma_0^2$, i.e., no fault state is defined other than the normal state. It shows clearly from (3.6) and (3.7) that $\mathrm{E}\left(S\left(\mathcal{Y}_j^k\right)\right)$ will have a downward trend with no fault and an upward trend with fault. Hence, the step change of variance can be detected.

Here a more rigorous proof of the detectability is provided referring to [51]. (3.2) implies that the partial sum satisfies the following properties of distribution:

$$S(\mathcal{Y}_j^k) + (k-j+1)\ln\frac{\sigma_1}{\sigma_0} \sim \begin{cases} \Gamma\left(\frac{k-j+1}{2},\ 1-\frac{\sigma_0^2}{\sigma_1^2}\right), \text{ without fault,} \\ \Gamma\left(\frac{k-j+1}{2},\ \frac{\sigma_1^2}{\sigma_0^2}-1\right), \text{ with fault.} \end{cases} \tag{3.8}$$

With the fault starting from $k = 1$,

$$\Pr_{\sigma_1}(S(\mathcal{Y}_1^n) < h) = \frac{1}{\Gamma\left(\frac{n}{2}\right)}\gamma\left(\frac{n}{2},\ \frac{\sigma_0^2}{\sigma_1^2-\sigma_0^2}\left(h + n\ln\frac{\sigma_1}{\sigma_0}\right)\right). \tag{3.9}$$

According to [51], a sufficient condition of a closed SPRT will apply if we can prove $\lim_{n\to\infty}\Pr_{\sigma_1}(S(\mathcal{Y}_1^n) < h) = 0$ for any fixed h and σ_1.

3.3 Assumption & Derivation of SPRT

Basseville and Nikiforov have introduced the general form of a CUSUM decision function $g(k)$ in [51], which can be rewritten as follows with the knowledge of (3.2)[1]:

$$g(k) = \max_{1\le j\le k} S(\mathcal{Y}_j^k) = \max_{1\le j\le k}\left\{-(k-j+1)\ln\frac{\sigma_1}{\sigma_0} + \frac{\sigma_1^2-\sigma_0^2}{2\sigma_0^2\sigma_1^2}\sum_{i=j}^{k}(y(i)-\mu)^2\right\}. \tag{3.10}$$

As (3.10) contains both σ_0 and σ_1, it is required that both σ_0 and σ_1 should be known as a priori for CUSUM detection.

For simplicity, we fix the fault time $j_f = 1$. Here we make a further assumption:

$$\max_{1\le j\le k} S(\mathcal{Y}_j^k) = S(\mathcal{Y}_1^k),\ k \ge 0, \tag{3.11}$$

which means every additive increment s_j is assumed positive after the fault occurrence. Note that it is the assumption that makes the detection not CUSUM, although it is CUSUM-based.

With the assumptions, the decision function becomes

$$g(k) = S(\mathcal{Y}_1^k) = -k\ln\frac{\sigma_1}{\sigma_0} + \frac{\sigma_1^2-\sigma_0^2}{2\sigma_0^2\sigma_1^2}\sum_{i=1}^{k}(y(i)-\mu)^2 \ge h, \tag{3.12}$$

[1] As the change on variance is the major research concentration in Chapter 3, it is assumed $\mu = 0$ from here to the end of the chapter.

which is equivalent to

$$\tilde{g}(k) \triangleq \sum_{i=1}^{k} \tilde{s}(i) \triangleq \frac{1}{\sigma_1^2}\sum_{i=1}^{k}(y(i)-\mu)^2 \geq \frac{2\sigma_0^2}{\sigma_1^2-\sigma_0^2}\left(h + k\ln\frac{\sigma_1}{\sigma_0}\right) \triangleq \tilde{h}(k). \tag{3.13}$$

As $\tilde{h}$ is affine upon k, define $\tilde{h}(k) \triangleq ak+b$, where $a = \frac{2\sigma_0^2}{\sigma_1^2-\sigma_0^2}\ln\frac{\sigma_1}{\sigma_0}$, $b = \frac{2\sigma_0^2}{\sigma_1^2-\sigma_0^2}h$.

Note that after the fault occurrence, the previous analysis shows

$$y(i)-\mu \sim \mathcal{N}(0,\sigma_1^2) \Rightarrow \frac{y(i)-\mu}{\sigma_1} \sim \mathcal{N}(0,1).$$

According to [106] and the i.i.d. property of $\{Y\}$, the following is true:

$$\begin{aligned} \tilde{s}(i) &= \frac{(y(i)-\mu)^2}{\sigma_1^2} \sim \chi^2(1), \\ \tilde{g}(k) &= \frac{1}{\sigma_1^2}\sum_{i=1}^{k}(y(i)-\mu)^2 \sim \chi^2(k). \end{aligned}$$

Now the problem is transformed into a $\chi^2(k)$ sequence $\tilde{g}(k)$ detected by the affine threshold $\tilde{h}(k)$. Here we make a further step in pursuing the probability of the first hitting time, i.e. the detection time k_d:

$$k_d : \begin{cases} \tilde{g}(j) < \tilde{h}(j),\ 1 \leq j < k_d; \\ \tilde{g}(k_d) \geq \tilde{h}(k_d). \end{cases} \tag{3.14}$$

Based on (3.14) we have the following derivation, with the knowledge $\tilde{s}(i) \geq 0$ in χ^2 distributions:

$$\Pr(k_d = 1) = \Pr(\tilde{g}(1) \geq \tilde{h}(1)) = \Pr(\tilde{s}(1) \geq \tilde{h}(1)) = 1 - \frac{1}{\Gamma\left(\frac{1}{2}\right)}\gamma\left(\frac{1}{2}, \frac{\tilde{h}(1)}{2}\right), \tag{3.15}$$

$$\begin{aligned} \Pr(k_d = 2) &= \Pr(\tilde{g}(1) < \tilde{h}(1), \tilde{g}(2) \geq \tilde{h}(2)) = \Pr(\tilde{s}(1) < \tilde{h}(1), \tilde{s}(2) \geq \tilde{h}(2) - \tilde{s}(1)) \\ &= \frac{1}{2\Gamma^2\left(\frac{1}{2}\right)}\int_0^{\tilde{h}(1)}\int_{\tilde{h}(2)-\tilde{s}(1)}^{\infty}(\tilde{s}(1)\tilde{s}(2))^{-\frac{1}{2}}e^{-\frac{\tilde{s}(1)+\tilde{s}(2)}{2}}\mathrm{d}\tilde{s}(2)\mathrm{d}\tilde{s}(1), \end{aligned} \tag{3.16}$$

$$\vdots$$

$$\begin{aligned} \Pr(k_d = k) &= \Pr(\tilde{g}(i) < \tilde{h}(i),\ i = 1, \cdots, k-1,\ g(k) \geq h(k)) \\ &= \Pr\left(\tilde{s}(i) < \tilde{h}(i) - \sum_{j=1}^{i-1}\tilde{s}(j),\ i = 1, \cdots, n-1,\ \tilde{s}(n) \geq \tilde{h}(n) - \sum_{j=1}^{n-1}\tilde{s}(j)\right) \\ &= \frac{1}{2^{\frac{k}{2}}\Gamma^k\left(\frac{1}{2}\right)}\int_0^{\tilde{h}(1)}\cdots\int_0^{\tilde{h}(k-1)-\sum_{i=1}^{k-2}\tilde{s}(i)}\int_{\tilde{h}(k)-\sum_{i=1}^{k-1}\tilde{s}(i)}^{\infty}\left(\prod_{i=1}^{k}\tilde{s}(i)\right)^{-\frac{1}{2}}e^{-\frac{\sum_{i=1}^{k}\tilde{s}(i)}{2}}\mathrm{d}\tilde{\mathbf{s}}_1^k. \end{aligned} \tag{3.17}$$

In the following parts, we will carry out deeper computations on some relevant performance indices and the analytical form of the probabilities in (3.16) and (3.17). Note that Γ and γ here are (in)complete Γ-functions as defined in [107], which are different from Γ-distribution as in (3.8).

3.4 Industrial Performance Indices

Here we discuss two commonly-accepted industrial performance indices [51]:

- The average run length (ARL) $\mathrm{E}_{\sigma_1}(k_d)$, i.e. the expectation of the detection time (FHT) given the fault occurs;
- The false alarm rate (FAR), i.e. the cumulative false alarm probability $\mathrm{Pr}_{\sigma_0}(k_d < \infty)$, given the fault does not occur.

3.4.1 ARL

An approximation of the ARL (named Average Sample Number (ASN)) regarding CUSUM-based detection is provided in [51]:

$$\mathbf{E}_{\sigma_1}(k_d) \approx \frac{-aQ(\sigma_1) + h(1 - Q(\sigma_1))}{\mathbf{E}_{\sigma_1}(s(y(i)))}, \text{ when } \mathbf{E}_{\sigma_1}(s(y(i))) \neq 0, \tag{3.18}$$

where $h > 0$, $-a < 0$ are respectively the threshold for determining $\mathcal{H}_0$ and $\mathcal{H}_1$, and

$$Q(\sigma_1) = \frac{e^{-h} - 1}{e^{-h} - e^{a}}.$$

In our detection problem, the lower bound does not exists, i.e. $a \to +\infty$. According to (3.18),

$$\begin{aligned} \lim_{a \to +\infty} Q(\sigma_1) &= \lim_{a \to +\infty} \frac{e^{-h} - 1}{e^{-h} - e^{a}} = 0, \\ \lim_{a \to +\infty} aQ(\sigma_1) &= \lim_{a \to +\infty} \frac{e^{-h} - 1}{\frac{e^{-h}}{a} - \frac{e^{a}}{a}} = 0. \end{aligned}$$

As a result of (3.7) and the expressions above, the ARL can be approximated as

$$\begin{aligned}\mathbf{E}_{\sigma_1}(k_d) &\approx \lim_{a\to+\infty}\frac{h}{E_{\sigma_1}(s(y(i)))} = \frac{h}{\frac{1}{2}\left(-\ln\frac{\sigma_1^2}{\sigma_0^2}+\frac{\sigma_1^2}{\sigma_0^2}-1\right)} \\ &= \frac{2\sigma_0^2}{\sigma_1^2-(1+2(\ln\sigma_1-\ln\sigma_0))\sigma_0^2}h. \end{aligned} \tag{3.19}$$

3.4.2 FAR

Wald's inequality shows for a open-ended test, an upper bound for false alarm rate exists, [51]:

$$\Pr_{\sigma_0}(k_d<\infty)\le e^{-h}. \tag{3.20}$$

On the other hand, [109], [110] have provided a less conservative upper bound for FAR: define the original likelihood ratio of the first step

$$\Lambda_1 \triangleq e^{S(\mathcal{Y}_1^1)} = \frac{p_{\sigma_1}(y(1))}{p_{\sigma_0}(y(1))} = \frac{\sigma_0}{\sigma_1}e^{\left(\frac{1}{2\sigma_0^2}-\frac{1}{2\sigma_1^2}\right)(y(1)-\mu)^2}. \tag{3.21}$$

As research in [109], [110] has shown

$$\Pr_{\sigma_0}(k_d<\infty)\le\frac{E_{\sigma_0}(\Lambda_1)}{e^h},\ \text{given } e^h>E_{\sigma_0}(\Lambda_1) \tag{3.22}$$

for nonnegative supermartingale $\Lambda_1,\Lambda_2,\cdots$, we have

$$\Pr_{\sigma_0}(k_d<\infty)\le\min\left\{\frac{E_{\sigma_0}(\Lambda_1)}{e^h}, e^{-h},\ 1\right\}, \tag{3.23}$$

with Λ_1 as defined in 3.21.[2]

3.5 Lower Bounds of the FHT Detection Probabilities

As it is difficult to work out an analytical form of the detection (FHT) probability, an alternative thought is to give a range of the probability by computing its bounds. Two lower bounds are provided in this section.

[2] $\Pr_{\sigma_0}(k_d<\infty)\le\min\{e^{-h},\ 1\}$ is used in simulation as no form of $E_{\sigma_0}(\Lambda_1)$ computable in MATLAB is worked out yet.

3.5.1 Detection delay

According to [107], we define the following linear variable transformation,

$$\mathbf{w}_1^k \triangleq \begin{bmatrix} \tilde{w}(k) \\ \tilde{w}(k-1) \\ \vdots \\ \tilde{w}(1) \end{bmatrix} \triangleq \begin{bmatrix} 1 & 1 & \cdots & 1 \\ 0 & 1 & \cdots & 1 \\ \vdots & \vdots & \ddots & \vdots \\ 0 & 0 & \cdots & 1 \end{bmatrix} \begin{bmatrix} \tilde{s}(k) \\ \tilde{s}(k-1) \\ \vdots \\ \tilde{s}(1) \end{bmatrix} \triangleq \mathbf{T}\tilde{\mathbf{s}}_1^k, \tag{3.24}$$

and substitute $\tilde{\mathbf{s}}_1^k$ with $\mathbf{w}_1^k$ in (3.17) to simplify the computations:

$$\begin{aligned} \Pr(k_d &= k) = \frac{1}{2^{\frac{k}{2}}\Gamma^k\left(\frac{1}{2}\right)} \int_0^{\tilde{h}(1)} \cdots \int_0^{\tilde{h}(k-1)-\sum\limits_{i=1}^{k-2}\tilde{s}(i)} \int_{\tilde{h}(k)-\sum\limits_{i=1}^{k-1}\tilde{s}(i)}^{\infty} \left(\prod_{i=1}^{k}\tilde{s}(i)\right)^{-\frac{1}{2}} e^{-\frac{\sum_{i=1}^{k}\tilde{s}(i)}{2}} \mathrm{d}\tilde{\mathbf{s}}_1^k \\ &= \frac{1}{(2\pi)^{\frac{k}{2}}} \int_0^{\tilde{h}(1)} \int_{w(1)}^{\tilde{h}(2)} \cdots \int_{w(k-2)}^{\tilde{h}(k-1)} \int_{\tilde{h}(k)}^{\infty} \frac{e^{-\frac{w(k)}{2}}}{\sqrt{w(1)\prod_{i=2}^{k}\left(w(i)-w(i-1)\right)}} \mathrm{d}\mathbf{w}_1^k. \end{aligned} \tag{3.25}$$

Here we look for a lower bound and an upper one for (3.25). A solution to the lower bound is provided in [107], using the inequality between the arithmetic and the geometric means, i.e. a form of the Cauchy-Schwarz inequality, in our research which is:

$$\sqrt[k]{w(1)\prod_{i=2}^{k}\left(w(i)-w(i-1)\right)} \leq \frac{w(1)+\sum_{i=2}^{k}\left(w(i)-w(i-1)\right)}{k} = \frac{w(k)}{k}, \tag{3.26}$$

and thus

$$\begin{aligned} (3.25) \quad &\geq \quad \frac{1}{(2\pi)^{\frac{k}{2}}} \int_0^{\tilde{h}(1)} \int_{w(1)}^{\tilde{h}(2)} \cdots \int_{w(k-2)}^{\tilde{h}(k-1)} \int_{\tilde{h}(k)}^{\infty} \frac{e^{-\frac{w(k)}{2}}}{\left(\frac{w(k)}{k}\right)^{\frac{k}{2}}} \mathrm{d}\mathbf{w}_1^k \\ &\triangleq \quad \left(\frac{k}{2\pi}\right)^{\frac{k}{2}} C(k,\ \tilde{h}(k)) \int_0^{\tilde{h}(1)} \int_{w(1)}^{\tilde{h}(2)} \cdots \int_{w(k-2)}^{\tilde{h}(k-1)} \mathrm{d}\mathbf{w}_1^{k-1}, \end{aligned} \tag{3.27}$$

where $C(k,\ x)$ is defined and with its analytical form[3] as in (3.28):

$$C(k,\ x) \triangleq \int_x^{\infty} \frac{e^{-\frac{u}{2}}}{u^{\frac{k}{2}}} \mathrm{d}u = \frac{1}{2^{\frac{k}{2}-1}} \Gamma\left(-\frac{k}{2}+1,\ \frac{x}{2}\right). \tag{3.28}$$

In order to provide a form compatible in MATLAB, we hereby use Maple to expand integrals as (3.28) and summarize inductive results throughout the

[3] Definition of $\Gamma(s,\ x)$ with negative s is controversial but defined and calculated as a result in Maple. Similar case for (3.37).

rest of the chapter. The following analytical form is worked out for $C(k,\ x)$:

$$C(k,\ x)=\begin{cases}\sqrt{2}\Gamma\left(\frac{1}{2},\ \frac{x}{2}\right), & k=1,\\ \Gamma\left(0,\ \frac{x}{2}\right), & k=2,\\ -\sqrt{2}\Gamma\left(\frac{1}{2},\ \frac{x}{2}\right)+2e^{-\frac{1}{2}x}x^{-\frac{1}{2}}, & k=3,\\ -\frac{1}{2}\left[\Gamma\left(0,\ \frac{x}{2}\right)-2e^{-\frac{1}{2}x}x^{-1}\right], & k=4,\\ \frac{(-1)^{\frac{k-1}{2}}}{(k-2)!!}\left[\sqrt{2}\Gamma\left(\frac{1}{2},\ \frac{x}{2}\right)-\frac{2\left(1+\sum\limits_{i=1}^{\frac{k-3}{2}}(2i-1)!!(-x)^{-i}\right)}{e^{\frac{1}{2}x}x^{\frac{1}{2}}}\right], & k=5,\ 7,\ \ldots\\ \frac{(-1)^{\frac{k}{2}-1}}{(k-2)!!}\left[\Gamma\left(0,\ \frac{x}{2}\right)-\frac{2\left(1+\sum\limits_{i=1}^{\frac{k}{2}-2}(2i)!!(-x)^{-i}\right)}{e^{\frac{1}{2}x}x}\right], & k=6,\ 8,\ \ldots\end{cases}\tag{3.29}$$

where the double factorial is defined following [105]:

$$n!!\triangleq\prod_{i=0}^{\left[\frac{n-1}{2}\right]}(n-2i).$$

Here we step further on the relationships between the value of C and its parameters $k,\ x$. A three-dimensional plot is then provided in Fig. 3.1. The figure tells the value of $C(k,\ x)$ decreases upon x-axis and generally upon k-axis; the latter case is no longer valid for small x.

Likewise, we can provide the visualized relationship between $C(k,\ \tilde{h}(k))$ and the parameters $k,\ \tilde{h}(k)$. As $\tilde{h}(k)=ak+b$ is a function of k, the relationship is a curve across the three-dimensional space. Fig. 3.2 gives an example, in which the value of $C(k,\ \tilde{h}(k))$ decrease with k increasing.

Another lower bound can be given by the thought of the arithmetic mean of the natural logarithms as in [107]:

$$\begin{aligned}\prod_{i=1}^{k}\tilde{s}(i) &= e^{\sum\limits_{i=1}^{k}\ln\tilde{s}(i)}\\ \Rightarrow \Pr(k_d=k) &= \frac{1}{(2\pi)^{\frac{k}{2}}}\int_0^{\tilde{h}(1)}\cdots\int_0^{\tilde{h}(k-1)-\sum\limits_{i=1}^{k-2}\tilde{s}(i)}\int_{\tilde{h}(k)-\sum\limits_{i=1}^{k-1}\tilde{s}(i)}^{\infty}e^{-\frac{\sum_{i=1}^{k}(\tilde{s}(i)+\ln\tilde{s}(i))}{2}}\mathrm{d}\tilde{\mathbf{s}}_1^k.\end{aligned}\tag{3.30}$$

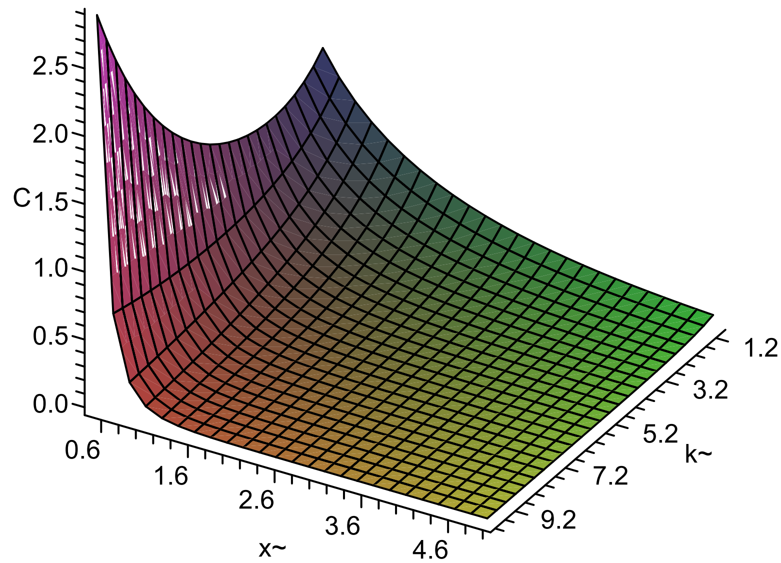

Figure 3.1: Three-dimensional plot of $C(k,\ x)$.

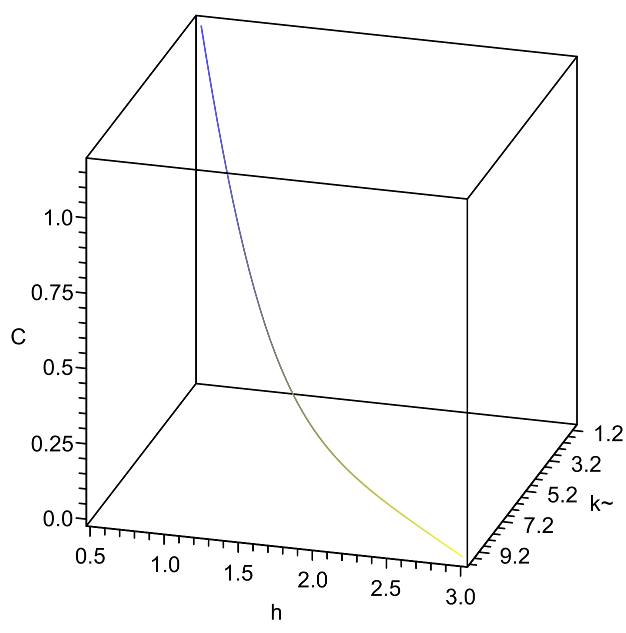

Figure 3.2: $C(k,\ \tilde{h}(k))$ with $\tilde{h}(k) = ak + b$, given $\sigma_0 = 0.1$ and $\sigma_1 = 0.3$.

Based on the natural logarithm inequalities provided in (3.5), the lower bound of FHT detection could be formed:

$$
\begin{aligned}
(3.30) \quad \geq\ & \frac{1}{(2\pi)^{\frac{k}{2}}}\int_0^{\tilde{h}(1)}\cdots\int_0^{\tilde{h}(k-1)-\sum_{i=1}^{k-2}\tilde{s}(i)}\int_{\tilde{h}(k)-\sum_{i=1}^{k-1}\tilde{s}(i)}^{\infty} e^{-\sum_{i=1}^{k}\left(\tilde{s}(i)-\frac{1}{2}\right)}\mathrm{d}\tilde{\mathbf{s}}_1^k \\
=\ & \left(\frac{e}{2\pi}\right)^{\frac{k}{2}}\int_0^{\tilde{h}(1)}\int_{w(1)}^{\tilde{h}(2)}\cdots\int_{w(k-2)}^{\tilde{h}(k-1)}\int_{\tilde{h}(k)}^{\infty} e^{-w_k}\mathrm{d}\mathbf{w}_1^k \\
=\ & \frac{e^{\frac{k}{2}-\tilde{h}(k)}}{(2\pi)^{\frac{k}{2}}}\int_0^{\tilde{h}(1)}\int_{w(1)}^{\tilde{h}(2)}\cdots\int_{w(k-2)}^{\tilde{h}(k-1)}\mathrm{d}\mathbf{w}_1^{k-1}. \qquad (3.31)
\end{aligned}
$$

3.5.2 Time between false alarms

Here we make a further step on the case in which no fault occurs. A positive probability of detection exists with respect to the method provide above. It is common knowledge that

$$
y(i)-\mu \sim \mathcal{N}(0,\sigma_1^2) \Rightarrow \frac{y(i)-\mu}{\sigma_1} \sim \mathcal{N}(0,\frac{\sigma_0^2}{\sigma_1^2}),
$$

According to [106], the distribution type of $\tilde{s}(i)$ and its probabilistic density function are available:

$$
\tilde{s}(i) = \frac{(y(i)-\mu)^2}{\sigma_1^2} \sim \Gamma\left(\frac{1}{2},\frac{2\sigma_0^2}{\sigma_1^2}\right), \qquad (3.32)
$$

$$
f(\tilde{s}(i)) = \frac{1}{\sqrt{2\pi\theta}}\cdot\frac{e^{\frac{-\tilde{s}(i)}{2\theta}}}{\sqrt{\tilde{s}(i)}}, \text{ where } \theta \triangleq \frac{\sigma_0^2}{\sigma_1^2} \in (0,\ 1). \qquad (3.33)
$$

Similar to (3.17) and (3.25), we can work out the general expressions of the false detection probabilities at each step:

$$
\begin{aligned}
\Pr(k_f = k) &= \Pr(\tilde{g}(i) < \tilde{h}(i),\ i=1,\cdots,k-1,\ g(k)\geq h(k)) \\
&= \Pr\left(\tilde{s}(i) < \tilde{h}(i)-\sum_{j=1}^{i-1}\tilde{s}(j),\ i=1,\cdots,n-1,\ \tilde{s}(n)\geq \tilde{h}(n)-\sum_{j=1}^{n-1}\tilde{s}(j)\right) \\
&= \frac{1}{(2\pi\theta)^{\frac{k}{2}}}\int_0^{\tilde{h}(1)}\cdots\int_0^{\tilde{h}(k-1)-\sum\limits_{i=1}^{k-2}\tilde{s}(i)}\int_{\tilde{h}(k)-\sum\limits_{i=1}^{k-1}\tilde{s}(i)}^{\infty}\left(\prod_{i=1}^{k}\tilde{s}(i)\right)^{-\frac{1}{2}} e^{-\frac{\sum_{i=1}^{k}\tilde{s}(i)}{2\theta}}\mathrm{d}\tilde{\mathbf{s}}_1^k. \qquad (3.34) \\
&= \frac{1}{(2\pi\theta)^{\frac{k}{2}}}\int_0^{\tilde{h}(1)}\int_{w(1)}^{\tilde{h}(2)}\cdots\int_{w(k-2)}^{\tilde{h}(k-1)}\int_{\tilde{h}(k)}^{\infty}\frac{e^{-\frac{w(k)}{2\theta}}}{\sqrt{w(1)\prod_{i=2}^{k}(w(i)-w(i-1))}}\mathrm{d}\mathbf{w}_1^k, \qquad (3.35)
\end{aligned}
$$

and from (3.35) we may work out the lower bound of the false alarm probabilities.

Define

$$C_f(k,\ \theta,\ x) \triangleq \int_x^{\infty} \frac{e^{-\frac{u}{2\theta}}}{u^{\frac{k}{2}}} \mathrm{d}u = \frac{1}{\theta^{\frac{k}{2}-1}} C\Big(k,\ \frac{x}{\theta}\Big) \tag{3.36}$$

$$= \frac{1}{(2\theta)^{\frac{k}{2}-1}} \Gamma\Big(-\frac{k}{2}+1,\ \frac{x}{2\theta}\Big), \tag{3.37}$$

where $C(k,\ x)$ is as defined in (3.28) and expanded in (3.29). Combine (3.26)(3.27)(3.35), we can get

$$\Pr(k_f = k) \geq \Big(\frac{k}{2\pi\theta}\Big)^{\frac{k}{2}} \int_0^{\tilde{h}(1)} \int_{w(1)}^{\tilde{h}(2)} \cdots \int_{w(k-2)}^{\tilde{h}(k-1)} \int_{\tilde{h}(k)}^{\infty} \frac{e^{-\frac{w(k)}{2}}}{w(k)^{\frac{k}{2}}} \mathrm{d}\mathbf{w}_1^k$$

$$= \Big(\frac{k}{2\pi}\Big)^{\frac{k}{2}} \theta^{1-k} C\Big(k,\ \frac{\tilde{h}(k)}{\theta}\Big) \int_0^{\tilde{h}(1)} \int_{w(1)}^{\tilde{h}(2)} \cdots \int_{w(k-2)}^{\tilde{h}(k-1)} \mathrm{d}\mathbf{w}_1^{k-1}. \tag{3.38}$$

(3.38) is a lower bound of the false alarm based on the Cauchy-Schwarz inequality.

Regarding the way of the arithmetic mean of the natural logarithms as in (3.5), the derivation in (3.30) becomes

$$\Pr(k_f = k) = \frac{1}{(2\pi\theta)^{\frac{k}{2}}} \int_0^{\tilde{h}(1)} \cdots \int_0^{\tilde{h}(k-1)-\sum\limits_{i=1}^{k-2}\tilde{s}(i)} \int_{\tilde{h}(k)-\sum\limits_{i=1}^{k-1}\tilde{s}(i)}^{\infty} e^{-\frac{\sum\limits_{i=1}^{k}\left(\frac{\tilde{s}(i)}{\theta}+\ln\tilde{s}(i)\right)}{2}} \mathrm{d}\tilde{\mathbf{s}}_1^k.$$

$$\geq \frac{e^{\frac{k}{2}}}{(2\pi\theta)^{\frac{k}{2}}} \int_0^{\tilde{h}(1)} \cdots \int_0^{\tilde{h}(k-1)-\sum\limits_{i=1}^{k-2}\tilde{s}(i)} \int_{\tilde{h}(k)-\sum\limits_{i=1}^{k-1}\tilde{s}(i)}^{\infty} e^{-\frac{1}{2}\left(\frac{1}{\theta}+1\right)\sum\limits_{i=1}^{k}\tilde{s}(i)} \mathrm{d}\tilde{\mathbf{s}}_1^k$$

$$= \frac{e^{\frac{k}{2}}}{(2\pi\theta)^{\frac{k}{2}}} \int_0^{\tilde{h}(1)} \int_{w(1)}^{\tilde{h}(2)} \cdots \int_{w(k-2)}^{\tilde{h}(k-1)} \int_{\tilde{h}(k)}^{\infty} e^{-\frac{\theta+1}{2\theta}w(k)} \mathrm{d}\mathbf{w}_1^k$$

$$= \frac{e^{\frac{k}{2}-\frac{\theta+1}{2\theta}\tilde{h}(k)}}{\pi^{\frac{k}{2}}(\theta+1)} (2\theta)^{1-\frac{k}{2}} \int_0^{\tilde{h}(1)} \int_{w(1)}^{\tilde{h}(2)} \cdots \int_{w(k-2)}^{\tilde{h}(k-1)} \mathrm{d}\mathbf{w}_1^{k-1}. \tag{3.39}$$

(3.39) is a lower bound of the false alarm based on the arithmetic mean of the natural logarithms.

3.6 Simulation

We hereby carry out an SPRT test on a DC motor system with the prototype in [53] and [72], regarding the industrial FD performance indices ARL and

FAR. The feedback connection plan is shown in Fig. 3.3. Note that the speed output (speed sensor measurement) $w(t) = w_0(t) + v(t) \to v(t)$ as $t \to \infty$ with a step reference for the position. $v(t) \sim \mathcal{N}(0, \sigma^2)$ is the speed sensor noise, which is assumed to be Gaussian.

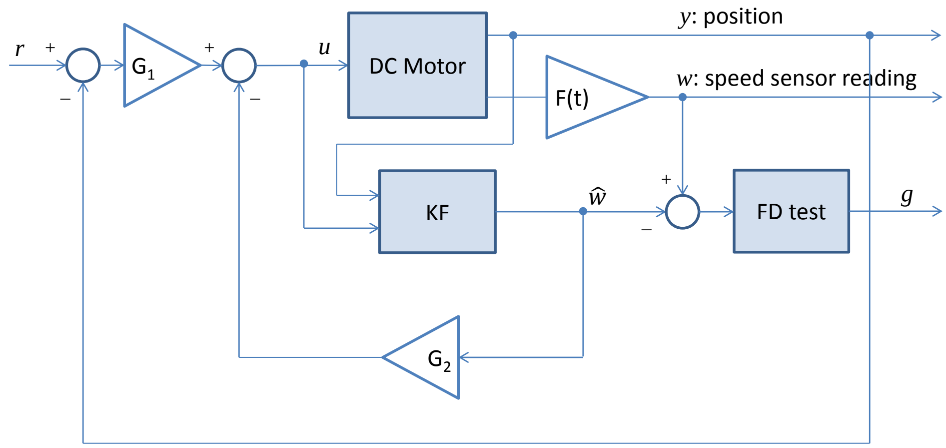

Figure 3.3: The DC motor model with multiplicative fault.

The gain shift on the speed sensor gain works as the multiplicative fault affecting variance. The observed speed $\hat{y}$ based on the position sensor measurement is used as the feedback signal, while the difference between the speed sensor measurement w and the observed speed $\hat{w}$ are defined as the decision function g. With an additional gain F appearing on the sensor output, the estimation $\hat{w}$ may have transient but will approach zero due to the nature of the step reference for the position, and the decision function becomes

$$g(t) \to w(t) = F(w_0(t) + v(t)) \to Fv(t) \sim \mathcal{N}(0, F^2\sigma^2), \text{ when } t \to \infty,$$

which is a variance change fault problem.

Select the parameters as $\sigma = 0.1$, $\sigma_1^2/\sigma_0^2 = F^2 = 4$, the sample time $T_s = 0.002$. Carry out the SPRT test as in (3.12) for 500 times and plot the histogram as in Fig. 3.4. The mean of the experimental ARL is 0.496; compared with the theoretical value from (3.19), the deviation is less than 0.7.

It has shown that the expression provided in (3.19) is a feasible approximation of ARL, as the accuracy is satisfactory.

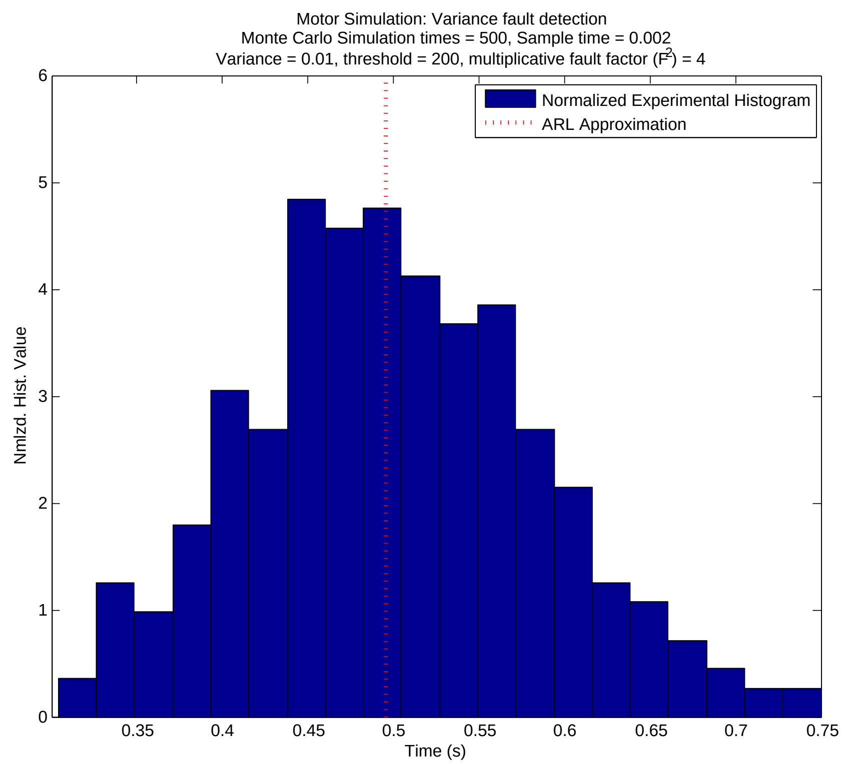

Figure 3.4: Distribution of detection delay with ARL approximation upon speed sensor gain shift of DC motor

As for the false alarm rate, we carried out two different tests to inspect the way that the FAR varies with respect to the selection of variance σ_0^2 and the threshold h. The other parameters, including F and T_s, remains the same as the experiment for detection delay. The first FAR test selects σ_0^2 from the range between 0.2 and 10 and a fixed $h = 1$, while the second test selects h from the range between 0.1 to 5 and a fixed $\sigma_0^2 = 1$. 500 Monte Carlo simulations have been done for each selection within the range, and the detections according to (3.12) within 1000 steps are considered as false alarms, based on which the experimental FAR is calculated. The experimental FAR and the upper bound of FAR share one plot axis, respectively in Fig. 3.5(a) and Fig. 3.5(b). The experimental results have shown that

- The variance does not affect FAR obviously.
- The threshold directly affects FAR, intuitively in an exponential way.
- $\min\{e^{-h},\ 1\}$ works as an upper bound of FAR.

3.7 Conclusion

This chapter has focused on providing quantitative descriptions for the fault detection against multiplicative fault affecting variances. It has provided analytical forms of industrial performance indices, including ARL and FAR, and made a further step by calculating lower bounds of the FHT detection probabilities. The simulations with sensor-faulted DC motor have not only shown the feasibility and effectiveness of these analytical descriptions, but also discussed the factors affecting the FHT.

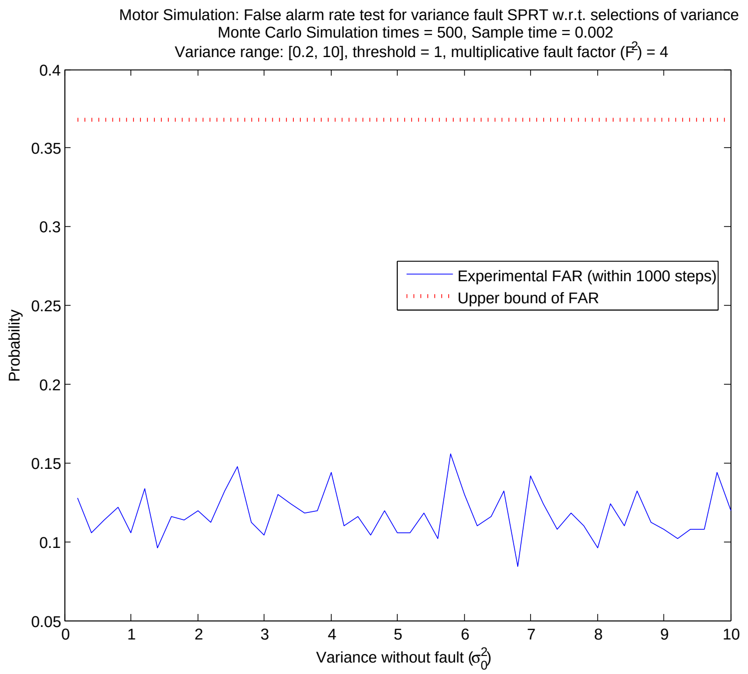

(a) $h = 1$, horizonal axis of σ_0^2

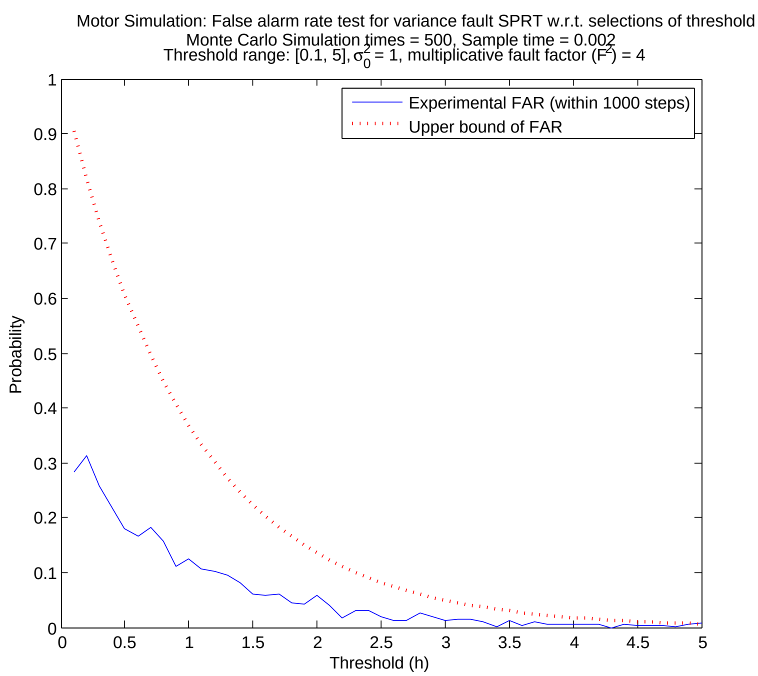

(b) $\sigma_0^2 = 1$, horizontal axis of h

Figure 3.5: Experimental FAR and the upper bound with respect to speed sensor gain shift in DC motor

Chapter 4

Real-time Frequency Estimation and Detection of Dynamic Fault

4.1 Introduction

Chapter 4[1] focuses on the real-time frequency estimation of sinusoidal signals with perturbation. A synthetic estimation strategies, i.e. parametric linear model based gradient estimator with leakage, is selected as the approach of estimation and thus researched. The theoretical basis is strictly proved, and its extension to fault diagnosis is discussed. Multiple case studies, i.e. machinery vibration data and various types of faults on a hydraulic rig model, are provided in the simulation part. Within the thesis scope, the chapter presents novel fault detection skills with respect to dynamic faults, faults affecting frequency, and the application as vibration/oscillation. From the perspective of estimation, the main contribution of this work is to improve the current existing frequency identifier especially when the signal is corrupted by disturbances. Furthermore, the application of the frequency identifier to robust fault detection is investigated. Both multiplicative and additive fault-induced

[1] Originally published as:
[69] S. Yang, Q. Zhao, "Real-time frequency estimation of sinusoids with low-frequency disturbances," *Proc. American Control Conference*, 2011, pp. 4275–4280.
[71] S. Yang, Q. Zhao, "Real-time frequency estimation for sinusoidal signals with application to robust fault detection," *Int. J. Adapt. Control Signal Process*, 26, 2012, DOI: 10.1002/acs.2308.

changes are considered. The simulations carried on a hydraulic rig model show satisfactory results.

The remainder of this chapter is organized as follows. Subtopic 4.2 formulates the problem by establishing a parametric linear model for the signal, Subtopic 4.3 introduces the estimator with the detailed analysis of the estimation error bounds, and Subtopic 4.4 discusses its application to fault detection (FD). Section 4.5 presents the simulation case studies. Firstly, the real-time frequency estimation using the method introduced in this chapter is compared with another existing method for a series of motor shaft vibration data, which demonstrates the improvement made by this work. Secondly, the simulation is performed on fault detection for a hydraulic rig model. At the end, Section 4.6 summarizes the chapter.

4.2 Linear Parametric Signal Model

Consider the following sinusoidal signal with n frequencies, perturbed by a disturbance:

$$y(t) = \sum_{i=1}^{n}(A_i \sin(w_i t + \phi_i)) + d(t) \triangleq \sum_{i=1}^{n} y_i(t) + d(t) \triangleq y_0(t) + d(t).$$

where $y_0(t)$ is the nominal signal, and $y_i = A_i \sin(w_i t + \phi_i)$ for $i = 1, 2, \cdots, n$. It is assumed that only $y(t)$ can be measured, but A_i, w_i, and ϕ_i, $i = 1, 2, \ldots n$ are unknown. The disturbance $d(t)$ is bounded as $d \in \mathcal{L}^\infty$ and thus $\delta \triangleq \|d\|_\infty = \sup_t |d(t)| < \infty$. Obviously y is also bounded in the same sense.

Based on the properties of sinusoids and the Laplace transform, the following equation stands:

$$\begin{aligned} & s^2 Y_i(s) - s y_i(0) - \dot{y}_i(0) = -w_i^2 Y_i(s) \\ \Rightarrow \quad & Y_i(s) = \frac{s y_i(0) + \dot{y}_i(0)}{s^2 + w_i^2}, \end{aligned}$$

where $y_i(0)$ and $\dot{y}_i(0)$ are the initial values with respect to $y_i(t)$ and its first order derivative $\dot{y}_i(t)$. Then we have

$$Y(s) = \sum_{i=1}^{n} Y_i(s) + d(s) \triangleq \frac{p(s)}{q(s)} + d(s), \tag{4.1}$$

$$\text{with } q(s) \triangleq \prod_{i=1}^{n}(s^2 + w_i^2) \triangleq s^{2n} + q_{n-1}s^{2(n-1)} + \cdots + q_1 s^2 + q_0. \tag{4.2}$$

where $\{q_i : i = 0, 1, ...n-1\}$ contains information of the n frequencies of the nominal signal, and can be used to determine these frequencies. In this chapter we will focus on estimation of these coefficients.

A common modeling method is to establish a parametric linear model referring to the prototype in [92]. Define a k^{th} order Hurwitz polynomial

$$\Lambda(s) \triangleq s^k + \lambda_{k-1}s^{k-1} + \cdots + \lambda_1 s + \lambda_0$$

with k tunable coefficients so that $1/\Lambda(s)$ is a stable filter, then

$$\frac{q(s)}{\Lambda(s)}Y(s) = \frac{q(s)}{\Lambda(s)}d(s) + \frac{p(s)}{\Lambda(s)} \triangleq \eta(s) + \eta_0(s) \tag{4.3}$$

$$\text{with} \qquad \eta(s) = H_d(s)d(s) \triangleq \frac{q(s)}{\Lambda(s)}d(s), \qquad \eta_0(s) \triangleq \frac{p(s)}{\Lambda(s)} \tag{4.4}$$

Here $\eta(s)$ denotes the perturbation caused by $d(s)$, and $\eta_0(s)$ reflects the response to initial values $y_i(0)$ and $\dot{y}_i(0)$. Due to the fact that η_0 exponentially decays to zero [92], it is dropped off for simplicity in the following analysis. If η_0 is considered, we just need to replace η with $\eta + \eta_0$ in the following derivation; the boundedness and the convergence will not be affected. For $\Lambda(s)$, it is required that $k \geq 2n$ in order for the noise in actual systems not to be amplified due to a non-causal $q(s)/\Lambda(s)$. Since $d(t)$ is bounded, $y(t)$ is bounded. Furthermore, because $H_d(s) \triangleq q(s)/\Lambda(s)$ is a proper stable transfer function, η is bounded [93].

With the definitions

$$Z(s) \triangleq \frac{s^{2n}}{\Lambda(s)}Y(s),\ \phi \triangleq -\frac{\left[s^{2(n-1)}, \ \cdots, \ s^2, \ 1\right]^T}{\Lambda(s)}Y(s),\ \theta \triangleq \left[q_{n-1} \ \ \cdots \ \ q_1 \ \ q_0\right]^T,$$

the equation (4.3) can be rewritten as:

$$Z(s) = \theta^T \phi(s) + \eta + \eta_0, \tag{4.5}$$

which is a linear regression form as found in [92] and [54] for the parameter estimation problem. In the equation (4.5), $z(t)$ and $\phi(t)$, the filtered signals of the original measurement y are used so that more information about the nominal frequencies can be gained. Various approaches, such as the gradient-based method, Strictly Positive Real(SPR)-Lyapunov design, and the least square method, can be used for estimating θ. In this chapter, the gradient based method is selected as the frequency estimator, which is presented in Section 4.2.

4.3 Gradient Estimator with Leakage

For the parameter estimation problem defined in section 2, the following adaptive gradient estimator with leakage is adopted, [92]:

$$\begin{aligned}
\dot{\hat{\theta}} &= \Gamma\epsilon\phi - \sigma\Gamma\hat{\theta} && (4.6)\\
\hat{z} &= \hat{\theta}^T\phi && (4.7)\\
\epsilon &\triangleq \frac{z-\hat{z}}{m^2} = \frac{\tilde{\theta}^T\phi + \eta}{m^2} && (4.8)\\
m^2 &\triangleq 1 + m_\eta^2 + m_\phi^2, && (4.9)
\end{aligned}$$

where Γ is a tunable positive (definite) gain, σ is a customized constant, m_η and m_ϕ are parameters to be designed to make $\eta/m, \phi/m \in \mathcal{L}^\infty$.

A general way of defining m_η and m_ϕ is presented here:

$$m_\eta^2 = y^T y, \quad m_\phi^2 = \phi^T\phi, \tag{4.10}$$

which is to ensure that $\eta/m, \phi/m \in \mathcal{L}^\infty$ as required in [92] .

Substitute (4.8) in (4.6), it shows

$$\dot{\tilde{\theta}} = -\dot{\hat{\theta}} = -\Gamma\frac{\phi\phi^T}{m^2}\tilde{\theta} + \sigma\Gamma\hat{\theta} - \Gamma\frac{\eta\phi}{m^2} = -\Gamma\left(\frac{\phi\phi^T}{m^2} + \sigma\mathbf{I}\right)\tilde{\theta} + \sigma\Gamma\theta - \Gamma\frac{\eta\phi}{m^2}, \tag{4.11}$$

Obviously, $\frac{\phi\phi^T}{m^2} \geq \mathbf{0}$, and a positive σ can be selected such that $-\left(\frac{\phi\phi^T}{m^2} + \sigma\mathbf{I}\right)$ is Hurwitz. Note that in (4.11) the term $\sigma\Gamma\theta - \Gamma\frac{\eta\phi}{m^2}$ acts as a bounded input, which helps the derivation in Section 4.3.2.

By further analyzing the effects of the disturbance, i.e. η in (4.4), it is found that for a strictly proper $H_d(s)$ (by selecting $\Lambda(s)$ with the order $k > 2n$), its impulse response $h_d \in \mathcal{L}^1$, and the following inequality holds [92], [94]:

$$\|\eta\|_\infty \leq \|h_d * d\|_\infty \leq \|h_d\|_1\|d\|_\infty = \|h_d\|_1\delta. \tag{4.12}$$

Remark 5 *The Hurwitz polynomial $\Lambda(s)$ of the order $k = 2n$ may still be used; in this case $H_d(s)$ becomes biproper. Define*

$$H_1(s) = H_d(s) - 1$$

which is a stable strict proper transfer function and thus its impulse response $h_1 \in \mathcal{L}^1$ [92]. Then (4.12) becomes,

$$\begin{aligned}
\eta(s) &= d(s) + H_1 d(s) \\
\Leftrightarrow \eta(t) &= d(t) + h_1(t) * d(t) \\
\Rightarrow \|\eta\|_\infty &\leq \|d\|_\infty + \|h_1 * d\|_\infty \leq \|d\|_\infty + \|h_1\|_1\|d\|_\infty \\
&= (1 + \|h_1\|_1)\,\delta
\end{aligned} \tag{4.13}$$

Now we are ready to develop a bounded zone to which $\tilde{\theta}$ will be attracted. Following the method in [92], the zero-input (autonomous) response $\tilde{\theta}_{zi}$ and the zero-state response $\tilde{\theta}_{zs}$ in (4.11) are analyzed; the real-time estimation error is the sum, i.e., $\tilde{\theta}(t) = \tilde{\theta}_{zi}(t) + \tilde{\theta}_{zs}(t)$.

4.3.1 Zero-input response

In (4.11), by assuming the unknown 'input' terms as zero, the autonomous system is in the form

$$\dot{\tilde{\theta}}_{zi} = -\Gamma\left(\frac{\phi\phi^T}{m^2} + \sigma\mathbf{I}\right)\tilde{\theta}_{zi}. \tag{4.14}$$

In [92] the convergence of $\tilde{\theta}_{zi}$ is discussed with an additional property $m \leq 1$, which is to be expanded to all positive m with a known inferior bound in the current research: firstly ϕ is required to satisfy the Persistency of Excitation (PE) condition, i.e.,

- $\exists \alpha_0,\ T_0 > 0$, s.t. $\int_t^{t+T_0} \phi(\tau)\phi^T(\tau)d\tau \geq \alpha_0 T_0 \mathbf{I}$.

For (4.14), define the Lyapunov function as

$$V_{zi}(t) \triangleq \frac{\tilde{\theta}_{zi}^T \Gamma^{-1} \tilde{\theta}_{zi}}{2},$$

then the following is true [92]:

$$V_{zi}(t) \leq \rho^{\left[\frac{t}{T_0}\right]} V_{zi}(0), \tag{4.15}$$

in which $\rho \in (0,\ 1)$, and ρ is calculated as

$$\rho \triangleq 1 - \frac{2\alpha_0 T_0 \lambda_{\min}(\Gamma)\underline{m}}{2\bar{m}\underline{m} + \bar{\phi}^4 T_0^2 \lambda_{\max}^2(\Gamma)}, \tag{4.16}$$

and $\bar{\phi} \triangleq \sup_t |\phi(t)|$, $\bar{m} \triangleq \sup_t m^2(t)$, $\underline{m} \triangleq \inf_t m^2(t)$.

It is then found that

$$\begin{aligned} V_{zi}(t) &\geq \lambda_{\min}(\Gamma^{-1}) \frac{|\tilde{\theta}_{zi}(t)|^2}{2} = \frac{|\tilde{\theta}_{zi}(t)|^2}{2\lambda_{\max}(\Gamma)} \\ V_{zi}(0) &\leq \lambda_{\max}(\Gamma^{-1}) \frac{|\tilde{\theta}_{zi}(0)|^2}{2} = \frac{|\tilde{\theta}(0)|^2}{2\lambda_{\min}(\Gamma)}. \end{aligned}$$

Based on the convergence analysis in [92], $|\theta_{zi}(t)|$ decays exponentially to zero. As a result, (4.15) can be transformed into

$$\begin{aligned} \left|\tilde{\theta}_{zi}(t)\right| &\leq \sqrt{\frac{\lambda_{\max}(\Gamma)}{\lambda_{\min}(\Gamma)}} \rho^{\frac{1}{2}\left[\frac{t}{T_0}\right]} \left|\tilde{\theta}(0)\right| \\ &< \sqrt{\frac{\lambda_{\max}(\Gamma)}{\lambda_{\min}(\Gamma)}} \rho^{\frac{t}{2T_0} - \frac{1}{2}} \left|\tilde{\theta}(0)\right|, \end{aligned} \tag{4.17}$$

which is also a result complementary for the research in [95].

4.3.2 Zero-state response

The equation (4.14) describes a linear time-varying autonomous system, whose solution can be written as [93]

$$\tilde{\theta}_{zi}(t) = \Phi(t,0)\tilde{\theta}(0)$$

where $\Phi(t,0)$ is the state transition matrix from $\tilde{\theta}(0)$ to $\tilde{\theta}_{zs}(t)$.

On the basis of (4.17), the following is true

$$\left|\tilde{\theta}_{zi}(t)\right| = \left|\Phi(t,0)\tilde{\theta}(0)\right| < \sqrt{\frac{\lambda_{\max}(\Gamma)}{\lambda_{\min}(\Gamma)}}\rho^{\frac{t}{2T_0}-\frac{1}{2}}\left|\tilde{\theta}(0)\right|,$$

From the above, similarly one can have the following expression by replacing the initial condition with the input signal:

$$|\Phi(t,\tau)\mathbf{u}(\tau)| < \sqrt{\frac{\lambda_{\max}(\Gamma)}{\lambda_{\min}(\Gamma)}}\rho^{\frac{t-\tau}{2T_0}-\frac{1}{2}}\left|\mathbf{u}(\tau)\right|, \forall t,\tau \in \mathbb{R}, u(\tau) \in \mathbb{R}^n.$$

Define

$$\mathbf{u}(t) \triangleq -\Gamma\frac{\eta(t)\phi(t)}{m^2(t)} + \sigma\Gamma\theta \triangleq \Gamma\mathbf{v}(t), \tag{4.18}$$

then based on [93] we can derive that,

$$\begin{aligned}
\left|\tilde{\theta}_{zs}(t)\right| &= \left|\int_0^t \Phi(t,\tau)\mathbf{u}(\tau)d\tau\right| \le \int_0^t \left|\Phi(t,\tau)\mathbf{u}(\tau)\right| d\tau \\
&< \sqrt{\frac{\lambda_{\max}(\Gamma)}{\lambda_{\min}(\Gamma)}}\int_0^t \rho^{\frac{t-\tau}{2T_0}-\frac{1}{2}}\left|\mathbf{u}(\tau)\right| d\tau \\
&\le \sqrt{\frac{\lambda_{\max}(\Gamma)}{\lambda_{\min}(\Gamma)}}\int_0^t \rho^{\frac{t-\tau}{2T_0}-\frac{1}{2}}\|\Gamma\|_2|\mathbf{v}(\tau)|d\tau \\
&\le \sqrt{\frac{\lambda_{\max}(\Gamma)}{\lambda_{\min}(\Gamma)}}\int_0^t \rho^{\frac{t-\tau}{2T_0}-\frac{1}{2}}d\tau\|\Gamma\|_2\|\mathbf{v}\|_\infty \\
&\le \sqrt{\frac{\lambda_{\max}(\Gamma)}{\lambda_{\min}(\Gamma)}}\cdot\frac{1-\rho^{\frac{t}{2T_0}}}{-2T_0\rho^{\frac{1}{2}}\ln\rho}\|\Gamma\|_2\left(\frac{\|\eta\|_\infty\bar{\phi}}{\underline{m}} + \sigma|\theta|\right) \\
&\le \sqrt{\frac{\lambda_{\max}(\Gamma)}{\lambda_{\min}(\Gamma)}}\cdot\frac{\|\Gamma\|_2}{-2T_0\rho^{\frac{1}{2}}\ln\rho}\left(\frac{\bar{\phi}\|h_d\|_1}{\underline{m}}\delta + \sigma|\theta|\right),
\end{aligned} \tag{4.19}$$

where h_d, δ, and θ are unknown.

Combine (4.17) and (4.19), we have formed a contour of $\tilde{\theta}(t)$:

$$\left|\tilde{\theta}(t)\right| < \sqrt{\frac{\lambda_{\max}(\Gamma)}{\lambda_{\min}(\Gamma)}} \left\{ \rho^{\frac{t-T_0}{2T_0}} \left|\tilde{\theta}(0)\right| + \frac{\|\Gamma\|_2}{-2T_0\rho^{\frac{1}{2}} \ln \rho} \left(\frac{\bar{\phi}\|h_d\|_1}{\underline{m}} \delta + \sigma|\theta| \right) \right\}. \quad (4.20)$$

As the autonomous part will exponentially decay to zero, $\tilde{\theta}(t)$ will enter and stay in the bounded zone, i.e.

$$\exists t_0 \geq 0, \forall t \geq t_0, \quad \left|\tilde{\theta}(t)\right| \leq \sqrt{\frac{\lambda_{\max}(\Gamma)}{\lambda_{\min}(\Gamma)}} \cdot \frac{\|\Gamma\|_2}{-2T_0\rho^{\frac{1}{2}} \ln \rho} \left(\frac{\bar{\phi}\|h_d\|_1}{\underline{m}} \delta + \sigma|\theta| \right) \triangleq b_f, \quad (4.21)$$

where b_f is the bound of the estimation error $\left|\tilde{\theta}(t)\right|$.

From the above, efforts can be made to reduce the error bound by tuning the user-defined parameters, Γ, m, σ. For example, selecting smaller σ can help reduce the bound at a cost of slower convergence; bigger (more positive-definite) Γ will result in faster convergence but bigger noise in estimation, which is shown in the simulation.

Remark 6 *The inequality in (4.21) clearly shows the effects of disturbance on the frequency estimation. When there is no disturbance, i.e. $\delta = 0$, then σ is selected as 0, the frequency identifier will be reduced to a standard gradient estimator as in [96], [92], generating exponentially convergent estimates with zero errors. Similar results for frequency identifier design for pure sinusoidal signals have been developed in [86]. The proposed frequency identifier in this chapter is more general in the sense that it can be applied to estimate frequencies of both nominal sinusoidal signals and sinusoidal signals with disturbances.*

4.4 Application to Fault Detection

The above gradient based frequency identifier with leakage has demonstrated its robustness on disturbance d when the nominal frequencies are estimated.

In this section, we investigate the application of such robust frequency identifier to fault detection problem. More specifically, we extend the results in Section 4.3 to the case when the signal is subject to faults. Compared to the disturbance, the fault is not only unexpected but also manifest more drastic and harmful changes in many cases, hence it needs to be detected and isolated. A well designed fault detection scheme should be robust to the disturbance but sensitive to the faults.

Regarding the frequency estimation problem discussed above, faults can occur in various forms. In this section, both multiplicative type and additive type of faults are considered. Particularly, the fault induced frequency shift and additional frequency components are investigated. In this case, the signal (4.5) may be rewritten into two forms:

$$Z(s) = \theta'^T \phi'(s) + \eta'(s) + \eta_0'(s) \quad \text{or} \tag{4.22}$$

$$Z(s) = \theta^T \phi(s) + \eta_f(s) + \eta_0(s). \tag{4.23}$$

Here (4.22) is the signal model with the fault-induced frequency shift, while (4.23) is the model with additive fault components.

$$\eta'(s) \triangleq \frac{q'(s)}{\Lambda(s)} d(s) \triangleq H_d'(s) d(s), \qquad \eta_0'(s) \triangleq \frac{p'(s)}{\Lambda(s)},$$
$$\eta_f(s) \triangleq \frac{q(s)}{\Lambda(s)} d(s) + (\theta' - \theta)^T \phi(s) \triangleq H_d(s) d(s) + f_\theta^T \phi(s),$$

where q', p', ϕ', η', and η_0' have the same expressions as q, p, ϕ, η, and η_0 respectively, but are determined by the new frequency θ' caused by the fault.

4.4.1 Frequency shift

One type of fault (commonly seen in the rotational machine fault detection and condition monitoring problem) many cause the shift (variation) on the original frequencies. Hereby we assume that the nominal frequencies $\mathbf{w}$ are known. Hence the parameter vector θ and the parameter bound b_f for the fault-free case are also known. After the occurrence of the fault, the frequency vector (excluding d) shifts from the nominal value $\mathbf{w}$ to $\mathbf{w}'$, the unknown fault induced frequencies. As a result, the corresponding parameter θ changes to the new value θ', which can be written as $\theta' = \theta + f_\theta$. The problem of interests is to detect such a change based on the signal measurement, which is also corrupted with external disturbances. In this case, the residual signal is generated by using the frequency identifier developed in Section 2 and defined as:

$$r(t) = \theta - \hat{\theta}(t) \tag{4.24}$$

For the signal model in (4.22), the boundary expression (4.21) can be rewritten as

$$|r(t) + f_\theta| = \left|\theta' - \hat{\theta}(t)\right| \leq \sqrt{\frac{\lambda_{\max}(\Gamma)}{\lambda_{\min}(\Gamma)}} \cdot \frac{\|\Gamma\|_2}{-2T_0\rho^{\frac{1}{2}}\ln\rho}\left(\frac{\bar{\phi}\|h_d'\|_1}{\underline{m}}\delta + \sigma|\theta'|\right) \triangleq b_f', \tag{4.25}$$

where $h_d'(t)$ is the impulse response of $H_d'(s)$, and b_f' is the counterpart of b_f but determined by θ'. ρ, $\underline{m}$, T_0 may be different from those in the fault-free case due to the fault's effect on y, whereas they still have the same parametric form as defined above.

We perform further analysis of the above inequality by using the triangular inequality properties:

$$\begin{aligned} b_f' \geq |r(t) + f_\theta| \geq |r(t)| - |f_\theta| \quad &\Rightarrow \quad |r(t)| \leq |f_\theta| + b_f', \\ |f_\theta| - b_f' \leq |f_\theta| - |r(t) + f_\theta| \leq |f_\theta - (r(t) + f_\theta)| \quad &\Rightarrow \quad |r(t)| \geq |f_\theta| - b_f'. \end{aligned}$$

The second inequality is under the assumption that $|f_\theta| - b_f' > 0$. We may summarize the above as

$$\max\left\{|f_\theta| - b_f', 0\right\} \leq |r(t)| \leq |f_\theta| + b_f' \tag{4.26}$$

Based on the above analysis, we have

$$\begin{cases} 0 \leq |r(t)| \leq b'_f & \text{when} \quad |f_\theta| = 0 \\ 0 \leq |r(t)| \leq 2b'_f & \text{when} \quad 0 \leq |f_\theta| \leq b'_f \\ |r(t)| > 0 & \text{when} \quad |f_\theta| > b'_f \\ |r(t)| \geq b_f & \text{when} \quad |f_\theta| \geq b'_f + b_f \end{cases}$$

In this case, one way to detect the fault is to adopt the estimation bound b_f in the noise-free case as the threshold. When the fault $f_\theta = 0$, the residual is mainly caused by the disturbance d and its norm is bounded by the threshold. When the fault starts to develop but is still less than the new estimation bound, the residual signal starts to change but is centered around zero. The residual vector is restricted in an spherical shell with the radius $2b'_f$. In this case, the fault is hard to be detected since it resembles the effects caused by disturbances. When the fault is developing and eventually becomes obvious enough so that $|f_\theta| > b'_f + b_f$, the fault can be flagged. Obviously, when fault size is small it may not be detected. To increase the sensitivity, one can select a lower threshold, for example, choose it as αb_f, where $\alpha \in (0,\ 1]$. As a trade-off, the chance of false alarm also increases.

4.4.2 Additive fault

Another type of frequently occurring fault is the appearance of additional frequency components in an additive fault signal. The general form of the fault f is

$$f = \begin{cases} 0, & 0 \leq t < t_f \\ \sum_{i=1}^{m} A_{f_i} \sin\left(w_{f_i}(t - t_f) + \phi_{f_i}\right), & t \geq t_f \end{cases} \tag{4.27}$$

with t_f as the fault occurrence time, $A_{f_i}(> 0)$, w_{f_i} , and ϕ_{f_i} respectively as the magnitude, the frequency, and the phase of the i^{th} fault component. Here we assume $t_f = 0$ in the following derivation.

(4.23) is suitable for modeling the signal in this case. Define

$$d' \triangleq d + f = d + \sum_{i=1}^{m} A_{f_i} \sin\left(w_{f_i} t + \phi_{f_i}\right). \tag{4.28}$$

Then following (4.19) we have the following derivation:

$$\begin{aligned}
|r(t)| = \left|\tilde{\theta}(t)\right| &\le \sqrt{\frac{\lambda_{\max}(\Gamma)}{\lambda_{\min}(\Gamma)}} \cdot \frac{\|\Gamma\|_2}{-2T_0\rho^{\frac{1}{2}}\ln\rho}\left(\frac{\|h_d * d'\|_\infty \bar{\phi}}{m} + \sigma|\theta|\right) \\
&= \sqrt{\frac{\lambda_{\max}(\Gamma)}{\lambda_{\min}(\Gamma)}} \cdot \frac{\|\Gamma\|_2}{-2T_0\rho^{\frac{1}{2}}\ln\rho}\left(\frac{\|h_d\|_1\|d'\|_\infty}{m}\bar{\phi} + \sigma|\theta|\right) \\
&\le \sqrt{\frac{\lambda_{\max}(\Gamma)}{\lambda_{\min}(\Gamma)}} \cdot \frac{\|\Gamma\|_2}{-2T_0\rho^{\frac{1}{2}}\ln\rho}\left(\frac{\delta + \sum_{i=1}^m A_{f_i}}{m}\|h_d\|_1\bar{\phi} + \sigma|\theta|\right) \\
&= b_f + \sqrt{\frac{\lambda_{\max}(\Gamma)}{\lambda_{\min}(\Gamma)}} \cdot \frac{\|\Gamma\|_2}{-2T_0\rho^{\frac{1}{2}}\ln\rho} \cdot \frac{\|h_d\|_1\bar{\phi}}{m}\sum_{i=1}^m A_{f_i}. \qquad (4.29)
\end{aligned}$$

b_f is the original bound shown in (4.21) and it can be calculated based on the assumption that the nominal frequencies are known (so is θ). The additional frequency components increase the estimation error which can be taken as a sign of fault. However by compounding f and d in this model, the fault detection becomes less effective compared to the case with multiplicative frequency shift discussed before.

4.5 Simulation

Simulation is firstly carried out with respect to the estimation of the frequency of a machinery vibration signal collected from a motor shaft. The fault detection function listed in subtopic 4.4 is then tested on a hydraulic rig model. The simulation results are presented and discussed.

4.5.1 Frequency estimation (gradient estimator with leakage)

In this simulation study, frequency identifier is tested to estimate the major frequency(-ies) of a sequence of vibration data recorded from a motor, . Cracks on the motor gears may cause the vibration on the shaft, i.e., the oscillation on the coordinates of the axis.

Define m^2 as in (4.9) and the linear filter $\Lambda(s) = (s + 10)^3$, whose order is higher than $2n = 2$: it makes $H_d(s)$ strictly proper so that (4.21) applies. Select parameters as $\Gamma = 3.0 \times 10^4$, $\sigma = 2.8 \times 10^{-7}$, with the initial guess $w_0 = 0.4$. Besides, the estimate curve generated by the methodology in [54] is used for comparison, with the gain selected as $\gamma_{\text{Hou}} = 1$. The estimation results, along with the original vibration data sequence and its frequency spectrum, is shown in Fig. 4.1.

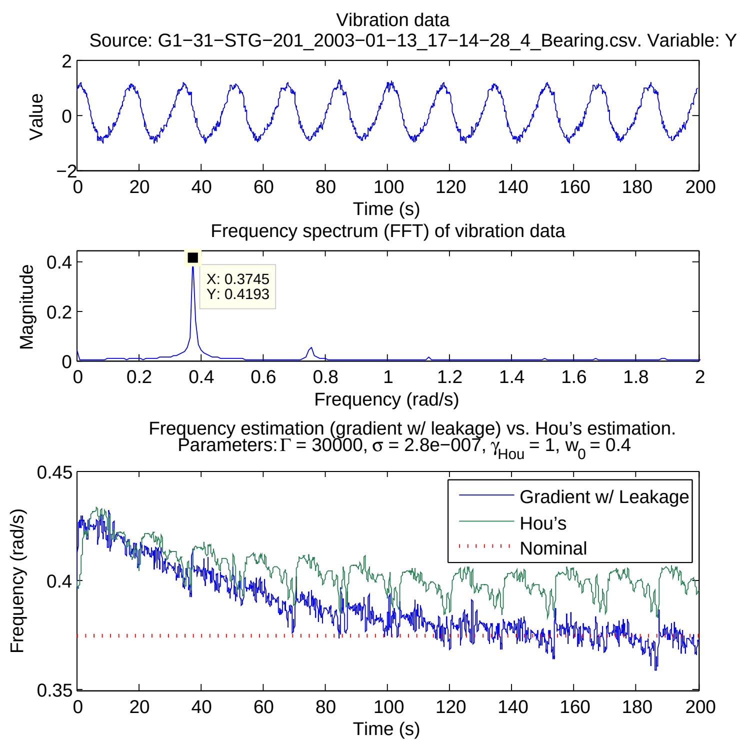

Figure 4.1: Vibration data and the frequency estimate using the gradient estimator with leakage, compared with the estimate using the method in [54].

Fig. 4.1 shows that the estimation result based on the gradient estimator with leakage agrees with the main frequency of the vibration. Although it presents noticeable oscillation, it converges relatively fast. In contrast, the estimation from the methodology in [54] failed to converge to the nominal frequency, reflecting the improvement of the proposed frequency when treating disturbances/noises in the signal.

Further analysis has been carried out for retrieving more properties. Firstly the experiment with different initial guesses was carried out, in order to show the impact of the initial guess on convergence. The result is shown in Fig. 4.2, where $\Gamma = 2 \times 10^4$, $\Lambda(s) = (s + 10)^3$, and $\sigma = 2.8 \times 10^{-7}$.

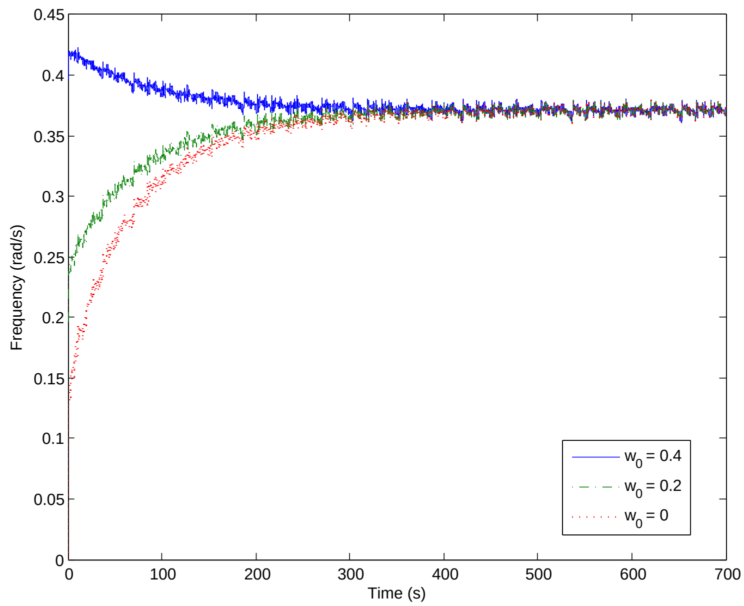

Figure 4.2: Frequency estimates of vibration data with multiple choices of w_0.

In Fig. 4.2, the estimates all approach to the same value, regardless of different initial values, 0, 0.2, or 0.4. It indicates in this design, the initial guess does not affect the convergence and the final value.

Secondly, we study the effect of the tuning parameter Γ on the estimation. Fig. 4.3 provides the estimation result with different Γ $(3\times10^4, 2\times10^4, 1\times10^4)$, where $\Lambda(s) = (s + 10)^3$, $w_0 = 0.2$, and $\sigma = 2.8 \times 10^{-7}$.

Fig. 4.3 shows that with Γ increasing, the convergence will be faster but with more noticeable oscillations. It reflects a trade-off in selecting Γ.

4.5.2 Fault detection (hydraulic rig model)

The fault detection tests have also been carried out on a hydraulic rig model. The key part of the hydraulic is a stiff shaft, with a hydraulic motor giving

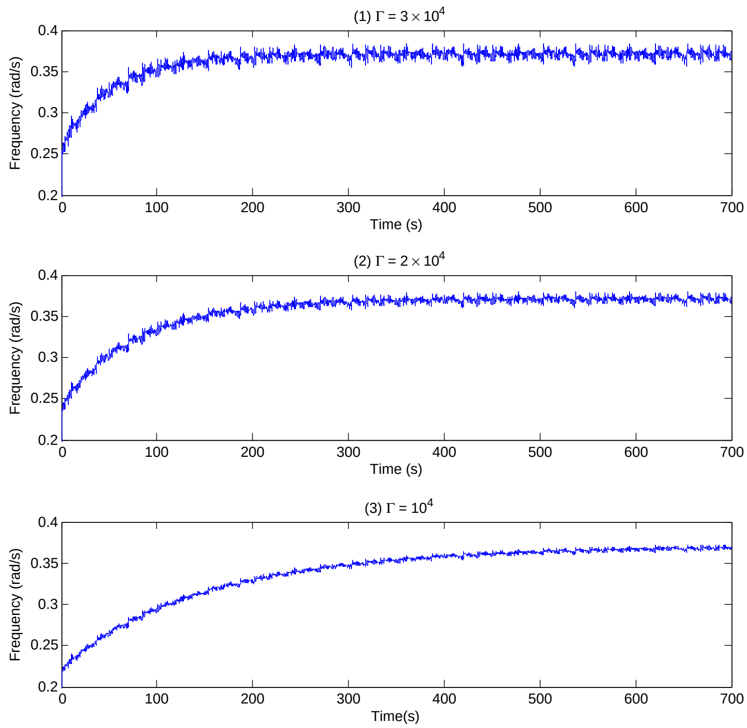

Figure 4.3: Frequency estimates of vibration data with multiple choices of Γ.

driving force and a hydraulic pump giving load [97]. Fig. 4.4 provides its systematic structure [98]:

The list of parameters is in Table 4.1:[2]

In [97] a second-order model for the servo motor is adopted; i.e. its displacement X_s is of a second order dynamics with its voltage input v. According to [99], the servo motor displacement X_s, along with the pressure differential across the motor P_m, control the oil flow rate across the hydraulic motor, so that the servo valve affects the hydraulic motor rotating speed $\dot{\theta}$. Based on the mechanic properties of the hydraulic motor itself, a first-order dynamics between $\dot{\theta}$ and the pressure differential across the pump P_p [98]. In summary, a nonlinear model of the hydraulic rig is established, with the definition of the state vector $\mathbf{x} = \begin{bmatrix} P_m, & \dot{\theta}, & X_s, & \dot{X}_s \end{bmatrix}^T \triangleq \begin{bmatrix} x_1, & x_2, & x_3, & x_4 \end{bmatrix}^T$, the input vector

[2] K_s is treated as time-varying in the second fault case.

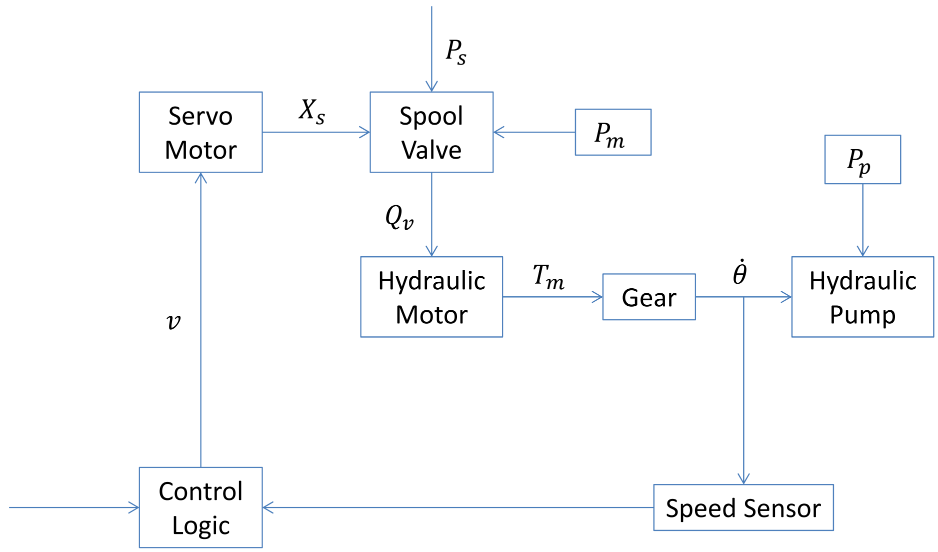

Figure 4.4: Hydraulic rig scheme [98]

Table 4.1: List of the parameters of the hydraulic model [99]

Parameter	Value	Description
P_s	140bar	Supply pressure (constant)
T_1	0.02s	Electro-magnetic time constant of the valve
T_2	0.01s	Electro-mechanic time constant of the valve
V_t	0.01gallon	Total trapped volume
K_s	-0.48	The valve electro-magnetic gain
K_θ	2.4	The valve flow coefficient
C_r	0.01cc	Motor displacement
β	3.30	Oil bulk modulus
K_l	0.15	Leakage coefficient
η_m	0.95	Motor efficiency
η_p	0.89	Pump efficiency
I	1.0×10^{-5}	Total inertia of pump, motor & shaft
D	9.0×10^{-5}	Viscous friction coefficient

$\mathbf{u} = \begin{bmatrix} v, & P_p \end{bmatrix}^T \triangleq \begin{bmatrix} u_1, & u_2 \end{bmatrix}^T$ [97], [98], [99]:

$$\begin{aligned} \dot{\mathbf{x}} &= f(\mathbf{x}) + g(\mathbf{x})\mathbf{u} \\ &\triangleq \begin{bmatrix} -\frac{2\beta K_l}{V_t}x_1 - \frac{2\beta C_r}{V_t}x_2 + \frac{2\beta K_\theta}{V_t}x_3\sqrt{P_s - x_1} \\ \frac{C_r\eta_m}{I}x_1 - \frac{D}{I}x_2 \\ x_4 \\ -\frac{1}{T_1T_2}x_3 - \frac{T_1+T_2}{T_1T_2}x_4 \end{bmatrix} + \begin{bmatrix} 0 & 0 \\ 0 & -\frac{C_r}{I\eta_p} \\ 0 & 0 \\ \frac{K_s}{T_1T_2} & 0 \end{bmatrix}\mathbf{u}. \end{aligned} \tag{4.30}$$

Two types of faults are respectively investigated: (1) frequency shift on the input v, and (2) oscillation on the parameter K_s. Due to the properties of the fault cases studied, we may only monitor $x_3 = X_s$ as the output and decouple $\begin{bmatrix} x_3, & x_4 \end{bmatrix}^T$ as the reduced state vector.

The input is set to $v(t) = \sin(1.2\pi t)$ with its main frequency $w = 0.6$rad/s before the fault occurrence. Note that in a stable system only the frequencies of the input will be preserved in long term; thus the frequency of x_3 is to be estimated as $\hat{w}(t)$, from which $\hat{\theta}$ and the residual r are defined. In order to inspect its sensitivity and robustness, a disturbance $d = 0.1\sin(3.6\pi t + \frac{5\pi}{11})$ with the frequency $w_d = 1.8$rad/s and a Gaussian white noise with the distribution $\mathcal{N}(0, 0.01)$ are introduced to the output sensor.

Frequency shift on v

Firstly we investigate the effect of frequency shift on v on the gradient estimator with the leakage. Ding categorizes it as an additive actuator fault [1]. It is expected not only the capability of detecting the fault, but also the robustness with the existence of the output disturbance and noise.

Assume the fault occurs at $t_f = 50$s and changes the frequency of v from $w = 1.2\pi$rad/s to $w_f = 2.4\pi$rad/s. Select $\Gamma = 4.0 \times 10^6$, $\sigma = 1.0 \times 10^{-9}$ and define the residual signal r as in (4.24). The input $v(t)$, the real-time frequency estimate $\hat{w}(t)$, and $|r(t)|$ are plotted in Fig. 4.5:

Fig. 4.5 shows obvious transient and final value change in $\hat{w}(t)$ and $r(t)$ after the fault occurs, indicating that the gradient estimator with leakage

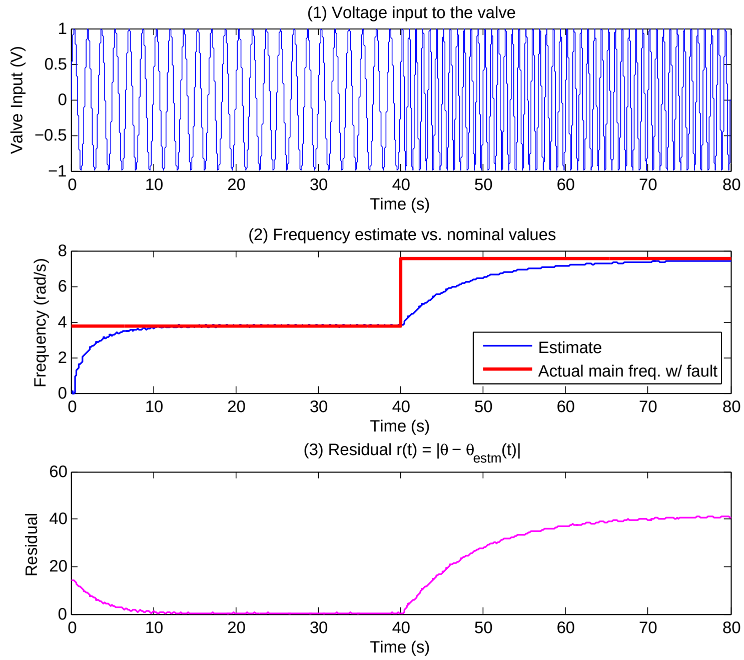

Figure 4.5: Fault detection of the hydraulic rig: frequency shift on v

is capable of detecting such a fault effectively. The results in the second subplot demonstrates the effectiveness of this gradient estimator in estimating frequencies and tracking changes in real-time.

Oscillation on K_s

Here a different case of fault is studied: the parameter K_s changes from a constant to an oscillating one, which is categorized as a multiplicative actuator fault in [1]. Assume the fault occurs at $t_f = 50$s, leading to a time-varying K_s:

$$K_s = \begin{cases} -0.48, & 0 \leq t < t_f \\ -0.48\left(1 + 0.6\sin(1.2\pi(t - t_f))\right), & t \geq t_f \end{cases}$$

Select $\Gamma = 4.0 \times 10^6$, $\sigma = 1.0 \times 10^{-9}$ and define the residual r as in (4.24). The time-varying $K_s(t)$, the valve displacement (output) $X_s(t)$ passed by the sensor, and $|r(t)|$ are plotted in Fig. 4.6:

According to Fig. 4.6, the dominant status of the major frequency is weakened by the multiplicative fault. As a result, the residual rise from a level near zero to around some obvious value, and thus the fault will be detected if

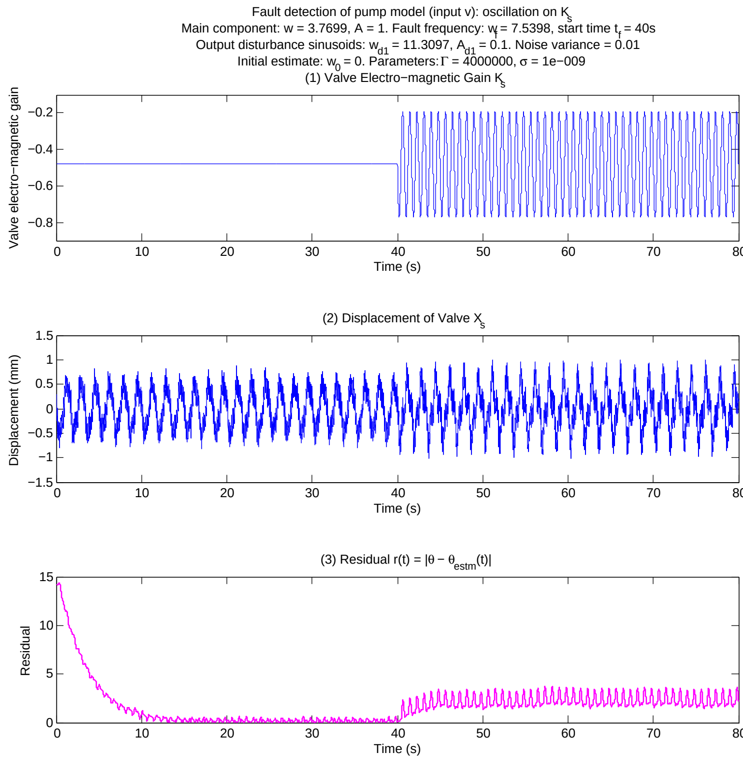

Figure 4.6: Fault detection of the hydraulic rig: oscillation K_s

the threshold is set properly.

4.6 Conclusion

This chapter has investigated the problem of estimating unknown frequencies of a given sinusoidal signal with disturbances and noises, as well as its usages for fault detection. The framework combining a parametric linear model and a gradient estimator with leakage forms the core of the thesis, under which the stability, the adaptivity, and the robustness are inspected. The parametric linear model builds up states providing sufficient information to get the frequency estimated, based on which the gradient estimator generates frequency estimates with the estimation error restricted to a certain bounded zone. The estimation mechanism can be also used for fault detection, as it achieves not only the tolerance to disturbances but also the sensitivity of faults. Simulations have verified its feasibility and capability of estimating frequencies and detecting faults.

Chapter 5

Upper-level Reliability Analysis

5.1 Introduction

Different from the other three research chapters, Chapter 5 concentrates on the contour of long term behaviors of faulted sequences. With well-defined states and transition behaviors among them, probabilistic kernel equations are introduced to describe the dynamic behavior of the fault. A commonly accepted definition of reliability is adopted to picturing the probabilistic usefulness of the detection upon time. Within the thesis scope, this chapter explores the top layer of the structure scheme as in Fig. 1.3, mainly characterization analysis, and gives FD performance evaluation from a different perspective compared with Chapter 3.

The rest part of the chapter is organized as follows. Under the assumption of Gaussian noises, two models of joint semi-Markov process are respectively provided in Section 5.2 and 5.4. The first (simple) model is for examining the feasibility of this kernel-based description, while the second (complex) model is a closer approximation of the actual fault/detection sequences. Section 5.5 provides the probabilistic reliability analysis based on the second model, while Section 5.6 examines the theoretical deduction in the simulation. The result indicates the feasibility and preciseness of the kernel-based reliability index.

5.2 Fault and Detection Processes

The research is about the reliability analysis with respect to semi-Markov fault and detection processes. A conceptual model of fault tolerant control systems subject to fault process $\zeta(t)$ has been provided in [111] and [78], featured for its diagnostic control input $u(t)$ subject to the detection process $\eta(t)$:

$$\begin{cases} \dot{\mathbf{x}}(t) = \mathbf{A}(\zeta(t), \Delta)\mathbf{x}(t) + \mathbf{B}(\zeta(t), \Delta)\mathbf{u}(\eta(t), t) + \mathbf{E}(\zeta(t), \Delta)\mathbf{w}(t), \\ \mathbf{y}(t) = \mathbf{C}(\zeta(t), \Delta)\mathbf{x}(t) + \mathbf{D}(\zeta(t), \Delta)\mathbf{w}(t) + \mathbf{F}(\zeta(t), \Delta)\mathbf{u}(\eta(t), t). \end{cases} \tag{5.1}$$

The concepts of ζ and η are used in our research, where they appear in the discrete-time form ζ_n and η_n with n as the time index. The results in [111] and [78] require Markov fault and detection processes, which is replaced by a weaker assumption, i.e. semi-Markovian ζ and η, in our research.

Following [112], we formulate the processes using Markov renewal properties as the follows. Semi-Markov fault process $\{\zeta_n\}$ and detection process $\{\eta_n\}$ can be expressed using the corresponding Markov renewal process pair $(\zeta(k),\ m_\zeta(k))$ and $(\eta(k),\ m_\eta(k))$, where $k = 0, 1, 2, \cdots$ denotes the k^{th} jump, $m_\zeta(k)$ and $m_\eta(k)$ denotes the sojourn time at the state $\zeta(k)$ and $\eta(k)$. It is obvious that the state processes $\{\zeta(k)\}$ and $\{\eta(k)\}$ with respect to k are Markovian.

In order to simplify the problem, we have further assumptions, referring to the ideas from [63]:

1. Alternative jump: Given $\zeta(0) = \eta(0)$, $n_\zeta(1) < n_\eta(1) < n_\zeta(2) < n_\eta(2) < \cdots$, where $n_\zeta(k) \triangleq \sum_{i=0}^{k-1} m_\zeta(k)$, $n_\eta(k) \triangleq \sum_{i=0}^{k-1} m_\eta(k)$, respectively the k^{th} jump time of ζ and η.

2. For any n with $\zeta_n = \eta_n$, η will not jump until ζ does, where ζ comes with the jump-counts-invariant transition rate $g_{ij}(m_\zeta)$ for one step and the cumulative transition rate $G_{ij}(m_\zeta)$ with m_η defined as the sampling interval counts since the last jump time of η. For any n with $\zeta_n \neq \eta_n$, ζ

will not jump until η does, where η comes with the jump-counts-invariant transition rate $h_{ij}(m_\eta)$ for one step and the cumulative transition rate $H_{ij}(m_\eta)$ with m_η defined as the sampling interval counts since the last jump time of ζ.

A common way to define transition rate of ζ and η after corresponding jumping edges is provided here and will be used in the following parts:

$$G_{ii}(m_\zeta) = \prod_{m=1}^{m_\zeta} g_{ii}(m), \quad G_{ij}(m_\zeta) = g_{ij}(m_\zeta) \prod_{m=1}^{m_\zeta - 1} g_{ii}(m) = (1 - g_{ii}(m_\zeta)) \prod_{m=1}^{m_\zeta - 1} g_{ii}(m), \tag{5.2}$$

$$H_{ii}(m_\eta) = \prod_{m=1}^{m_\eta} h_{ii}(m), \quad H_{ij}(m_\eta) = h_{ij}(m_\eta) \prod_{m=1}^{m_\eta - 1} h_{ii}(m) = (1 - h_{ii}(m_\eta)) \prod_{m=1}^{m_\eta - 1} h_{ii}(m), \tag{5.3}$$

where $\{i,\ j\} = \{0,\ 1\}$, $i \neq j$, and the time-varying one-step transition probabilities satisfy $g_{ii}(m) + g_{ij}(m) = 1$ and $h_{ii}(m) + h_{ij}(m) = 1$, [112], [113].

5.3 Semi-Markov Modeling and Kernels

Referring to [112], we may also define a process X^R for reliability evolution, with respect to which the kernels for calculating conditional reliability will be defined. As X^R is concerning the reliability of FDI, it should cover both ζ and η. Here we set up four states for X^R as they covers all the combination patterns of ζ_n and η_n:

$$X_n^R = \begin{cases} 0, & \zeta_n = 0, \quad \eta_n = 0; \\ 1, & \zeta_n = 1, \quad \eta_n = 0; \\ 2, & \zeta_n = 1, \quad \eta_n = 1; \\ 3, & \zeta_n = 0, \quad \eta_n = 1. \end{cases} \tag{5.4}$$

With the assumptions above, the one-step state transition of X^R follows:

1. It may stay at its current state or transit to other states;

2. The alternation of states of X^R must follow the order: $0 \to 1 \to 2 \to 3 \to 0 \to \cdots$. No reverse or crossing flow.

The state flow diagram of X^R and an example of the triplet (ζ, η, X^R) are provided in Fig. 5.1 as a visual demonstration of the definitions and assumptions above:

According to the state flow diagram, one important property of $\{X_n^R\}$ is that X^R is a semi-Markov processes and thus can be expressed using the Markov renewal pair $(X^R(k),\ m_R(k))$, although neither ζ nor η is semi-Markov in the strict sense.

Now we start to calculate the semi-Markov kernels, i.e. the conditional probability of the sojourn time and the next state given the current state at the latest jump time. It is easy to conclude that the k^{th} sojourn (and jump) time of the corresponding Markovian state $X^R(k)$, respectively denoted with $m_R(k)$ (and $n_R(k)$), satisfies the following relation (given $\zeta(0) = \eta(0)$):

$$m_R(k) = \left\{ \begin{array}{ll} m_\zeta(2i+1) - m_\eta(2i), & k = 4i \\ m_\eta(2i+1) - m_\zeta(2i+1), & k = 4i+1 \\ m_\zeta(2i+2) - m_\eta(2i+1), & k = 4i+2 \\ m_\eta(2i+2) - m_\zeta(2i+2), & k = 4i+3 \end{array} \right\}, \text{ where } i = 0,\ 1,\ 2,\ \cdots . \tag{5.5}$$

Define the kernel form as[1] by following [112]:

$$Q^R(i,j,m) = \Pr\{X^R_{n_R(k)+m} = j,\ X^R_{n_R(k)+m-1} = \cdots = X^R_{n_R(k)+1} = i | X^R_{n_R(k)} = i\}, \tag{5.6}$$

$$\text{or } Q_s^R(i,j,m) = \Pr\{X^R(k+1) = j,\ m_R(k) = m | X^R(k) = i\}. \tag{5.7}$$

where the probability is irrelevant to the jump index k. As Q_s^R is defined regarding the sojourn time, only the case $i \neq j$ is considered in (5.7) without loss of generality.

Similar to [112], we give the specific expressions of kernels using transition

[1]Kernels defined in Section 5.3 and 5.4 are more similar to those used in [112]. In contrast, the kernel form defined in Section 5.5 are proposed in [114].

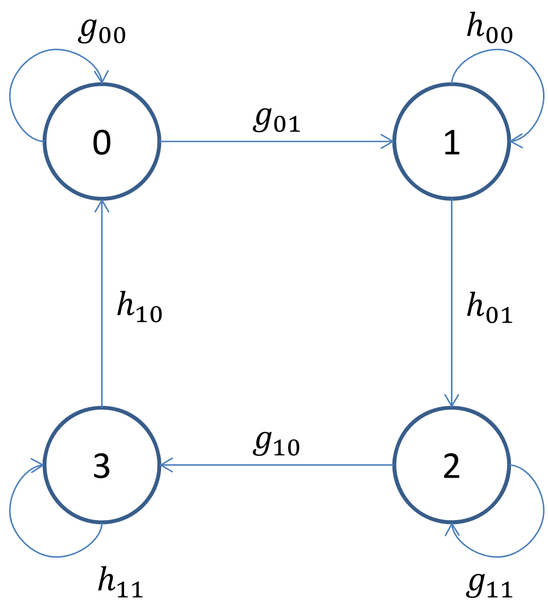

(a) State flow diagram, where the one-step transition rates may be time-varying

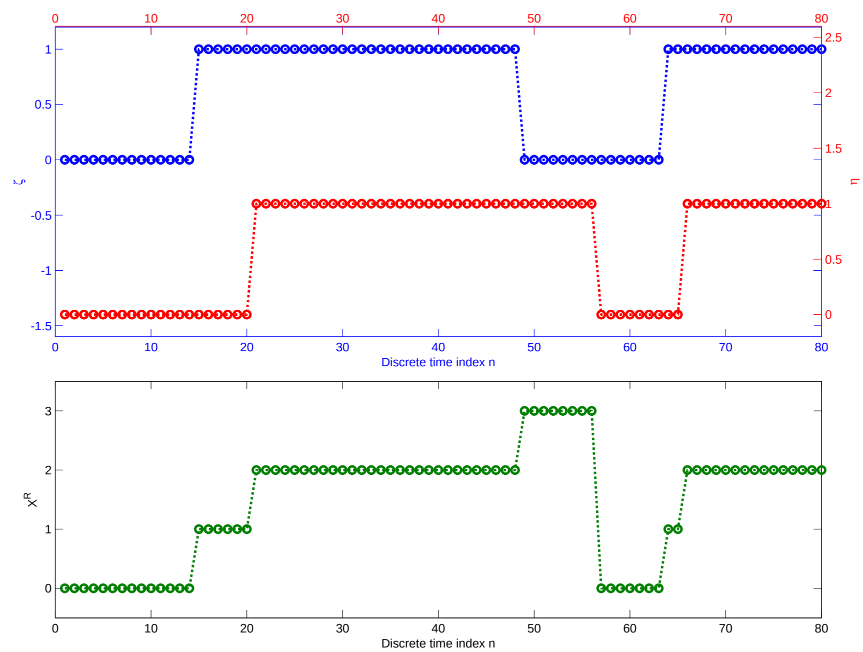

(b) Example of ζ (blue), η (red), and X^R (green)

Figure 5.1: Visual demonstration of the semi-Markov process X^R (one-way flow)

rates as in (5.2) and (5.3):

$$
\begin{aligned}
Q^R(0,0,m) &= G_{00}(m) = && \prod_{l=1}^{m} g_{00}(l);\\
Q^R(0,1,m) &= G_{01}(m) = && g_{01}(m)\prod_{l=1}^{m-1} g_{00}(l);\\
Q^R(1,1,m) &= H_{00}(m) = && \prod_{l=1}^{m} h_{00}(l);\\
Q^R(1,2,m) &= H_{01}(m) = && h_{01}(m)\prod_{l=1}^{m-1} h_{00}(l);\\
Q^R(2,2,m) &= G_{11}(m) = && \prod_{l=1}^{m} g_{11}(l);\\
Q^R(2,3,m) &= G_{10}(m) = && g_{10}(m)\prod_{l=1}^{m-1} g_{11}(l);\\
Q^R(3,3,m) &= H_{11}(m) = && \prod_{l=1}^{m} h_{11}(l);\\
Q^R(3,0,m) &= H_{10}(m) = && h_{10}(m)\prod_{l=1}^{m-1} h_{11}(l).
\end{aligned}
$$

5.4 Complex Modeling

Here we switch to a complex modeling of semi-Markov processes $(\zeta,\ \eta)$, which is more likely to occur in practice. The core idea is that the fault process ζ can have its states switched in a random manner independent from η, while the detection process η follows ζ with random delays. The desired state diagram and an example of the triplet $(\zeta,\ \eta,\ X^R)$ are as in Fig. 5.2:

A different set of assumptions applies to Fig. 5.2, compared with those in Section 5.2:

1. $\Pr(\eta_{n+m} = \eta_{n+m-1} = \cdots = \eta_{n+1} = i | \eta_n = i,\ \zeta_{n+m-1} = \cdots = \zeta_n = i,\ \zeta_{n+m} = j) = 1$, for $\{i,\ j\} \in \{0,\ 1\}$, $i \neq j$, $\forall n, m \in \mathbb{N}$. In other words, for identical state pairs $\zeta_n = \eta_n$, η keeps the state value until ζ jumps.

2. $\{\zeta_n\}$ is Markov;

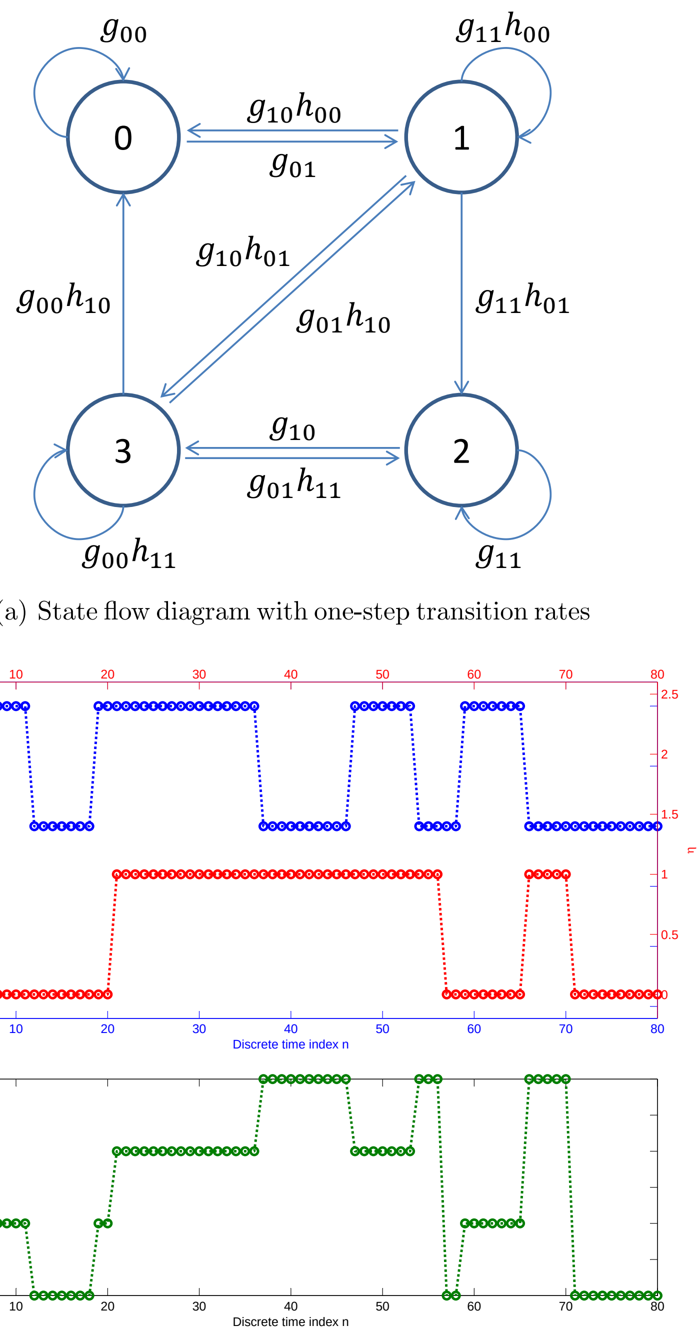

(a) State flow diagram with one-step transition rates

(b) Example of ζ (blue), η (red), and X^R (green)

Figure 5.2: Visual demonstration of the semi-Markov process X^R (complex modeling)

3. the dependent process $\{\eta_n\}$ is semi-Markov in time subsequence $\{n : \eta_n \neq \zeta_n\}$.

Remark 7 *If $\{\zeta_n\}$ is not Markov, the one-step transition probabilities of X^R rightly after jumps of X^R from 3 to 0 and from 1 to 2 depends on the states before the nearest jumping edge, which is a jumping edge of η. As a result, $\{X_n^R\}$ is not semi-Markov.*

Remark 8 *Note that $\{X_n^R : n \in \mathbb{N}\}\}$ is a semi-Markov process given the assumptions above, while $\{\eta_n\}$ is not a semi-Markov process along the entire time span in general cases. If The one-step jumping rates of η, i.e. $h_{00}(m)$, $h_{01}(m)$, $h_{11}(m)$, and $h_{10}(m)$, are time-varying upon the jumping edges, then $\{m_\eta(k)\}$ is not i.i.d. and thus not a renewal process. According to the definition, $(\eta(k),\ n_\eta(k))$ is not a Markov renewal process, and $\{\eta_n\}$ is not semi-Markov.*

More kernel equations exist for this model due to more complex state transitions. Similar to [112] and Section 5.3, here we derive the kernel equations following the definition in (5.6):

$$
\begin{aligned}
Q^R(0,0,m) &= g_{00}^m; \\
Q^R(0,1,m) &= g_{01} g_{00}^{m-1}; \\
Q^R(1,0,m) &= g_{10} g_{11}^{m-1} \prod_{l=1}^{m} h_{00}(l); \\
Q^R(1,1,m) &= g_{11}^m \prod_{l=1}^{m} h_{00}(l); \\
Q^R(1,2,m) &= g_{11}^m h_{01}(m) \prod_{l=1}^{m-1} h_{00}(l); \\
Q^R(1,3,m) &= g_{10} g_{11}^{m-1} h_{01}(m) \prod_{l=1}^{m-1} h_{00}(l); \\
Q^R(2,2,m) &= g_{11}^m; \\
Q^R(2,3,m) &= g_{10} g_{11}^{m-1};
\end{aligned}
$$

$$
\begin{aligned}
Q^R(3,0,m) &= g_{00}^m h_{10}(m) \prod_{l=1}^{m-1} h_{11}(l); \\
Q^R(3,1,m) &= g_{01} g_{00}^{m-1} h_{10}(m) \prod_{l=1}^{m-1} h_{11}(l); \\
Q^R(3,2,m) &= g_{01} g_{00}^{m-1} \prod_{l=1}^{m} h_{11}(l); \\
Q^R(3,3,m) &= g_{00}^m \prod_{l=1}^{m} h_{11}(l).
\end{aligned}
$$

5.5 Reliability Analysis with Up-Down States

After determining the semi-Markov process X^R and its kernel equations, we expect a reliability function upon time, reflecting the effectiveness of the fault detection. The reliability framework based on the research of [114] is now introduced, which highlights the difference and transition between the up (good, normal) states u and the down (bad, failure) states d. According to [114], the reliability $R(n)$ is defined as the probability for the first hitting time at any down state to appear later than the time n: equivalently it is opposite to the case that the down state occurs no later than n, i.e.

$$
R(n) \triangleq 1 - \Pr(\exists k \leq n,\ X^R(k) = -1) = 1 - \Pr(X^R(n) = -1) \tag{5.8}
$$

as the down state is absorbing.

Barbu has also proposed an algorithm to calculate the reliability $R(n)$, [114]:

$$
R(n) = \mu \cdot ((\delta I - q)^{(-1)} * (I - \Lambda))(n) \cdot \mathbf{1}_{u+d,u} = \mu_u((\delta I - q)_{u,u}^{(-1)} * (I - \Lambda_{u,u}))(n) \mathbf{1}_{u,u}, \tag{5.9}
$$

given the following definitions and assumptions [114]:

- Initial state probability (distribution) row vector $\mu = [\mu_u,\ \mu_d]$.

- Convolution of discrete-time matrix sequences has the element-wise definition:

$$C_{ij}(n) = (A * B)_{ij}(n) \triangleq \sum_{k} \sum_{l=0}^{n} A_{ik}(n-l) B_{kj}(l). \tag{5.10}$$

- Kernel matrix $q(n) = \begin{bmatrix} q_{u,u}, & q_{u,d} \\ q_{d,u} & q_{d,d} \end{bmatrix}$. The element in the i^{th} row and j^{th} column satisfies $q_{ij}(m) \triangleq \mathbf{1}_{\{i \neq j\}} \cdot \Pr\{X^R_{n_R(k)+m} = j,\ X^R_{n_R(k)+m-1} = \cdots = X^R_{n_R(k)+1} = i | X^R_{n_R(k)} = i\}$. Especially, $q_{ii}(m) = 0$ and $q_{ij}(0) = 0$ for any state $i,\ j$.

- For the square matrix sequence $(\delta I)(n)$, it satisfies

$$(\delta I)(n) = \mathbf{1}_{\{n=0\}} \cdot I = \begin{cases} I, & n = 0; \\ 0, & n \geq 1. \end{cases} \tag{5.11}$$

  and $(\delta I - q)^{(-1)}(n)$ obeys the following recursive algorithm:

$$(\delta I - q)^{(-1)}(n) = \begin{cases} I, & n = 0; \\ -\sum_{l=0}^{n-1} (\delta I - q)^{(-1)}(l)(\delta I - q)(n-l), & n \geq 1. \end{cases} \tag{5.12}$$

- $\Lambda(n) = \text{diag}\{\Lambda_u(n),\ \Lambda_d(n)\}$. Each element

$$\Lambda_i(n) \triangleq \sum_{l=1}^{n} \lambda_i(l) \triangleq \sum_{l=1}^{n} \sum_{k} q_{ik}(l). \tag{5.13}$$

  Physically, $\lambda_i(n)$ denotes the probability of sojourn time equal to n in State i, and $\Lambda_i(n)$ denotes the probability of sojourn time less than or equal to n in State i.

- $\mathbf{1}_{u+d,u} \triangleq [1,\ \cdots,\ 1,\ 0,\ \cdots,\ 0]^T$, where the first u elements equal to one and the rest d elements equal to zero, where u and d are respectively the dimension of up and down states. $\mathbf{1}_{u,u}$ is thus an all-one column vector.

Considering the FHT property of this reliability index and the definition of failure state in [112], we propose the following principles regarding the modeling of sequences as in Section 5.4, with the failure state considered:

- State 0, 1, 2, 3 are considered as up states.

- X^R enters the down (failure) state F if and only if it keeps stayed in either State 1 or State 3 for the time of N_{hd}.

- The down state is absorbing and may denote the system failure in practice.

Then the new kernel for the model in Section 5.4 has the form

$$q(n) = \begin{bmatrix} q_{u,u}(n) & q_{u,d}(n) \\ q_{d,u}(n) & q_{d,d}(n) \end{bmatrix} = \begin{bmatrix} q_{00}(n) & q_{01}(n) & q_{02}(n) & q_{03}(n) & q_{0F}(n) \\ q_{10}(n) & q_{11}(n) & q_{12}(n) & q_{13}(n) & q_{1F}(n) \\ q_{20}(n) & q_{21}(n) & q_{22}(n) & q_{23}(n) & q_{2F}(n) \\ q_{30}(n) & q_{31}(n) & q_{32}(n) & q_{33}(n) & q_{3F}(n) \\ q_{F0}(n) & q_{F1}(n) & q_{F2}(n) & q_{F3}(n) & q_{FF}(n) \end{bmatrix},$$

in which the non-zero constant elements are

$$\begin{aligned}
q_{01}(n) &= g_{01}g_{00}^{n-1}, \\
q_{10}(n) &= \mathbf{1}_{\{n\le N_{hd}\}} \cdot g_{10}g_{11}^{n-1}\prod_{l=1}^{n} h_{00}(l), \\
q_{12}(n) &= \mathbf{1}_{\{n\le N_{hd}\}} \cdot g_{11}^{n}h_{01}(n)\prod_{l=1}^{n-1} h_{00}(l), \\
q_{13}(n) &= \mathbf{1}_{\{n\le N_{hd}\}} \cdot g_{10}g_{11}^{n-1}h_{01}(n)\prod_{l=1}^{n-1} h_{00}(l), \\
q_{1F}(n) &= \mathbf{1}_{\{n=N_{hd}\}} \cdot g_{01}g_{00}^{n-1}, \\
q_{23}(n) &= g_{10}g_{11}^{n-1}, \\
q_{32}(n) &= \mathbf{1}_{\{n\le N_{hd}\}} \cdot g_{01}g_{00}^{n-1}\prod_{l=1}^{n} h_{11}(l), \\
q_{30}(n) &= \mathbf{1}_{\{n\le N_{hd}\}} \cdot g_{00}^{n}h_{10}(n)\prod_{l=1}^{n-1} h_{11}(l), \\
q_{31}(n) &= \mathbf{1}_{\{n\le N_{hd}\}} \cdot g_{01}g_{00}^{n-1}h_{10}(n)\prod_{l=1}^{n-1} h_{11}(l), \\
q_{3F}(n) &= \mathbf{1}_{\{n=N_{hd}\}} \cdot g_{10}g_{11}^{n-1}.
\end{aligned}$$

Compared with $Q^R(i,j,n)$ introduced in the previous subtopic, $q_{ij}(n)$ considers the effects brought by the absorbing failure state. In addition, only combinations of different i and j are taken into account in $q_{ij}(n)$.

The list of $\lambda(n)$ and $\Lambda(n)$ are then calculated as follows:

$$
\begin{aligned}
\lambda_0(n) &= (1-g_{00})g_{00}^{n-1};\\
\lambda_1(n) &= \begin{cases} g_{11}^{n-1}(1-g_{11}h_{00}(n))\prod_{l=1}^{n-1} h_{00}(l), & n < N_{hd}\\ g_{11}^{n-1}\prod_{l=1}^{n-1} h_{00}(l), & n = N_{hd}\\ 0, & n > N_{hd}\end{cases};\\
\lambda_2(n) &= (1-g_{11})g_{11}^{n-1};\\
\lambda_3(n) &= \begin{cases} g_{00}^{n-1}(1-g_{00}h_{11}(n))\prod_{l=1}^{n-1} h_{11}(l), & n < N_{hd}\\ g_{00}^{n-1}\prod_{l=1}^{n-1} h_{11}(l), & n = N_{hd}\\ 0, & n > N_{hd}\end{cases};\\
\lambda_F(n) &= 0.
\end{aligned}
$$

$$
\begin{aligned}
\Lambda_0(n) &= 1-g_{00}^{n};\\
\Lambda_1(n) &= \begin{cases} 1-g_{11}^{n}\prod_{l=1}^{n} h_{00}(l), & n < N_{hd}\\ 1, & n \geq N_{hd}\end{cases};\\
\Lambda_2(n) &= 1-g_{11}^{n};\\
\Lambda_3(n) &= \begin{cases} 1-g_{00}^{n}\prod_{l=1}^{n} h_{11}(l), & n < N_{hd}\\ 1, & n \geq N_{hd}\end{cases};\\
\Lambda_F(n) &= 0.
\end{aligned}
$$

5.6 Simulation

We hereby provide a simulation example to verify the validity of preciseness of the reliability algorithm with respect to our transition model (kernel). Select a process X^R, which follows the rules in Section 5.4 and has one-step transition probabilities

$$
\begin{array}{ll} g_{00} = 0.5, & h_{00}(m) = 0.8 + 0.1\sin(m+1),\\ g_{11} = 0.8, & h_{11}(m) = 0.75 + 0.25(1-e^{-m-1}). \end{array} \tag{5.14}
$$

It is easy to compute the reliability function $R(n)$ upon the time index following (5.9). Fig. 5.3 gives the plots of $R(n)$ with two sample processes of X^R, where the four states are defined as discussed above and the failure state is marked with -1.

Define the experimental reliability function as

$$
R_{ex}(n) = 1 - \frac{1}{N}\sum_{i=1}^{N} \mathbf{1}_{\{X_i^R(n)=-1\}}, \tag{5.15}
$$

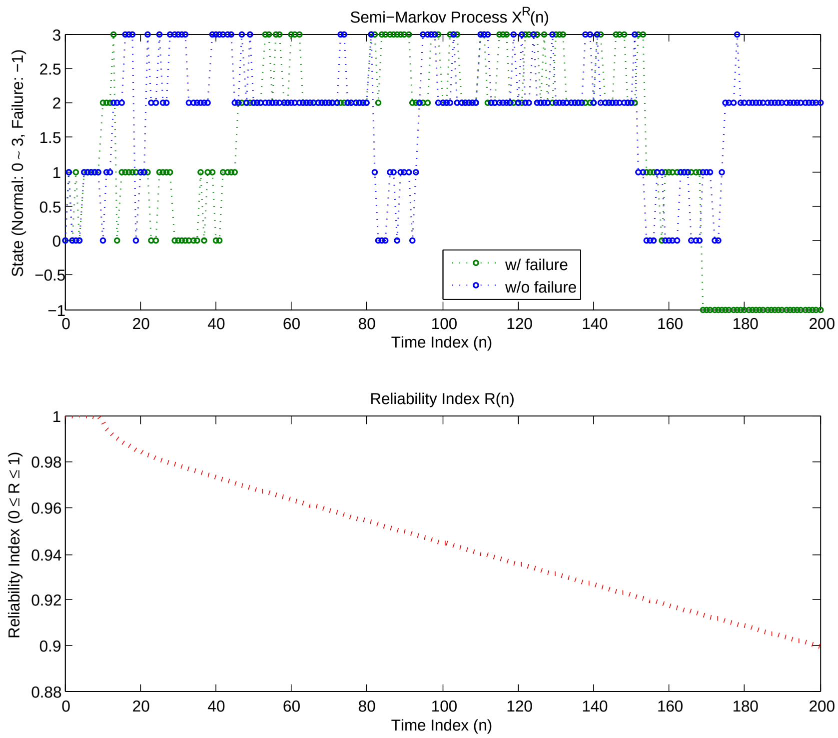

Figure 5.3: $R(n)$ with two sample processes of X^R, one of which with fault state appearance

where N is the total counts of the Monte-Carlo simulations. X_i^R denotes the i^{th} sample process of X^R. $R_{ex}(n)$ gives the statistical proportion of unfaulted experiments among the total samples.

Run Monte-Carlo simulation for 2000 times, and Fig. 5.4 shows the result of both $R(n)$ and $R_{ex}(n)$. The figure has shown that the experimental result matches the theoretical index, and thus confirmed the preciseness of the probability-based reliability index function $R(n)$.

5.7 Conclusion

This chapter presents in-depth analysis of long-term properties of fault and detection processes upon time. Two types of semi-markov kernel models have been established, given different assumptions/simplifications on the state-transition behavior. A quantitative reliability is then contoured with respect

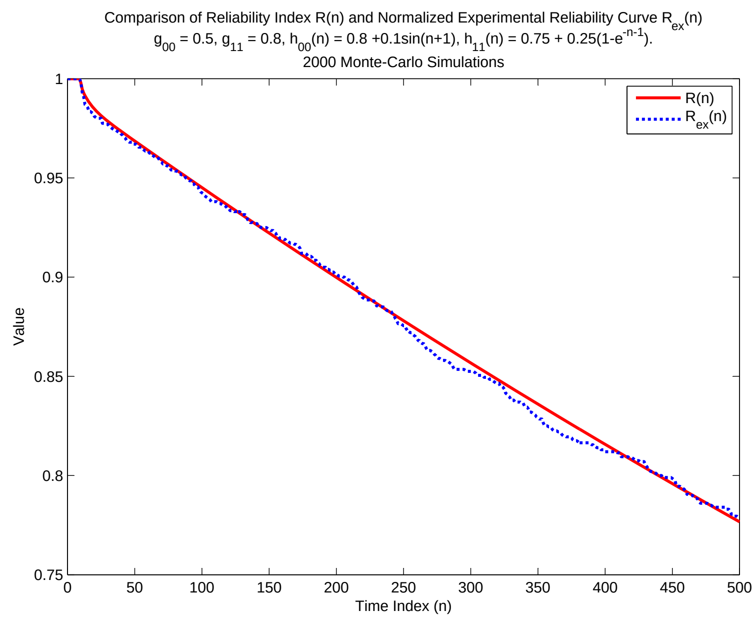

Figure 5.4: Comparison between $R(n)$ and $R_{ex}(n)$

to the kernel model provided, with the simulation reflecting its correctness. Research in this chapter will be helpful in the long-term FD evaluation and FTC for systems subject to structured faults. As a substantial part completing the research work for the thesis, it expands our research by filling the blank of the top layer in the three-layer integrate FD framework.

Chapter 6

Summary and Future Work

6.1 Research Summary

Under the real-time integrated FDI framework posed in Chapter 1, the thesis has carried out insightful research from Chapter 2 to 5 with the following highlights:

- Exploration of multiple types of faults

One of the most important thoughts of the thesis is the coverage of multiple types of faults, and contributions have been made following this direction. Besides the traditional step fault on mean mainly researched in Chapter 2, the fault on variance has appeared as a new fault, requiring different way of solution. Chapter 3 has established provided both single value-based and probability-based indices, respectively ARL (FAR) and approximated FHT probabilities, which succeed to characterize that fault. Besides, Chapter 4 introduces two types of dynamic faults (frequency shift and additive sinusoids), which can also be categorized as structured or unstructured fault depending on whether the fault occurs on system parameter(s). With the trade-off between robust estimation and FD of the perturbation, the analytical FD characterization results is realized and implemented with respect to problems including frequency shift and new fault frequency.

- FD characterization methodologies

With the mind to explore new types of faults, the methodologies used for FD characterization are also sparkling. As the main result of Chapter 2, CLR (BCLR) is an important simplification for the GLR-based probabilistic characterization as well as a breakthrough in continuous time domain, before which the deduction of the original GLR considering sample period is carried out for guaranteeing the correctness of GLR FTCS with different sampling periods. Due to the complexity of the multi-layer integral, mathematical approximations, including Cauchy-Schwarz inequality and the arithmetic mean inequality of the natural logarithm, are the solution to the analytical form of the FHT probabilities regarding the multiplicative fault affecting variances in Chapter 3. The analytical form of mapping range of the FD signal is given, providing grounds for the detectableness of the frequency perturbation faults.

- Real-time (online) estimation/detection

Committing to provide practical solutions, we have tried to cover more practical factor in our research results. One of the most crucial factors is the real-time consideration: nearly all of our research highlights involves real-time elements, making them useful techniques. In Chapter 2 and 3, analytical versions of detection (FHT) probabilities upon time for additive and multiplicative faults are worked out and integrated in real-time DC motor FTCS. A real-time frequency estimator is directly usable for signal monitoring in Chapter 4, and the kernel models in Chapter 5 as fundamental transition behavior description decide the failure rate and the reliability upon time. With such characteristics, they are potentially implementable to industries such as chemical/process engineering, mechanical engineering, power engineering, reliability engineering and system safety.

- FD long-term performance analysis

Listed in Chapter 5, this part of research seems standing alone, while it is the one completing the thesis in the view of systematic structure. This park sparkles as it provides a feasible model explaining the transition among the well-defined states of the joint fault and detection process, upon which the higher-end Barbu's time-reliability function is rewritten in a more computable way. Besides, the fact that the research stands on the commonly-accepted previous research benchmarks, especially transition state concepts as posted in [112] and Barbu's reliability index [114], will reduce the cost of application/modification/upgrade of equipments, giving high practicality to the research so that it is suitable for large engineering sites/projects, e.g. power/mining plants.

6.2 Future Work

In summary, the thesis has made broad research and provided a solid base for further research. The future work can be developed following the potential topics.

First of all, the research on more types of faults may be covered in the future, although major types have already been researched in the thesis. Some existing techniques may be helpful to our future research. Regarding the fault's effect on mean/variance and its occurrence style, the moving average/variance filter techniques (e.g., exponential window moving average/variance (EWMA/EWMV), [65], [66], [67]) can be used for better coverage of dynamic faults featured for time-varying mean/variance with non-abrupt changes. It is also noticeable that the power of a sinusoid keeps positive while the sinusoid itself does not, so researchers may take advantage of IAE [41] or IAE-like techniques for topics as further research on perturbed sinusoid signal estimation and processing. Besides, industry projects may require more than two states (normal-fault pair) available in the joint fault-detection process; in this case the function of multiple hypotheses testing [68] may be introduced, in order to make the integrated FD adapt to multiple types of signals.

In the three-layer integrated FD structure, the thesis contains research in at least two layers with four different subtopics. Upcoming research may attempt subtopics connecting two or more layers, e.g. a complete design of CLR-based FTCS with long-term transition probability analysis and prediction. This systematic outline may need more opinions and knowledge of integration of modules other than those mentioned in the thesis. System design tools, such as flow charts and system topology, will be useful for such collaboration work [38], [47], [45].

At last, the tailing of the integrated FDI to a real engineering project will be meaningful. Occurring frequently in chemical/petro-engineering sites, random jitter, where the false and missing detection rates are high due to a large variance compared with the mean difference, may be treated as the next topic. It causes the difficulty in identifying whether the FHT denotes time between false alarms or detection delay and in calculating the FHT or run length distribution in general. One potential solution is that forming the distribution as a weighted sum of the two computable distributions respectively under H_0 and H_1, and the weights depends on the probability of fault occurrence at the beginning (end) of each time duration. Common oscillation processing methods, such as PCA [3], IAE [41], ACF [42], spectral methods [37], root causes [37], [43], [119], [120] will be crucial references.

Bibliography

[1] S.X. Ding, *Model-based fault diagnosis techniques: design schemes, algorithms, and tools*. Springer-Verlag, 2008.

[2] F. Gustafsson, “Statistical signal processing approaches to fault detection,” *Annual Reviews in Control*, 31(1), 2007, pp. 41–54.

[3] V. Venkatasubramanian, R. Rengaswamy, K. Yin, S.N. Kavuri, “A review of process fault detection and diagnosis: Part I: Quantitative model-based methods,” *Comp. & Chem. Eng.*, 27(3), 2003, pp. 293–311.

[4] V. Venkatasubramanian, R. Rengaswamy, S.N. Kavuri,“A review of process fault detection and diagnosis: Part II: Qualitative models and search strategies,” *Comp. & Chem. Eng.*, 27(3), 2003, pp. 313–326

[5] V. Venkatasubramanian, R. Rengaswamy, S.N. Kavuri, K. Yin, “A review of process fault detection and diagnosis: Part III: Process history based methods,” *Comp. & Chem. Eng.*, 27(3), 2003, pp. 327–346.

[6] Q. Yang, “Model-based and data-driven fault diagnosis methods with applications to process monitoring,” Ph.D. dissertation, Dept. Elec. Eng. & Comp. Sci., Case Western Resv. Univ., Cleveland, OH, 2004.

[7] H. Wang, T.-Y. Chai, J.-L. Ding, B. Martin, “Data driven fault diagnosis and fault tolerant control: some advances and possible new directions,” *Acta Automatica Sinica*, 35(6), 2009, pp. 739–747.

[8] P.M. Frank, “Fault diagnosis in dynamic systems using analytical and knowledge-based redundancy—A survey and some new results,” *Automatica*, 26(3), 1990, pp. 459–474.

[9] C.H. Lo, Y.K. Wong, A.B. Rad, “Model-based fault diagnosis in continuous dynamic systems,” *ISA Trans.*, 43(3), 2004, pp. 459–475.

[10] C.-T. Chang, J.-I. Hwang, “Simplification techniques for EKF computations in fault diagnosis—suboptimal gains,” *Chem. Eng. Sci.*, 53(22), 1998, pp. 3853–3862.

[11] A.M. Pertew, H.J. Marquez, Q. Zhao, “LMI-based sensor fault diagnosis for nonlinear Lipschitz systems,” *Automatica*, 43(8), 2007, pp. 1464–1469.

[12] B. Yan, Z. Tian, S. Shi, Z. Weng, “Fault diagnosis for a class of nonlinear systems via ESO,” *ISA Trans.*, 47(4), 2005, pp. 386–394.

[13] H. Wang, H.-H. Ju, G.-H. Yang, "Fault detection filter design for linear polytopic uncertain continuous-time systems," *Acta Automatica Sinica*, 36(5), 2010, pp. 742–750.

[14] L. Yao, H. Wang, "Fault diagnosis of a class of singular nonlinear systems," *Proc. of the 6th IFAC Symposium on fault detection, supervision and safety of technical processes, SAFEPROCESS 2006*, 2007, pp. 42–47.

[15] P. Zhang, H. Ye, S.X. Ding, G.Z. Wang, D.H. Zhou, "On the relationship between parity space and H_2 approaches to previous termfault detection," *Systems & Control Letters*, 55(2), 2006, pp. 94–100.

[16] W.R. Becraft, P.L. Lee, "An integrated neural network/expert system approach for fault diagnosis," *Comp. & Chem. Eng.*, 17(10), 1993, pp. 1001–1014.

[17] D. Leung, J. Romagnoli, "An integration mechanism for multivariate knowledge-based fault diagnosis," *J. Proc. Ctrl.*, 12(1), 2002, pp. 15–26.

[18] R. Dunia, S.J. Qin, T.F. Edgar, T.J. McAvoy, "Identification of faulty sensors using principal component analysis," *American Institute of Chem. Eng. J.*, 42(10), 1996, pp. 2797–2812.

[19] W. Li, H. Yue, S. Valle-Cervantes, S. Qin, "Recursive PCA for adaptive process monitoring," *J. Proc. Ctrl.*, 10(5), 2000, pp. 471–486.

[20] J.-C. Jeng, "Adaptive process monitoring using efficient recursive PCA and moving window PCA algorithms," *Journal of the Taiwan Institute of Chemical Engineers*, 41(4), 2010, pp. 475–481.

[21] J.-M. Lee, C. Yoo, I.-B. Lee, "Statistical process monitoring with independent component analysis," *J. Proc. Ctrl.*, 14(5), 2004, pp. 467–485.

[22] S.X. Ding, P. Zhang, A. Naik, E.L. Ding, B. Huang, "Subspace method aided data-driven design of fault detection and isolation systems," *J. Proc. Ctrl.*, 19(9), 2009, pp. 1496–1510.

[23] P. Vachhani, S. Narasimhan, R. Rengaswamy, "An integrated qualitative-quantitative hypothesis driven approach for comprehensive fault diagnosis," *Chem. Eng. Research & Design*, 85(9), 2007, pp. 1281–1294.

[24] Y. Zhang, J. Jiang, "Design of integrated fault detection, diagnosis and reconfigurable control systems," *Proc. 38th IEEE Conf. on Dec. & Ctrl.*, vol. 4, 1999, pp. 3587–3592.

[25] Y. Ma, S.X. Ding, P. Zhang, T. Jeinsch, M. Schultalbers, "Integrated design of fault detection system with multi-objective optimization," *Proc. 6th IFAC symposium on fault detection, supervision and safety of technical processes, SAFEPROCESS 2006*, 2007, pp. 879–884.

[26] Y. Huang, J. Gertler, T.J. McAvoy, "Sensor and actuator fault isolation by structured partial PCA with nonlinear extensions," *Journal of Process Control*, 10(5), 2000, pp. 459–469.

[27] F.N. Pirmoradi, F. Sassani, C.W. de Silva, "Fault detection and diagnosis in a spacecraft attitude determination system," *Acta Astronautica*, 65(5–6), 2009, pp. 710–729.

[28] R.J. Patton, F.J. Uppal, S.Simani, B. Polle, "Robust FDI applied to thruster faults of a satellite system," *Ctrl. Eng. Practice*, 18(9), 2010, pp. 1093–1109.

[29] X. Wang, V. Makis, "Autoregressive model-based gear shaft fault diagnosis using the Kolmogorov-Smirnov test," *Journal of Sound and Vibration*, 327(3–5), 2009, pp. 413–423.

[30] Q. Hu, Z. He, Z. Zhang, Y. Zi, "Fault diagnosis of rotating machinery based on improved wavelet package transform and SVMs ensemble," *Mechanical Systems and Signal Processing*, 21(2), 2007, pp. 688–705.

[31] M. Saimurugan, K.I. Ramachandran, V. Sugumaran, N.R. Sakthivel, "Multi component fault diagnosis of rotational mechanical system based on decision tree and support vector machine," *Expert Systems with Applications*, 38(4), 2011, pp. 3819–3826.

[32] P.R.S. Jota, S.M. Islam, T. Wu, G. Ledwich, "A class of hybrid intelligent system for fault diagnosis in electric power systems," *Neurocomputing*, 23(1–3), 1998, pp. 207–224.

[33] C. Ma, X. Gu, Y. Wang, "Fault diagnosis of power electronic system based on fault gradation and neural network group," *Neurocomputing*, 72(13–15), 2009, pp. 2909–2914.

[34] F.B. Leão, R.A.F. Pereira, J.R.S. Mantovani, "Fault section estimation in electric power systems using an optimization immune algorithm," *Electric Power Systems Research*, 80(11), 2010, pp. 1341–1352.

[35] Q. Wu, "Car assembly line fault diagnosis based on modified support vector classifier machine," *Expert Systems with Applications*, 37(9), 2010, pp. 6352–6358.

[36] J.P. Shunta, *Achieving world class manufacturing through process control.* Englewood Cliffs, NJ: Prentice-Hall, 1995.

[37] H. Jiang, M.A.A.S. Choudhury, S.L. Shah. "Detection and diagnosis of plant-wide oscillations from industrial data using the spectral envelope method," *J. Proc. Ctrl.*, 17(2), 2007, pp. 143–155.

[38] A.K. Tangirala, K. Kanodia, S.L. Shah, "Applications of non-negative matrix factorization for detection and diagnosis of plant-wide oscillations," *Industrial Eng. Chemistry Res. & Development*, 46(3), 2007, pp. 801–817.

[39] K.W. Louie, P. Wilson, R.A. Rivas, A. Wang, P. Buchanan, "Discussion on power system harmonic analysis in the frequency domain," *IEEE/PES Transmission & Distribution Conference and Exposition*, 2006, pp. 1–6.

[40] N.F. Thornhill, A. Horch, "Advances and new directions in plant-wide disturbance detection and diagnosis," *Ctrl. Eng. Practice*, 15(10), 2007, pp. 1196–1206.

[41] N.F. Thornhill, T. Hägglund, "Detection and diagnosis of oscillation in control loops," *Ctrl. Eng. Practice*, 5(10), 1997, pp. 1343–1354.

[42] N.F. Thornhill, B. Huang, H. Zhang, "Detection of multiple oscillations in control loops," *J. Proc. Ctrl.*, 13(1), 2003, pp. 91–100.

[43] N.F. Thornhill, "Finding the source of nonlinearity in a process with plant-wide oscillation," *IEEE Trans. Ctrl. Sys. Tech.*, 13(3), 2005, pp. 434–443.

[44] L. Desborough, R. Miller, "Increasing customer value of industrial control performance monitoring—Honeywell's experience," *Proc. AIChE Symp. Ser.*, vol. 98, 2002, pp. 153–186.

[45] M.A.A.S. Choudhury, S.L. Shah, N.F. Thornhill, "Diagnosis of poor control-loop performance using higher-order statistics," *Automatica*, 40(10), 2004, pp. 1719–1728.

[46] D. Törnqvist, F. Gustafsson, 2006, "Eliminating the initial state for the generalized likelihood ratio test," *Proc. 6th IFAC symposium on fault detection, supervision and safety of technical processes, SAFEPROCESS 2006)*, 2007, pp. 599–604.

[47] S.Y. Yim, H.G. Ananthakumar, L. Benabbas, A. Horch, R. Drath, N.F. Thornhill, "Using process topology in plant-wide control loop performance assessment," *Comp. & Chem. Eng.*, 31(2), 2006, pp. 86–99.

[48] O.L.V. Costa, F. Dufour, "Stability and ergodicity of piecewise deterministic Markov processes," *Proc. IEEE Conf. Decision & Ctrl. (CDC)*, 2008, pp. 1525–1530.

[49] Z. Lu, H.H.S. Ip, "Spatial Markov kernels for image categorization and annotation," *IEEE Trans. on Systems, Man, and Cybernetics, Part B: Cybernetics*, 41(4), 2011, pp. 976–989.

[50] M.L. Gamiz , "Smoothed estimation of a 3-state semi-Markov reliability model," *IEEE Trans. on Reliability*, 61(2), 2012, pp. 336–343.

[51] M. Basseville, I. Nikiforov, *Detection of abrupt changes: theory and application*, Prentice Hall, Inc., 1993.

[52] Y. Lin, *Applied stochastic processes.* Tsinghua University Press, Beijing, China, 2002.

[53] Q. Zhao, M. Kinnaert, "Statistical properties of CUSUM based fault detection schemes for fault tolerant control," *Joint 48th IEEE Conf. Decision and Control / 28th Chinese Control Conf.*, 2009, pp. 7831–7836.

[54] M. Hou, "Estimation of sinusoidal frequencies and amplitudes using adaptive identifier and observer," *IEEE Trans. Automat. Ctrl.*, 52(3), 2007, pp. 493–499.

[55] B.B. Sharma, I.N. Kar, "Design of asymptotically convergent frequency estimation using contraction theory," *IEEE Trans. Automat. Contr.*, 53(8), 2008, pp. 1932–1937.

[56] P.K. Dash, S. Hasan, B.K. Panigrahi, "Adaptive complex unscented Kalman filter for frequency estimation of time-varying signals", *IET Science, Measurement & Technology*, 4(2), 2010, pp. 93–103.

[57] Z. Gao, X. Dai, T. Breikin, H. Wang, "Novel parameter identification by using a high-gain observer with application to a gas turbine engine," *IEEE Trans. on Industrial Informatics*, 4(4), 2008, pp. 271–279.

[58] Z. Gao, T. Breikin, H. Wang, "High-gain estimator and fault-tolerant design with application to a gas turbine dynamic system," *IEEE Trans. Ctrl. Sys. Tech.*, 15(4), 2007, pp. 740–753.

[59] J. Durbin, "Boundary-crossing probabilities for the Brownian motion and Poisson processes and techniques for computing the power of the Kolmogorov-Smirnov test," *J. Appl. Prob.*, 8, 1971, pp. 431–453.

[60] S. Aberkane, J.C. Ponsart, M. Rodrigues, and D. Sauter, "Output feedback control of a Class of Stochastic Hybrid Systems," *Automatica*, 44(5), 2008, pp. 1325–1332.

[61] D.P. De Farias, J.C. Geromel, J.B.R. do Val, and O.L.V. Costa, "Output feedback control of Markov jump linear systems in continuous-time," *IEEE Trans. Automat. Cntrl.*, 45(5), 2000, pp. 944–949.

[62] F. Tao, Q. Zhao, "Synthesis of fault tolerant control with random FDI delay," *Proc. 44th IEEE Conf. Dec. Ctrl. (CDC) & European Ctrl. Conf. (ECC)*, 2005, pp. 3844–3849.

[63] F. Tao, Q. Zhao, "Synthesis of stochastic fault tolerant control with random FDI delay," *Int. J. Ctrl.*, 80(5), 2007, pp. 684–694.

[64] G. Lorden, "Open-ended tests for Koopman-Darmois families," *The Annals of Statistics*, 1(4), 1973, pp. 633–643.

[65] S.W. Roberts, "Control chart tests based on geometric moving averages," *Technometrics*, 1(3), 1959, pp. 239–250.

[66] P.E. Maravelakis, P. Castagliola, "An EWMA chart for monitoring the process standard deviation when parameters are estimated," *Computational Statistics & Data Analysis*, 53(7), 2009, pp. 2653–2664.

[67] D.A. Serel, H. Moskowitz, "Joint economic design of EWMA control charts for mean and variance," *European Journal of Operational Research*, 184(1), 2008, pp. 157–168.

[68] M. Basseville, I. Nikiforov, "Fault isolation for diagnosis: Nuisance rejection and multiple hypotheses testing," *Annual Reviews in Control*, 26(2), 2002, pp. 189–202.

[69] S. Yang, Q. Zhao, "Real-time frequency estimation of sinusoids with low-frequency disturbances," *Proc. American Control Conference*, 2011, pp. 4275–4280.

[70] S. Yang, Q. Zhao, "Statistical characterization of the GLR based fault detection," *Proc. American Control Conference*, 2011, pp. 3778–3783.

[71] S. Yang, Q. Zhao, "Real-time frequency estimation for sinusoidal signals with application to robust fault detection," *Int. J. Adapt. Control Signal Process*, 26, 2012, DOI: 10.1002/acs.2308.

[72] S. Yang, Q. Zhao, "Probability distribution characterisation of fault detection delays and false alarms," *IET Control Theory & Applications*, 6(7), 2012, pp. 953–962.

[73] M. Blanke, M. Kinnaert, J. Lunze, M. Staroswiecki, *Diagnosis and fault-tolerant control*. 2nd edn., Springer Verlag, 2006.

[74] P. Salminen, "On the first hitting time and the last exit time for a Brownian motion to/from a moving boundary," *Adv. Appl. Probab.*, 20(2), 1988, pp. 411–426.

[75] L. Wang, K. Pötzelberger, "Brownian motion hitting probabilities for general two-sided square root boundaries," *J. Appl. Probab.*, 34(1), 1997, pp.45–65.

[76] D.S. Donchev, "Brownian motion hitting probabilities for general two-sided square root boundaries," *Methodol. Comput. Appl. Probab.*, 12(2), 2009, pp. 237–245.

[77] J. Jiang, "Fault-tolerant control systems—an introductory overview," *ACTA Autom. Sin.*, 31(1), 2005, pp. 161–174.

[78] R. Srichander, B.K. Walker, "Stochastic stability analysis for continuous-time fault tolerant control systems," *Int. J. Control*, 57(2), 1993, pp. 433–452.

[79] H. Li, Q. Zhao, "Design of fault-tolerant control for mean time to failure)", *Int. J. Robust Nonlinear Control,* 2008, 18(16), pp. 1551–1574.

[80] I. Izadi, S.L. Shah, T. Chen, "Effective resource utilization for alarm management," *Proc. IEEE Conf. Decision & Ctrl.*, 2010, pp. 6803–6808.

[81] I.I.N.A. Adnan, T. Chen, "On expected detection delays for alarm systems with deadbands and delay times", *J. Process Control*, 21(9), 2011, pp. 1318–1331.

[82] B.K. Øksendal, "Stochastic differential equations: an introduction with applications," Springer, Berlin, Germany.

[83] J. Durbin, "The first passage density of the crossing of a continuous Gaussian process to a general boundary," *J. Appl. Probab.*, 22(1), 1985, pp. 99–122.

[84] L. Hsu, R. Ortega, G. Damm, "A globally convergent frequency estimator," *IEEE Trans. Automatic Ctrl.*, 44(4), 1999, pp. 698–713.

[85] R. Marino, P. Tomei, "Global estimation of n unknown frequencies," *IEEE Trans. Automatic Ctrl.*, 47(8), 2002, 1324–1328.

[86] M. Hou, "Amplitude and frequency estimator of a sinusoid," *IEEE Trans. Automatic Ctrl.*, 50(6), 2005, pp. 855–858.

[87] S.W. Lee, J.S. Lim, S.J. Baek, K.M. Sung, "Time-varying frequency estimation by VFF Kalman filtering," *Signal Processing*, 77(3), 1999, pp. 855–858.

[88] Q.W. Jia, "Disturbance rejection through disturbance observer with adaptive frequency estimation," *IEEE Trans. Magnetics*, 45(6), 2009, pp. 2675–2678.

[89] J. Yang, H. Xi, W. Guo, "Robust modified Newton algorithm for adaptive frequency estimation.," *IEEE Signal Processing Letters*, 14(11), 2007, pp. 879–882.

[90] J. Yang, H. Xi, F. Yang, "Adaptive modified Newton algorithm for multiple frequencies estimation," *Proc. World Cong. Intelligent Ctrl. Autom. (WCICA)*, 2008, pp. 2992–2995.

[91] H.C. So, P.C. Ching, "Adaptive algorithm for direct frequency estimation," *IEE Proc.-Radar, Sonar & Navigation*, 151(6), 2004, pp. 359–364.

[92] P.A. Ioannou, J. Sun, *Robust adaptive control.* Prentice Hall, Upper Saddle River, NJ, USA, 1996.

[93] C.T. Chen, *Linear system theory and design.* 3rd edn., Oxford University Press, NY, USA, 1999.

[94] C.A. Desoer, M. Vidyasagar, *Feedback systems: input-output properties.* Academic Press Inc., NY, USA, 1975.

[95] J.P. Hespanha, "Uniform stability of switched linear systems: extensions of LaSalle's Invariance Principle," *IEEE Trans. on Automatic Control*, 49(4), 2004, pp. 470–482.

[96] S. Sastry, M. Bodson, *Adaptive control: stability, convergence, and robustness.* Prentice Hall, Upper Saddle River, NJ, USA, 1989.

[97] G.J. Preston, D.N. Sheilds, S. Daley, "Application of a robust nonlinear fault detection observer to a hydraulic system," *Proc. UKACC Int. Conf. Ctrl.*, 2, 1996, pp. 1484–1489.

[98] D. Yu, G.J. Preston, D.N. Sheilds, S. Daley, "A bilinear fault detection observer and its application to a hydraulic drive system," *Int. J. Ctrl.*, 64(6), 1996, pp. 1023–1047.

[99] X. Wen, "Observer based fault detection method for a hydraulic rig," *M. Eng. Report*, University of Alberta, Edmonton, Canada, 2008.

[100] M. Timusk, M. Lipsett, C.K. Mechefske, "Fault detection using transient machine signals," *Mechanical Sys. & Signal Proc.*, 22(7), 2008, pp. 1724–1749.

[101] F. Caliskan, C.M. Hajiyev, "Innovation sequence application to aircraft sensor fault detection: comparison of checking covariance matrix algorithms," *ISA Transactions*, 39(1), 2000, pp. 47–56.

[102] H. Hung and A. Chen, "Test of covariance changes without a large sample and its application to fault detection classification," *J. Proc. Ctrl.*, 22(6), 2012, pp. 1113–1121.

[103] L.H. Chiang, R.D. Braatz, "Process monitoring using causal map and multivariate statistics: fault detection and identification," *Chemometrics & Intelligent Lab. Sys.*, 65(2), 2003, pp. 159–178.

[104] J. Yu and S.J. Qin, "Statistical MIMO controller performance monitoring. Part I: Data-driven covariance benchmark," *J. Proc. Ctrl.*, 18(3–4), 2008, pp. 277–296.

[105] F.J. O'Brien, Jr. *Double factorials: selected proofs and notes.* Aquidneck Indian Council, Newport, RI, 2009.

[106] S.M. Kay, *Fundamentals of statistical signal processing: volume II, detection theory.* Prentice Hall, Upper Saddle River, NJ, 1998.

[107] M. Abramowitz, I.A. Stegun, *Handbook of mathematical functions with formulas, graphs, and mathematical tables.* Dover Publications, Inc., NY, 1964.

[108] W.H. Greene, *Econometric analysis.* 5th edn., Prentice-Hall, Upper Saddle River, NJ, 1993.

[109] H. Robbins, "Statistical methods related to the law of the iterated logarithm," *Annals Mathematical Statistics*, 41(5), 1970, pp. 1397–1409.

[110] M. Pollak, D. Siegmund, "Approximations to the expected sample size of certain sequential tests," *Annals Statistics*, 3(6), 1975, pp. 1267C1282.

[111] M. Mahmoud, J. Jiang, Y. Zhang. *Active fault tolerant control systems: stochastic analysis and synthesis.* Springer-Verlag, Berlin, 2003.

[112] H. Li, "Reliability-based fault tolerant control systems—analysis and design," *PhD thesis*, University of Alberta, Edmonton, Canada, 2007.

[113] G. Latouche, V. Ramaswami, *Introduction to matrix analytic methods in stochastic modeling.* SIAM, 1999.

[114] V. Barbu, M. Boussemart, N. Limnios, "Discrete-time semi-Markov model for reliability and survival analysis," *Communications in Statistics—Theory and Methods*, 33(11), 2004, pp. 2833–2868.

[115] Y. Fang, K.A. Loparo, "Stabilization of continuous-time jump linear systems," *IEEE Transactions on Automatic Control*, 47(10), 2002, pp. 1590–1603.

[116] P.K. Anderson, O. Borgan, R.D. Gill, and N. Keiding, *Statistical models based on counting processes.* Springer, New York, 1993.

[117] A. Csenki, "Transition analysis of semi-Markov reliability models—A tutorial review with emphasis on discrete-parameter approaches," In: S. Osaki, ed. *Stochastic Models in Reliability and Maintenance.* Springer, Berlin, 2002, pp. 219–251.

[118] J. Janssen, R. Manca, "Numerical solution of non-homogeneous semi-Markov processes." *Insurance Math Econom.*, 3, 2001, pp. 271–294.

[119] Ender, "Process control performance: not as good as you think," *Control Eng.*, Vol. 40, 1993, pp. 180–190.

[120] H. Jiang, R. Patwardhan, S.L. Shah. "Root cause diagnosis of plantwide oscillations using the concept of adjacency matrix," *J. Proc. Ctrl.*, 19(8), 2009, pp. 1347–1354.